# Iodine-125 Induced DNA Strand Breakage: Contributions of Different Physical and Chemical Radiation Action Mechanisms

Dissertation

zur Erlangung des Grades eines Doktors
der Naturwissenschaften

der Fakultät für Physik
der Technischen Universität München

vorgelegt von

## Weibo Li

aus Luoyang VR China

Juni 2002

**Technische Universität München**


E22 Lehrstuhl für Experimentalphysik


Iodine-125 Induced DNA Strand Breakage:

Contributions of Different Physical and Chemical Radiation Action Mechanisms


Weibo Li


Vollständiger Abdruck der von der Fakultät für Physik
der Technischen Universität München zur Erlangung des akademischen Grades eines
Doktors der Naturwissenschaften
genehmigten Dissertation.


Vorsitzender: Univ.−Prof. Dr. S. Fischer
Prüfer der Dissertation:
  1.  Hon.−Prof. Dr. H. G. Paretzke
  2.  Univ.−Prof. Dr. E. Sackmann


Die Dissertation wurde am 04.07.2002 bei der Technischen Universität München
eingereicht und durch die Fakultät für Physik
am 16.09.2002 angenommen.

*To my parents and Ying*

# Contents

I

# List of Figures

# List of Tables

# Chapter 1

# Introduction

## 1.1    I-125 Decays and their Biological Effects

The radioisotope $^{125}$I is of high importance in radiation biology. It is of widespread use in diagnostic nuclear medicine. Its radiation action has often been experimentally studied. If an $^{125}$I atom is incorporated into a deoxyribonucleic acid (DNA)$^\dagger$ molecule, besides the biological damage of the low-energy Auger electrons the toxic effect resulting from the neutralization of the metastable $^{125m}$Te atom is dominant. The present work tries to evaluate the fraction of this neutralization effect on the basis of Monte Carlo simulations and experimental data available. An attempt using charge transfer theory was also made to explore the contribution of the neutralization effect in $^{125}$I-induced DNA damage.

There are two steps in $^{125}$I decay. When the nucleus of an $^{125}$I atom captures an inner-shell orbital electron, which mostly comes from the K-shell, the $^{125}$I nucleus decays to a metastable state $^{125m}$Te with an excitation energy 35.4 keV. This step is called electron capture (EC), which is finished at about $10^{-16}$ to $10^{-15}$ s. This time is shorter than the molecular vibration period ($10^{-14}$ to $10^{-13}$ s), so that the atom remains in its equilibrium state in the molecule. If the $^{125}$I atom is a part of a molecule, the atom will be in neutral. In this period of time, the binding energy of the captured inner electron will be released by emission of characteristic X-rays, Auger and Coster-Kronig electrons, shake-off electrons and soft X-rays. This is the first electron cascade. In the second step, which takes time of $1.6 \times 10^{-9}$ s, the excitation energy can be released by $\gamma$ photon emission, but 93% of it is transferred directly to shell electrons, emits internal electrons and produces a vacancy. An outer-shell electron will fill it and release also characteristic X-rays and Auger electrons as in the first step. This process is called isomeric transition (IT). During this process the

---

$^\dagger$Abbreviations see Appendix C.

| Mammalian Cellular DNA | |
|---|---|
| $^{125}$IdCTP | [BRFB73], [PYB74], [BCA75], [CLLA76], [CLLA78], [PY78] |
| $^{125}$IdU | [MF81], [KSA87], [KFK$^+$89], [CHvLS94], [WAK98b], [WAK98b], |
| | [HLS00], [WDAK00], [YHD01], [WAK01] |
| $^{125}$IVME2 | [HvLSC92], [YHD01], [HPH69] |
| Plasmid DNA | |
| $^{125}$IH | [AK96], [WDR$^+$99], [KHA99b] |
| $^{125}$IAP | [AK96], [KHA99b] |
| $^{125}$I-TFO | [NMC$^+$96], [PLPN01] |
| Pyrimidine in Synthetic Oligodexynucleotide | |
| $^{125}$I | [CH88], [Pom91], [PT94], [LFJ00] |
| $^{125}$IdCTP | [KL74], [KKS76], [MH81], [LM00a], [LM00b] |
| $^{125}$I-TFO | [PN94], [PN96], [PN97], [NLT$^+$00], [NPT$^+$00], [PLPN01] |

Table 1.1: Literature on positions and forms of the $^{125}$I atom in different targets commonly used in experiments and calculations

atom emits internal conversion (IC) electrons and $\gamma$-rays, and it produces a second electron cascade. If the $^{125}$I atom is incorporated into a molecule, e.g. DNA in solution, during the two Auger electron cascades, the $^{125m}$Te atom is highly positive charged as a result of the emission of an average of 21.2 electrons [CJ81]. It will later extract electrons from the parent molecule in which $^{125}$I located and also from neighboring molecules. This is the so-called neutralization effect. A neutralization of the charge on the parent moiety will deposit tens to hundreds of eV excitation energy in this molecule, leading to its superexcited state. This energy exceeds by much the chemical bond energy or even the dissociation energy of most radicals and the molecule should be expected to collapse. After this transmutation, the atom $^{125}$Te is stable.

The biological effects after $^{125}$I decays have been extensively investigated experimentally and theoretically at the molecular and cellular level [Ade92], [Sas92], [Hof00]. Table 1.1 gives relevant literature about positions and forms of the $^{125}$I atom in different targets commonly used in experiments and simulations. In the following we describe in detail experimental studies from the cellular level to the genetic level and the current situation of the Monte Carlo simulation using radiation

track structure and an atomic DNA model; indeed, this was the motivation of the present work.

## Studies on $^{125}I$ in Mammalian Cellular DNA

In earlier years, Carlson and White [CW64] showed that the decay of $^{125}I$ in methyl or ethyl iodide leads to molecular fragmentation. A few years later, Feinendegen et al. [FEB71], Ertl et al. [EFH70] and Hofer et al. [HPH69], [HH71] reported that $^{125}I$ incorporated into DNA in the form of $^{125}IdU$ was obviously toxic to mammalian cells. Walicka et al. [WAK98b] showed that chromatin structure fosters some DSBs (double strand breaks) formation by an indirect mechanism when $^{125}I$ is incorporated into DNA in cells and indicated that radiotoxicity of $^{125}I$ decay in the Chinese hamster V79 cells is caused by the indirect mechanism [WAK98a], [WDAK00]. In a recent publication, Kassis et al. [KWA00] concluded that DSB production depends on the conformation and/or environment of DNA. Yasui et al. [YHD96], [YHD01] found an 8-10 fold increase in the induction of DSBs by accumulation of $^{125}IVME2$ decays compared to accumulation of the thymine analog $^{125}IdU$ in CHOER cells. They also indicated that a biophysical model of the DNA damage based on the synthetic oligodeoxynucleotide and naked DNA (plasmid) is inadequate for explaining radiobiological effects at the cellular level, especially for the multiple DSBs in mammalian cellular DNA which arise as a result of biological damage magnification [KWA00]. Hofer et al. [HLS00] developed a new model which represents differential spatial arrangements for parent and daughter DNA in the genome, with DNA strands organized such that a single $^{125}I$ decay originating in daughter DNA damages two targets during the first $G_2$ phase, but identical decays occurring during the second $G_2$ phase damage only one of the targets.

## Studies on $^{125}I$ in Plasmid DNA

Kassis et al. [KHA99a] pointed out that the yield of SSBs induced by $^{125}IH$ incorporated into the minor groove and at a distance from pUC19 plasmid DNA by $^{125}IAP$ was equal per decay, but that the DSB yield was 6.7 fold different. They [KHA99b], [WDR$^+$99] found also that DMSO is efficient in protecting super plasmid DNA from the decay of $^{125}I$ free in solution, and less efficient when the $^{125}I$ decays close to DNA.

Panyutin and Neumann [PN94], [PN96], [PN97] measured DNA DSBs induced by triplex-forming oligodeoxynucleotides. The $^{125}I$ atom was incorporated into a cytosine on an oligonucleotide that formed a triplex helix with a DNA double helix. They found that 90% of all the breaks in the target double helix were located within 10 bp (base pairs) around the decay site. Panyutin et al. [PLPN01] have recently

measured the DNA strand breaks produced by the decay of $^{125}I$ positioned against a specific site in pUC19*MDR1* via an $^{125}I$-TFO. They found that the localized breaks are distributed within 10 bp in each direction from the decay site. The distributions of breaks in the two DNA strands are almost symmetrical. About 25% of the DSBs were located outside the 90-bp fragment containing the TFO binding sequence. They demonstrated that, in addition to DNA breaks confined to a helical turn around the $^{125}I$ atom, the decay can produce breaks hundreds of base pairs away in the plasmid DNA. The results agreed with the data of Linz and Stöcklin [LS85] and of Kassis et al. [KHA99a]. However, Linz and Stöcklin explained that these DNA strand breaks may be induced by the charge transfer along the DNA chain via $\pi$-electrons which are delocalized in the stacking bases. Panyutin et al. believe that these breaks result from the high-energy Auger electrons released in $^{125}I$ decay.

### Studies on $^{125}I$ in Synthetic Oligodeoxynucleotide

Krisch et al. [KL74], [KKS76] and Painter et al. [PYB74] first demonstrated that $^{125}I$ decays in DNA induced double strand breaks. Martin and Haseltine [MH81] showed that DNA strand breaks mostly occurred within four to five nucleotides from an $^{125}I$ decay site. Labochevsky and Martin [LM00a], [LM00b] concluded that for synthetic oligoDNA there should be three components contributing to the DNA strand breaks, and that the non-radiation component constitutes 50 percent.

### Monte Carlo Simulation of $^{125}I$ Induced DNA Strand Breaks

Those impressive experimental studies stimulate modelers to simulate the biological endpoint to test working-hypotheses on the mechanisms of radiation action. This task needs not only theoretical calculations on the $^{125}I$ decay in physical aspects but also appropriate models of DNA used in the measurements. Charlton and Booz [CJ81] first developed a Monte Carlo method for simulating individual radionuclide decays and for calculating the electron spectrum following the decay of an $^{125}I$ atom. Their results showed that the number of electrons emitted per decay depends on the environment of the atom; different numbers of electrons are emitted depending on whether the atom is in isolated or in condensed phase.

With these physical data, Charlton [Cha86] calculated the consequences of $^{125}I$ decays using an electron track structure code [Par80]. Pomplun et al. [PBC87] developed a new theoretical method based on a relativistic Dirac-Fock program and using rigorous bookkeeping [Des75] and estimated a total ionization energy of 1.1 keV released from the charged $^{125m}Te$ atom by neutralization effect. Recently, the same author has calculated the bond length between the decaying iodine and the $C_5$ atom of thymine molecule as a function of charge when an $^{125}I$ atom was incorporated

into the thymine residue in a DNA chain, using a semiempirical quantum-mechanical program [Pom00]. He also pointed out that the second cascade induced by internal conversion after the decay of the metastable state would occur when the atom is perhaps no longer a part of the molecule and may have moved away from the original incorporated position. Charlton et al. [CPB87] and Booz et al. [BPPO87] calculated the potential energy produced by the Auger cascade due to the charging of atoms.

After these physical studies, Charlton and Humm [CH88] developed a simple DNA model, in which the molecule was divided into three volumes representing a base and two individual sugar-phosphate chains separately, and successfully simulated the DNA SSBs measured by Martin and Haseltine [MH81]. Later Pomplun [Pom91] developed a new DNA target model for track structure calculations and applied it to $^{125}$I decay studies. Terrissol [Ter94] built up a more complex model of nucleosome and tested working-hypotheses on the action of $^{125}$I decay on the DNA in mammalian cells. Pomplun and Terrissol [PT94] investigated also the behavior of chemical radicals produced by $^{125}$I atom in a DNA unit and attempted to elucidate the radiation action mechanism. Charlton et al. [CHvLS94] applied a simple volume DNA model and the track structure code [Par80] to simulate DSBs of the DNA associated with a nucleosome induced by $^{125}$I incorporated into the DNA and compared with the experimental data [HvLSC92].

Nikjoo et al. [NMC$^+$96] modeled the fragment length distributions induced by incorporated $^{125}$I in a synthetic oligodeoxynucleotide using a volume model of B-DNA. Recently, Nikjoo et al. [NLT$^+$00], [NPT$^+$00] have calculated the fragment size distributions for triplex DNA induced by TFO-$^{125}$I. In their simulations for DNA and TFO, they did not show the total DNA strand break distributions in both strands.

The radionuclide $^{125}$I is widely used in cancer therapy. Because of the tumor heterogeneity and the incorporation of $^{125}$I atoms into normal body tissues, data on both subcellular $^{125}$I carriers distribution and on the heterogeneity in cellular activity within tumors are required. The inhomogeneity in the dose distribution for low-energy Auger electrons emitted by $^{125}$I decays is a serious problem. Dosimetry calculations [HRS89], [LFP$^+$01] show that $^{125}$I atoms should be more effective in treating mircometastases than high-energy $\beta$-emitters, e.g. $^{131}$I atoms. For further information, see e.g. ref. [Hof96], [Hof00].

## 1.2 Motivation and Concept of the Present Work

In spite of all those efforts in experiments and theoretical calculations, the actual mechanism of DNA damage by the Auger emitter $^{125}$I atom is not yet fully understood [Hof00]. Some questions are still open:

1. Different $^{125}$I compounds, e.g. $^{125}$IVME2 and $^{125}$IdU induce strikingly different yields of DSBs in CHOER cells [YHD01], Are these differences due to different radiosensitivity to $^{125}$I atoms or to the structure of DNA conformation in mammalian cells or to both?

2. DNA strand breaks occur 100 base pairs away from the decay site [LS85], [PLPN01]. Is this due to charge transfer, or to physical direct interactions or to chemical radicals?

3. Theoretical simulations [CH88], [NMC$^+$96], [NLT$^+$00], [NPT$^+$00] so far compared only the fragment size distribution of DNA strand breaks with experimental data. The neutralization effect was always neglected, which might be of the same importance as the radiation effect [Hal90], [LM00a], [LM00b].

4. Experiments [LM00a], [LM00b] suggest that DNA strand breaks may be due to radiation action as well as to non-radiation action. The non-radiation action may be due to the highly charged daughter ion $^{125m}$Te. Is it possible to apply a charge transfer theory [MS85], [BJ99] to the highly dynamic neutralization effect of $^{125m}$Te?

5. A highly charged daughter ion $^{125m}$Te represents a high ionization potential energy, and may transfer a part of the energy to neighboring bases. What is the mechanism or the pathway in which these energy induces DNA strand breaks?

The present work is originally designed to investigate and to test working-hypotheses on the causes of the DNA strand breaks induced by $^{125}$I incorporated into a CAP-DNA complex. This is done by using the refined track structure calculation code PARTRAC (cf. Appendix A) with the crystallized spatial model of this complex. Preliminary calculated results [LFJ00] agreed well in shape of the curve with the experimental data [KZG$^+$99] on the strand in which an $^{125}$I atom is incorporated. However, there is an unexplained shift on the opposite strand. We realized that this kind of shift might arise from the neutralization effect or from the electron/charge/energy transfer, which is emphasized by Halpern [Hal90] and Fuciarelli [FSMZ94]. At the same time, Labochevsky and Martin [LM00a], [LM00b] published their new experimental data of DNA strand breaks induced by an $^{125}$I atom incorporated into a cytosine located in the middle of a 41-mer synthetic oligodeoxynucleotide and derived the contribution of neutralization component, which may be as high as 50% according to an estimate based on a simple model. Thus, we were stimulated to calculate the number of DNA strand breaks contributed from the radiation component, and to compare our simulation results with the experimentally

derived total DNA strand breaks. Our new simulation results are much lower than the experiment derived data around the $^{125}$I atom located site, whereas the strand breaks on the distant bases agree quite well. This implies that the mere comparison, e.g. between simulations and experiments [CH88], [NMC$^+$96], [NLT$^+$00], [NPT$^+$00] of the fragment size distribution, (i.e. the only quantity that can be measured in experiments) is inadequate, in part because the fragment size distribution has been normalized to be unity. During the course of this normalization, the neutralization effect will always be overlooked.

The first task of the present work is to assess the DNA strand break contribution from the neutralization effect by combining simulation results based on the refined biophysical model — the PARTRAC code (cf. Appendix A) and experimental data [LM00a], [LM00b]. The second task is to try to understand the underlying mechanism of the neutralization effect of the multiply positive charged daughter ion $^{125m}$Te from the point of view of the charge transfer theory.

In plasmid DNA, the experimental data agree well among themselves, but different authors [LS85], [PLPN01] gave different explanations for the DSBs which occurred up to 100 bp away from the decay site. Linz and Stöcklin [LS85] explained this phenomenon by energy transfer mechanism along the DNA, which is supported by investigators using other irradiation sources [vLWdHH86], [CMS90]. However, Panyutin et al. [PLPN01] believe that these DSBs could be contributed from the action of high-energy electrons produced by $^{125}$I decay. They could not distinguish between a molecule in which the decay actually occurred and nearby molecules that were hit by the high-energy Auger electrons, since they applied the Monte Carlo track structure simulations to a larger volumes encompassing the whole plasmid DNA. Thus, another task of the present work is to calculate the DNA strand breaks induced by an $^{125}$I atom incorporated in a plasmid DNA. We expect that comparison between simulation results and experimental data will give some clues for the electron transfer along the DNA chain.

In mammalian cellular DNA, the situation becomes even more complicated because of higher-order organization of DNA and of effects of protein. We simulated two cases of $^{125}$I: (1) incorporated into DNA thymine bases and (2) distributed homogeneously in cellular nuclei. Comparison with experimental data [WAK98b], [WAK98a], [WDAK00], [WAK01], [KWA00], [HLS00], [BRB$^+$94], [YHD01] should give some insights into radiation action mechanisms of $^{125}$I decay in mammalian cell nuclei.

# Chapter 2

# Simulation of I-125 Induced DNA Strand Breaks

## 2.1   Simulation of I-125 Decay

The decay of $^{125}$I occurs by electron capture (EC), which results in vacancies in the atomic subshells of the metastable daughter nucleus $^{125m}$Te. The metastable level of the $^{125m}$Te nucleus has an excitation energy of 35.4 keV. It will lose its excess energy by transition of 7% $\gamma$ emission and 93% internal conversion, and thus transmutes to the stable atom $^{125}$Te; this process is called isomeric transition (IT). The decay scheme of $^{125}$I is shown in Figure 2.1, which is based on data given by [ICR83]. The $Q_{EC}$ in the Figure 2.1 is the energy difference in the electron capture (EC) decay between the ground states of the parent nuclide, $^{125}_{53}$I, and the daughter nuclide, $^{125m}_{52}$Te, in the metastable state.

The spectra of Auger electrons and photons for individual $^{125}$I decays have been calculated by a Monte Carlo technique [CJ81], [PBC87], [BPPO87]. The primary hole leading to an excited state of the nucleus is created by electron capture mainly from the K-shell, at a relative frequency higher than 80% [LZ64], whereas other shells are affected only to a minor degree. For the de-excitation both radiative as well as Auger and Coster-Kronig transitions, and moreover, shake-off and double Auger processes have been considered. (The meanings of an Auger and a Coster-Kronig transitions, and other special terms are given in ref. [ICR83] and [PBC87].) Other processes were neglected here either due to very low intensities or in view of lacking data.

Starting from the primary vacancy, the first transition has been selected according to its probability by using random numbers for creating one X-ray photon or two new vacancies (Auger transition). By checking the energy conditions the code

EC-decay 100%        $\frac{5}{2}+$  $^{125}_{53}$I (59.4 d)                0.0 MeV

$Q_{\mathrm{EC}} = 0.1781$ MeV

Electron Capture

$\frac{3}{2}+$        $^{125m}_{52}$Te        $(1.6{\times}10^{-9}$ s)     0.0354 MeV

93% Internal Conversion

$\gamma_1$

7% $\gamma$-Emission

$\frac{1}{2}+$      $^{125}_{52}$Te (stable)                 0.0 MeV
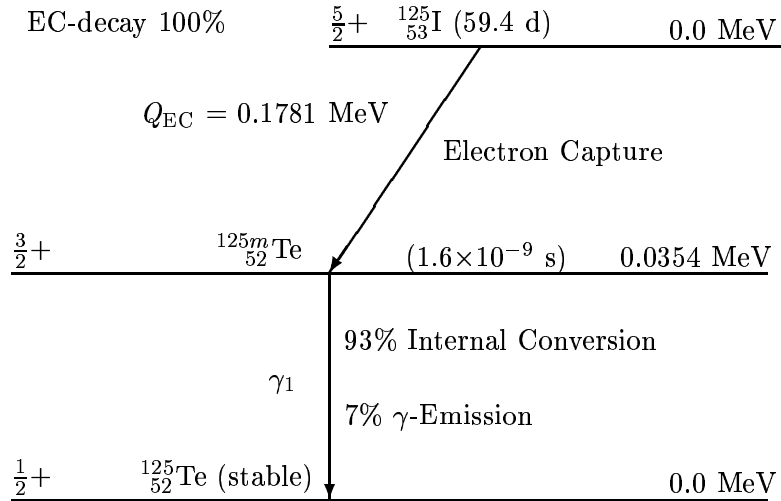
Figure 2.1: Decay scheme of $^{125}I$

allows or refuses the transition. If a selected transition is energetically not possible, it is canceled from the list of transitions and another one is chosen. An energetically allowed transition is definitely accepted and the deepest lying vacancy is the new starting point for the next transition. In this way, a whole cascade of transitions is followed until all positive charges are located in the outer shells which cannot be filled any longer by electrons from the same atom.

According to the decay mode of $^{125}I$ (Figure 2.1), the metastable state of $^{125m}$Te with a half life of $1.6{\times}10^{-9}$ s (it takes about $10^{-16}$ to $10^{-15}$ s for the complete cascade) is assumed to live sufficiently long to allow a complete neutralization of the charge by electrons from surroundings. This state decays in about 93% of all cases by internal conversion, which again creates a hole in an inner shell resulting in a second Auger cascade. Because probabilities for transitions in multiply ionized atoms are not available, the probabilities for singly ionized atoms have been used and modified by a factor accounting the number of electrons available for a certain transition. To determine the energies of the emitted Auger electrons or X-rays, the total energies of the atom before and after the transition are calculated and the difference between the two is equal to the energy released. For references of the used probabilities for electron capture, internal conversion, radiative and radiationless transitions see Pomplun et al. [PBC87]. Another way of simulation of $^{125}I$ decays can be found in [CJ81], [BPPO87].

Results on spectra of Auger electrons and photons for individual $^{125}I$ decays,

| Radiation | $y(i)$ (Bq-s)$^{-1}$ | $E(i)$ (MeV) | $y(i) \times E(i)$ |
|---|---|---|---|
| $\gamma_1$ | 6.860E-02 | 3.548E-02 | 2.434E-03 |
| ce-K, $\gamma_1$ | 8.000E-01 | 3.643E-03 | 2.914E-03 |
| ce-L$_1$, $\gamma_1$ | 9.440E-02 | 3.052E-02 | 2.881E-03 |
| ce-L$_2$, $\gamma_1$ | 9.500E-03 | 3.084E-02 | 2.930E-04 |
| ce-L$_3$, $\gamma_1$ | 1.900E-03 | 3.112E-02 | 5.913E-05 |
| ce-M$_1$, $\gamma_1$ | 1.700E-02 | 3.445E-02 | 5.857E-04 |
| ce-M$_2$, $\gamma_1$ | 2.800E-03 | 3.459E-02 | 9.685E-05 |
| ce-M$_3$, $\gamma_1$ | 1.000E-03 | 3.464E-02 | 3.464E-05 |
| ce-N$_1$, $\gamma_1$ | 4.000E-03 | 3.529E-02 | 1.412E-04 |
| ce-N$_2$, $\gamma_1$ | 8.000E-04 | 3.534E-02 | 2.827E-05 |
| K$_{\alpha_1}$ X-ray | 7.587E-01 | 2.746E-02 | 2.083E-02 |
| K$_{\alpha_2}$ X-ray | 4.060E-01 | 2.722E-02 | 1.105E-02 |
| K$_{\beta_1}$ X-ray | 1.345E-01 | 3.099E-02 | 4.168E-03 |
| K$_{\beta_2}$ X-ray | 3.710E-02 | 3.169E-02 | 1.176E-03 |
| K$_{\beta_3}$ X-ray | 6.900E-02 | 3.093E-02 | 2.135E-03 |
| K$_{\beta_5}$ X-ray | 1.300E-03 | 3.124E-02 | 4.061E-05 |
| L   X-ray | 1.396E-01 | 3.938E-03 | 5.497E-04 |
| Auger-KLL | 1.327E-01 | 2.248E-02 | 2.983E-03 |
| Auger-KLX | 5.700E-02 | 2.639E-02 | 1.504E-03 |
| Auger-KXY | 6.300E-03 | 3.022E-02 | 1.904E-04 |
| C-K LLX | 2.626E-01 | 2.805E-04 | 7.365E-05 |
| Auger-LMM | 1.252E 00 | 3.018E-03 | 3.779E-03 |
| Auger-LMX | 3.372E-01 | 3.656E-03 | 1.233E-03 |
| Auger-LXY | 2.140E-02 | 4.292E-03 | 9.186E-05 |
| C-K MMX | 1.449E 00 | 9.071E-05 | 1.315E-04 |
| Auger-MXY | 3.315E 00 | 3.768E-04 | 1.249E-03 |
| Auger-NXY | 3.439E 00 | 3.263E-05 | 1.122E-04 |

| | |
|---|---|
| Average electron energy (MeV) | 1.839E-02 |
| Average photon energy (MeV) | 4.239E-02 |
| Average potential energy (MeV) | 1.083E-03 |
| Average number of electrons | 13.36 |
| Average number of shake-off electrons | 2.15 |
| Average number of photons | 1.61 |
| Average charge per decay | 14.36 |
| Average energy per decay (MeV) | 6.186E-02 |

Table 2.1: Yields and energies of emissions in the $^{125}$I decay. For the meanings of the designations, see text

simulated by Monte Carlo technique described above, have been used in the present study. Yields and energies of emissions in the $^{125}$I decay are listed in Table 2.1, which has been taken from Pomplun et al. [PBC87]. Designations in the Table 2.1 are explained as follows: $y(i)$ is the yield of the emission of kind $i$, the unit, $(Bq\text{-}s)^{-1}$, is equivalent to that of per transformation; $E(i)$ is the energy of the emission of kind $i$; $y(i) \times E(i)$ is the average energy of the emission of kind $i$; $\gamma_1$ is the isomeric transition of $^{125m}$Te; ce-K, $\gamma_1$ is the internal conversion electron from the K-shell associated with the $\gamma_1$-ray; $K_{\alpha_1}$ X-ray is the characteristic X-ray emitted when an electron makes a transition from the subshell $L_3$ of the major L-shell to the K-shell; $K_{\beta_1}$ and $K_{\beta_2}$ X-rays are the characteristic X-rays emitted when electrons make transitions from the subshells $M_5$ and $M_4$ of the major M-shell to the K-shell respectively; L X-ray is characteristic X-ray emitted when an electron makes a transition from any shells beyond the L-shell to the L-shell; Auger-KLL is an Auger electron emission from the L-shell when a vacancy occurs in the K-shell and an orbital electron from L-shell fills the vacancy and transfers the energy directly to the emitted Auger electron; the designations of X and Y in Auger-KLX and Auger-KXY mean any shells higher than the L-shell for K series Auger transitions; Auger-LXY is L series Auger transitions; C-K LLX is a Coster-Kronig transition, a special type of the Auger transition involving transitions between subshells of the same major shell.

Some characteristics of the individual electron spectra used in the present study are shown in Figure 2.2, based on data given by Pomplun et al. [PBC87]. From Figure 2.2a one can get an idea of the number of electrons with various energies released per decay; Figure 2.2b gives the probabilities of the total electron energies released per decay.

## 2.2 Geometric Structures of DNA Models

According to the goals and concepts of the present work, five structures of DNA models in different scale of base pairs, i.e. a 12-mer free B-DNA, a 30-base pair DNA-protein complex, a 41-mer synthetic oligodeoxynucleotide, a pUC19 plasmid DNA in length of 2700 base pairs and a higher-oder organization of DNA in mammalian cells were developed and used in the PARTRAC code.

### 2.2.1 CAP-DNA Complex and Free B-DNA

The catabolite gene activator protein (CAP) or cAMP receptor protein (CRP) of the CAP-DNA complex is a dimer of two identical subunits, each of which is 209 amino acids in length and contains a helix-turn-helix DNA binding motif (Figure 2.3) [VV95]. CAP complexed with a specific 30-base pair DNA sequence shows that the
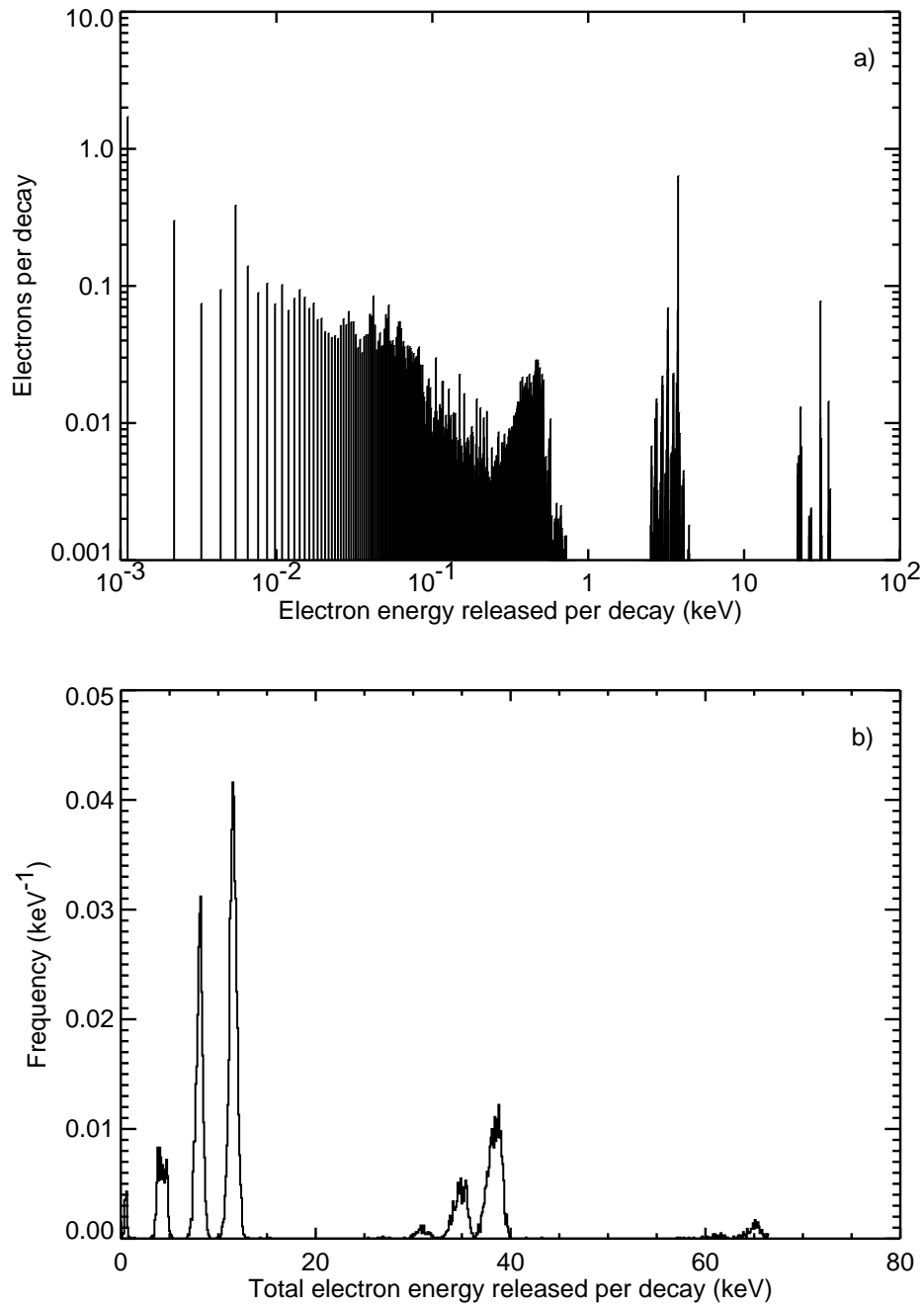
Figure 2.2: Average electron spectra (a) and the frequency of total electron energy released (b) in the simulated $^{125}$I decays

DNA is bent by 90° [PWG$^+$96], [SSS91], [SSS90]. The structure data set of the CAP-DNA complex was obtained from the Protein Data Bank (PDB) [BWF$^+$00]; its PDB ID entry number is 1GCP. In the PDB CAP-DNA data set, all the H-atoms in sugars of the nucleoside and some H-atoms in the 4 bases are missing and there are two single-phosphate gaps [PWG$^+$96] between bases T(2)G(3) in the "top" strand and between bases G(-3)T(-2) in the "bottom" strand (Figure 2.3). Before the PDB CAP-DNA data were used in our simulation, all the H-atoms were added and the two phosphate gaps were also filled using an algorithm described in Appendix B.

The naked free B-DNA model is a 12-base pair piece of DNA with so called intrinsic or preexisting twisting and bent in the DNA duplex [GZO95]. Figure 2.4 shows this kind of the free B-DNA with the $^{125}$I atom incorporation into the position of atom $C_9$, i.e. the $^{125}$I atom substitutes the methyl group $CH_3$ and bonds to $C_5$ atom in one thymine, which was used as a control example for the bent CAP-DNA in the experiment [KZG$^+$99]. This was designed to test whether the Auger emitter $^{125}$I atom could play the role of a radioprobe for the bent CAP-DNA like other chemical and biological assays.

### 2.2.2 Synthetic Oligodeoxynucleotide

The 41-mer synthetic oligodeoxynucleotide, containing the $^{125}$I atom which replaced the $C_5$ atom of the middle cytosine base, was used as a conventional system for investigation of $^{125}$I decays induced DNA strand breakage in previous experiments [KLDM96], [LM96] and in simulation calculations [NMC$^+$96]. Recently, experiments [LM00a] were performed by labeling $^{32}$P at the 3′ and 5′-ends on both stands of this model and incubating in 20 m$M$ sodium phosphate buffer (PB) and PB plus DMSO (Dimethyl sulphoxide) (Figure 2.4). After 18 $\sim$ 20 decays incubation, samples were analyzed on a denaturing DNA sequencing gel, 8 measured data sets, i.e. fragments size distribution from the $^{32}$P-labeled end were obtained for the "top" strand: (1) 5′-end $^{32}$P-labeled in PB, (2) 5′-end in PB+DMSO, (3) 3′-end in PB, (4) 5′-end in PB+DMSO and the "bottom" strand: (5) 5′-end $^{32}$P-labeled in PB, (6) 5′-end in PB+DMSO, (7) 3′-end in PB, (8) 5′-end in PB+DMSO (Figure 2.4). From these 8 systematic data sets, total DNA strand breaks and the non-radiation induced DNA strand breaks on both strands were derived with the assumption that the induction probability for DNA strand breaks induced by radiation declines as an inverse square of the distance from the decay point to a sensitive target [LM00b].

### 2.2.3 Plasmid DNA

DNA strand breakage was detectable up to 70 Å, which is equivalent to about 20 base pairs, from the $^{125}$I decay site by using a 59 and an 121 bp DNA double

Numbering    -15 -14 -13 -12 -11 -10 -9 -8 -7 -6 -5 -4 -3 -2 -1 1 2 3 4 5 6 7 8 9 10 11 12 13 14 15 16

Bottom   $3'$ $^{32}$P-   G C T T T T C A C A C T G T A T A C A G T G T G A A A A G C G $5'$

Top   $5'$ $^{32}$P- G C G A A A A G T G T G A C A T A T G T C A C* A C T T T T C G   $3'$
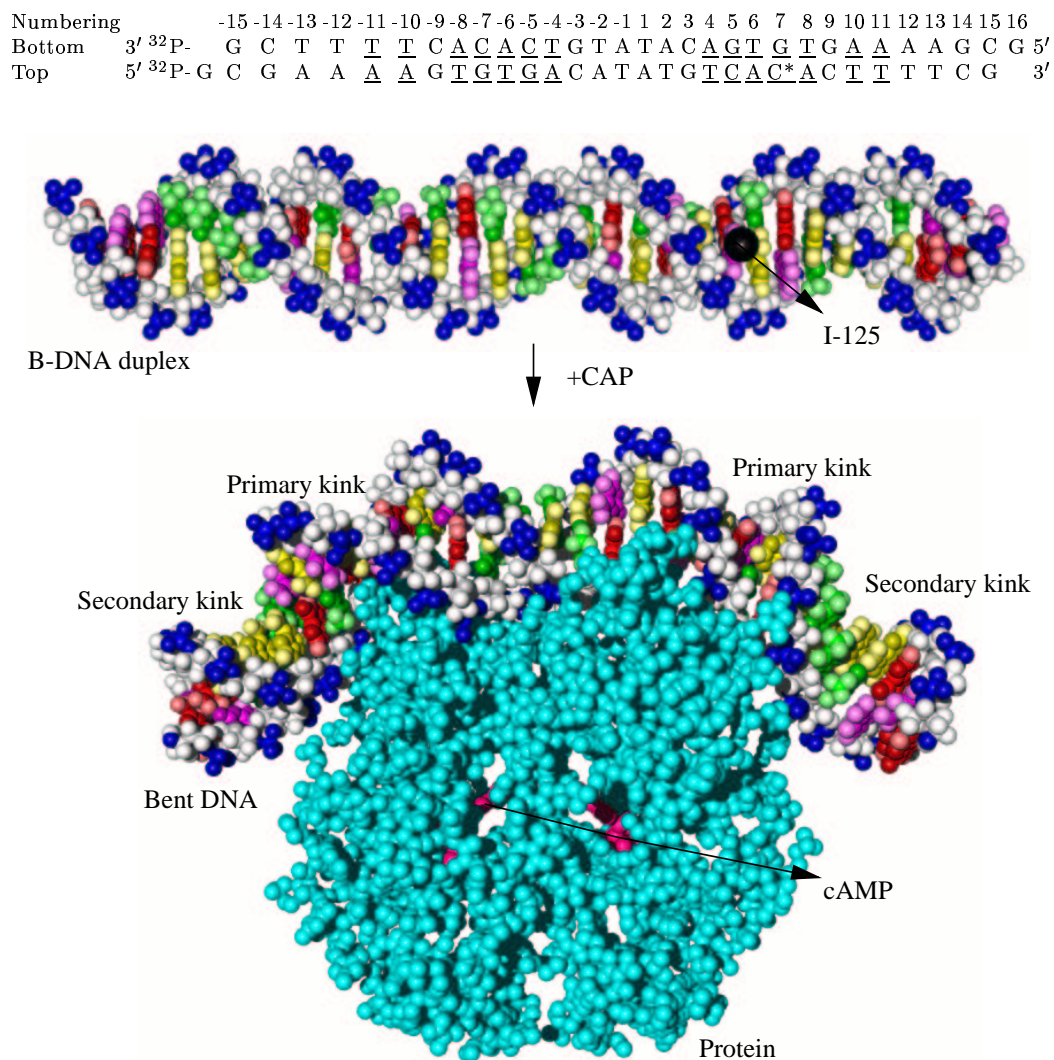


Figure 2.3: CAP-DNA complex. The numbering of base pairs is according to Schultz et al. [SSS91]. The bases are shown in colors (AGCT). The iodine atom $^{125}$I is shown in black (at the $H_5$ position of cytosine 7, i.e. C*). The $^{125}$I atom in the bent DNA is hidden by other atoms. The protein is presented in cyan and the cAMP is shown in orange red. The white and the blue atoms are the sugar-phosphate backbone of the DNA duplex. The strand, in which the $^{125}$I atom is located, is called the "top" strand and the opposite the "bottom" strand. The underlined nucleotides are connected with the protein (all the color pictures of the DNA models in this dissertation are visualized by using Persistence of Vision$^{TM}$ Raytracer (POV-Ray$^{TM}$) freeware.)

Top     5′- C C T C T T C A A G A A T T C T C A C T Cⁱ G G C T C C G G T A A G C A T C T A G C 3′
Bottom 3′- G G A G A A G T T C T T A A G A G T G A G   C C G A G G C C A T T C G T A G A T C G 5′

Incubation in (1) PB and (2) PB+DMSO

Symbols used: $\star - {}^{32}P$, $\text{i} - {}^{125}I$, $C^{i} - {}^{125}I$ incorporated cytosine
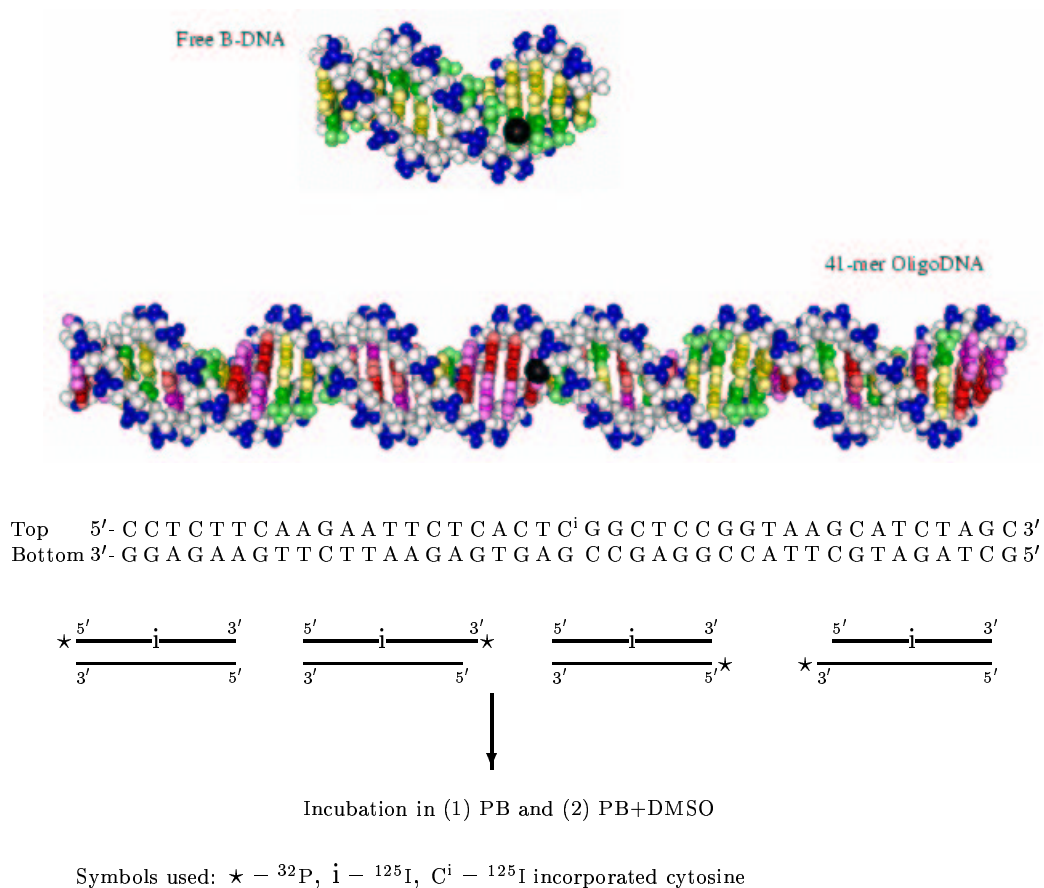
Figure 2.4: A free B-DNA and a 41-mer synthetic oligoDNA (upper part). The black ball denotes the $^{125}I$ atom. The colors of the atoms are the same as in Figure 2.3. The sequence of the 41-mer synthetic oligoDNA is listed in the middle, its spatial atomic co-ordinates are generated by the Biosym modules `Insight` and `Biopolymer`. The free B-DNA is comprised by only adenine (A) and thymine (T). The outline of experimental procedures used to synthesize four possible combinations of the $^{32}P$ and labeling of the $^{125}I$-dC containing oligoDNA (lower part)
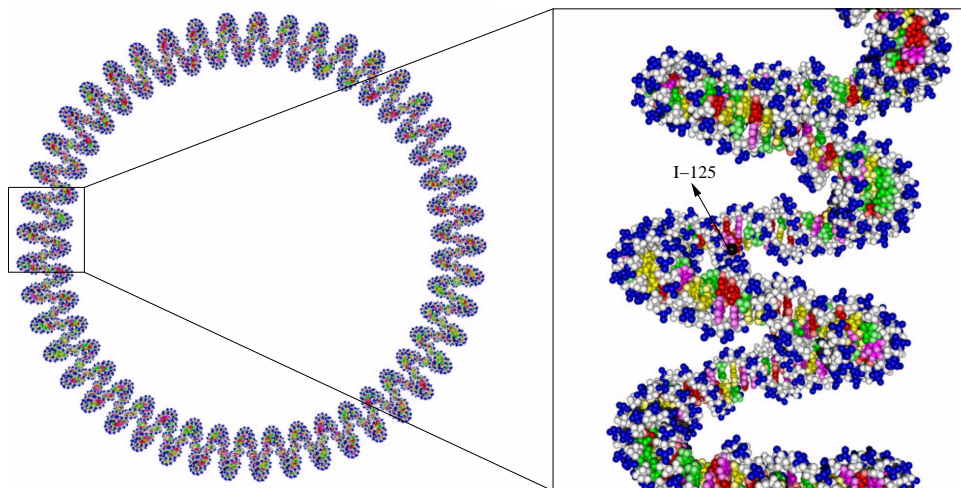
Figure 2.5: A pUC19 plasmid DNA model. The black ball denotes the location of the $^{125}$I atom

strand fragments with $^{125}$I-dC containing at known position [MH81]. Experiments with long bp plasmid DNA pBR322 [LS85] and pUC19 [PLPN01] demonstrated that DSBs may also occur as far as hundreds of base pairs apart from the $^{125}$I site which were explained to be due to transport of excitation energy via the $\pi$-electrons systems by the former investigator and by radiation action by the latter one. From the physical tracks of $^{125}$I decays presented in Figure 3.1, one can see that the ionization and excitation events densely occurred up to 200 Å apart from the $^{125}$I atom and even extend up to 2000 Å away. These events and the chemical radicals produced by those events can also interact with and attack DNA molecules, giving rise to many strand breaks. In the present work a simple geometrical model of plasmid pUC19 DNA was set up using parameters suggested by Vologodskii et al. [VLK$^+$92] and Saenger [Sae84] to test, from the point of view of the radiation track structure theory, whether the portion of DNA strand breaks produced by those tracks are comparable to that measured in experiments and, further on, to give some hints for the understanding of the long distance damage to DNA by $^{125}$I decays. In the simulation the sequence of the plasmid pUC19 [YPVM85] was used instead of a random sequence to text the finding of predominant damage in the thymine-rich areas [LS85]. The geometry of the model is shown in Figure 2.5.
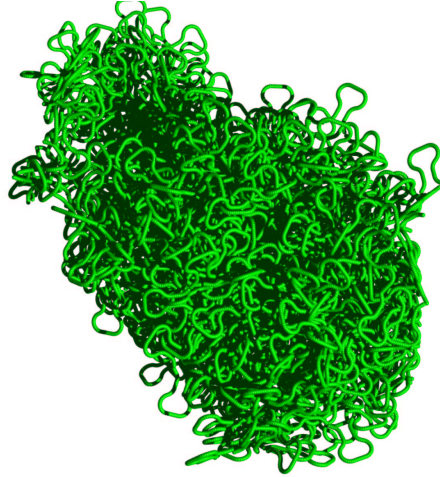
Figure 2.6: The chromosome geometry used to model the DNA organization in human cellular nuclei

### 2.2.4 Mammalian Cellular DNA

The higher toxicity of DNA-incorporated $^{125}I$ atoms in mammalian cellular nuclei was reported by many experimental investigators [LL84], [LHBL96], [WDAK00], [WAK01], [WAK98b], [WAK98a], [YHD01], [KWA00], [HLS00], [BRB+94]. With the higher-oder organization model of DNA in mammalian cellular nuclei [FJPS98] the DNA strand breaks and the fragment distribution were modeled in a larger scale. The model [FJP+99] used in our simulation is plotted in Figure 2.6 for reference, the $^{125}I$ atoms are asummed to be located at cytosines.

## 2.3 Modeling of I-125 Radiation Action on DNA

Regardless of the special chemical toxicity of the DNA-incorporated $^{125}I$ atom, it is without exception primarily a radioactive isotope. After EC decay, it releases about 21 Auger electrons with lower energy, mostly $\leq 1$ keV and photons with a main energy of 27.4 keV. Photons transfer a large fraction of their energy to many other electrons via inelastic and elastic interactions. These energetic electrons ionize and excite DNA and water molecules and deposit their energy. The residual electrons with energies lower than, say 10 eV, will lose their energy mostly by excitation of rotational, translational and vibrational modes of molecules. In addition, the

chemical new products, e.g. $^\bullet$OH and H$^\bullet$ radicals, produced by radiation interaction with water molecules, will also contribute to DNA damage via subsequent chemical reactions.

In the present study, the PARTRAC code (cf. Appendix A) was used to model the $^{125}$I atom interaction with DNA molecules in solution. The PARTRAC code is a self-consistent biophysical simulation code which models not only radiation interactions in liquid water of the earlier physical and later chemical processes but also provides a complete DNA geometric model from an atomic to a cellular nuclear level. It provides also a module which analyzes the initial interactions leading to a biological endpoint.

In the two following subsections, physical and chemical initial interaction mechanisms between radiation and DNA molecule and environments, e.g. water molecules will be introduced in detail; for the modeling and computational techniques, one can reference Appendix A. The mechanism and modeling of the neutralization effect will be discussed in Section 2.4.

### 2.3.1  Physical Action Mechanisms

According to the radiation interaction time scale listed in Table A.1, the physical processes of radiation interaction with matter complete at $10^{-15}$ s. Radiation interacts with matter in different processes due to its intrinsic quality, and the probabilities of interaction processes are expressed as cross sections (for introduction see ref. [Par87], [DHIP98]). For the simulation of physical action on DNA and its environment, the physical track structures of radiation, i.e. the spatial distributions of interaction events, e.g. ionizations and excitations are needed. In biological tissues, liquid water is the dominant component.

Electrons and photons released in individual decays of $^{125}$I atom were evaluated by Pomplun [PBC87]. Such spectra were read in by the PARTRAC code to generate tracks in the model substance — liquid water. DNA molecules in their geometry, which are considered as liquid water regarding their cross sections (since non DNA cross sections are available yet and the differences are expected to be small), was configured into the space where the tracks were produced by keeping the position of the DNA-incorporated $^{125}$I atom in the origin. With the superposition of the radiation track structures and the DNA geometrical structures, the coordinates of these two structures were analyzed with an assumption that a hit occurred when an event is found inside the van der Waals radii of atoms of the DNA molecules. The hit means that an event, e.g. ionization or excitation happens and deposits its energy inside DNA molecular atoms.

Where the energy deposits in the DNA molecule is important for leading to damages of DNA. A DNA molecule is a macromolecular chain which is constructed

by repeated motif — nucleotides. It is composed of a cyclic, furanoside-type sugar which is phosphorylated in the 5′ position and substituted at $C_{1'}$ by one of four different heterocycles attached by a $\beta$-glycosyl $C_{1'}$-N linkage. The heterocycles are purine bases adenine (Ade) and guanine (Gua) and the pyrimidine cytosine (Cyt), thymine (Thy) and uracil (Ura) which is only found in ribonucleic acid (RNA). The four bases (Ade, Gua, Cyt and Thy) and sugar compose the four nucleosides: adenosine (dAdo or dA), guanine (dGuo or dG), cytidine (dCyd or dC), thymine (dThd or dT), and the four nucleotides are denoted as 5′-dTMP or pdT, 5′-dCMP or pdC, 5′-dAMP or pdA and 5′-dGMP or pdG (for DNA and RNA see text books by Saenger [Sae84] and by Voet and Voet [VV95]). In literature as a convention, nucleotide bases and abbreviations, A, G, T and C are used to stand for the heterocycles, i.e. bases. The knowledge of the detailed structure of DNA molecule is essential for modeling its radiation damage especially for the simulation of radiolysis interaction which will be dealt with in the next section.

Hits or energy depositions inside atoms from different constituents of DNA molecules introduced above can break valence bonds of atoms and further destroy the intrinsic structures of the DNA molecules. This action was called direct action or direct hit of radiation in biological tissues. The direct radiation action is just a model which was abstracted from physical knowledge of radiation transport in matter and the experimental observations.

## 2.3.2   Chemical Action Mechanisms

Experiments concluded that DNA is heavily hydrated. Not only plays the aqueous solvent a central role in conserving the architecture of DNA molecule, these inhomogeneous hydration shells are also involved in the formation of hydration forces and play a role in folding and recognition events. As radiation penetrating the DNA molecule and its environment, e.g. the hydration water molecule, the active radicals produced by radiation in water will react with the radicals and enzymes produced by normal metabolism and further produce many products in the time scale $10^{-15}$ $\sim 10^{-12}$ s, which is called the physicochemical stage (cf. Appendix A.3). These initial radiolytic species will diffuse and react among themselves or attack the atoms of DNA molecules in the time scale which extends from $10^{-12}$ to $10^{-6}$ s; this is regarded as the chemical stage in modeling.

The hydration is described in terms of two discrete layers representing primary and secondary hydration shells. Generally, in the primary shell, there are at least 11 to 12 water molecules per nucleotide, hydration of the DNA bases is local. In the hydration of phosphate 5 to 6 water molecules are concentrated in six hydration sites per phosphate, and the positions and occupancies of these sites are dependent on the conformation and type of nucleotide. With 80% relative humidity, the DNA

double helix is completed with about 20 water molecules per nucleotide, which are not all in direct contact with DNA: $8 \sim 9$ of them are bonded to $11 \sim 12$ other water molecules in the inner primary hydration shell. The second, outer hydration shell is indistinguishable from bulk water. New investigations on this subject give even more detailed information [SPB98], [AW00].

A precise knowledge of the shape of the primary hydration shell at the nucleotide and base-pair level is required for the positions of the initially produced radiolysis produced at $10^{-15}$ s around DNA molecules. These radicals have a relative short life and will re-organize within $10^{-12}$ s. When ionized or electronically excited molecules undergo a dissociation process, the resulting kinetic energy is shared by the moving fragments which may also be electronically and/or vibrationally excited. Those fragments thermalize a few angstroms from each other, the distance is a function of the available energy and of the fragment mass. The channels through which the excited water molecules decay and the branching ratios associated with each of them, remain still largely unknown for liquid water. But the yield of directly excited molecules is relatively small and, in turn, has only limited consequences. The reorganization of excited electronic states of water molecule, electrons, positive and negative ions is dealt with in our simulation listed in Table A.2. For a detail description of the physicochemical stage simulation see Appendix A.3 and ref. [BBM$^+$00], [CFP$^+$98].

The species present at the end the physical and physicochemical stages are distributed in a highly nonhomogenous track structure which is the starting point for the so-called chemical stage which extends from $10^{-12}$ s up to $10^{-6}$ s. In these stage, the various species diffuse and react among themselves, or they can attack constituent parts of DNA molecules. To model the chemical stage, the diffusion coefficient of each species and the reaction rate constants between each species with the different DNA molecule constituents introduced in above section are needed. Two main modeling approaches for chemical reactions, i.e. the independent reaction time (IRT) technique [FGF$^+$98] and the step-by-step technique [TMW$^+$83] are accepted and were improved as stochastic models of diffusion and interaction of chemical species.

The IRT model is based on the assumption that the distribution of species can be modeled as independent reactant pairs. It is important to account for three phenomena for adoption of the IRT model: (1) the fact that most of the reactions involved in the chemical stage are partially diffusion-controlled, (2) effects related to the spin statistics of some of the radicals, and (3) pseudo-first-order reactions that involve various species that are distributed homogeneously in the medium. This model makes no provision to account for the systematic spatial correlations that exist between the radiolytic species left in a track. Following this approach, the competition between the different possible reactions can be described via a sorting

of the stochastically sampled reaction times of each pair. Its application is divided into two principal steps: the sampling of the reaction time of the species and the realization of selected reactions.

The step-by-step simulation applied in this nonhomogenous chemical stage describes the Brownian dynamics of each species through a sampling of their random diffusive steps and accounts for the Coulombic force influencing the trajectory of charged species. This model follows the diffusion of each individual species within time steps of the order of picoseconds, the position of all the species are known after each reaction time step and their encounters can be determined. Compared to the computionally fast IRT model, this model is very time-consuming. But with this technique, one can keep control of the spatial distribution of all radicals at all times, which is needed for modeling the interactions between radiation induced chemical species and the atomic structure of target DNA molecules in solution during the chemical stage.

During diffusions and reactions among themselves, radiolysis products can attack atoms of DNA in different moieties, e.g. base, sugar and phosphodieaster bond and lead to oxidation of bases and sugars, breakage of the backbone of the DNA chain. In which position the attack is easier to occur in the whole DNA molecule is still a complicated open problem. In the double helix DNA molecule, the base is wrapped inside and the sugar is outside the double helix. This implies that damage to sugar is the key action for double helix DNA. Experiments showed that the $^{\bullet}OH$ and $H^{\bullet}$ radicals and solvated electrons, $e_{aq}^{-}$, are the main chemical species which attack DNA molecules.

In the following damage to DNA from radical attack will be introduced in the base, sugar and phosphate [GV91]. For convenient discussion, the four nucleotide bases are listed in Figure 2.7.

**Base damage**: The $^{\bullet}OH$ and $H^{\bullet}$ radicals react with pyrimidine and purine via additive reaction (90% for $^{\bullet}OH$) and protonation reaction (10% for $^{\bullet}OH$, 3% for $H^{\bullet}$). Due to electrophilic nature the $^{\bullet}OH$ and $H^{\bullet}$ radicals preferentially attack the site of the highest electron density, e.g. first $C_5$ and next $C_6$ in thymine; among the four oxidation products in purine: $dA(2\text{-}OH)^{\bullet}$, $dA(4\text{-}OH)^{\bullet}$, $dA(5\text{-}OH)^{\bullet}$, $dA(8\text{-}OH)^{\bullet}$. The $dA(8\text{-}OH)^{\bullet}$ is more important due to its further oxidation under oxygen condition to 8-hydroxyadenosine, a hidden mutation which is not easy to be repaired. $e_{aq}^{-}$ reacts with bases mainly via additive reaction and produce charged free base radicals. Normally electron adducts to $C_4$ in pyrimidine and to $C_2$ and $C_8$ in purine. These electron adducts can be rearranged in their molecular structure via protonation reaction and further form different oxides. Due to the difference of the electron affinity of the four base (T>C>A>G), when one base is adducted by electron, the electron will transfer to the nearest base if its electron affinity is larger than that of
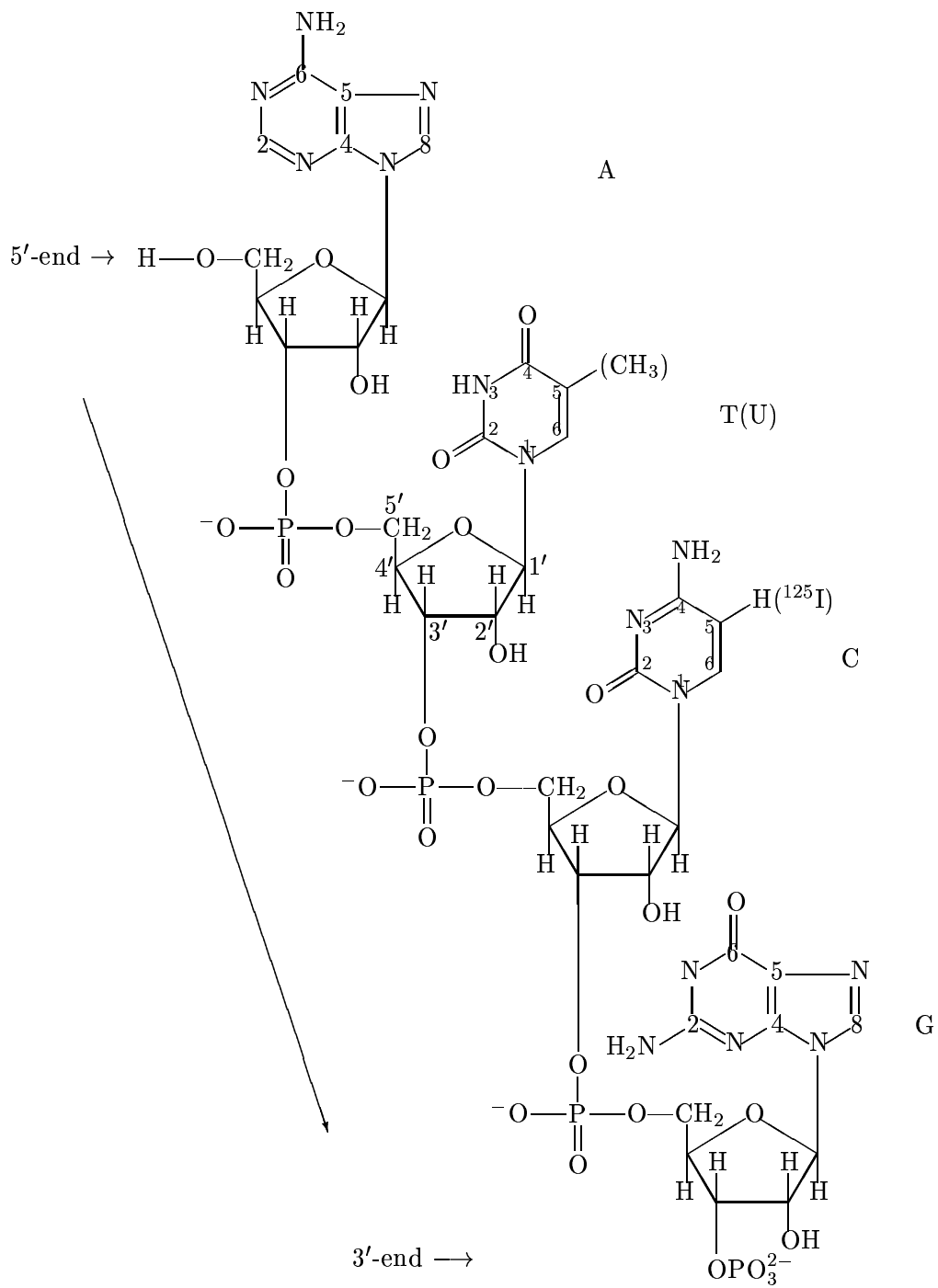
Figure 2.7: Nucleotide bases 5′–dApdTpdCpdG–3′

the nearest one. That is the reason why the base G is more easier damaged by $e_{aq}^-$.

**Sugar damage**: Sugar is the key moiety in the backbone chain structure of the DNA molecule. It connects with base and phosphate groups and forms the four bases via the connection hydroxyl and phosphate of the 5' and 3' C atoms to the DNA chain structure. The lesion of the sugar group is the precursor of deletion of undamaged base from the nucleic acid and strand breakage. Other than $^\bullet$OH, H$^\bullet$ and $e_{aq}^-$ do not react directly with sugar group. Attacks to the sugar moiety come more from the transfer of the base radicals (formed by $^\bullet$OH and H$^\bullet$ addition to the base moiety) to the 4' or 2' site in the sugar group. In another words, the lesion of sugar is the result of the base lesion. Sugar radicals is not stable and can release phosphate in a short time, and further release bases undergoing H-abstraction and hydrolysis reactions and form different oxidized products.

**Phosphate damage**: Damage of the phosphate group is mainly from the direct energy deposition. Phosphate absorbs radiation energy and changes to radical $(RO)_2P(O)O^\bullet$ and releases $e_{aq}^-$. This radical can oxidate the nearby base and protonate reaction on the site of 4' C atom in sugar groups which results in the release of phosphates and bases. This, in turn, will lead to strand breakage and base damage.

From the discussion above, it is obvious that the $^\bullet$OH radical is the main species attacking the DNA. In a cellular environment it can be scavenged with certain probabilities. In solution, scavenging depends on the density of DMSO and on the temperature. Due to experiments performed at $-70°$C [KZG$^+$99], in the simulation of CAP-DNA, free B-DNA damage, the effect of the protein on the transport of radiation induced radicals has been neglected. At this temperature, it is assumed that the radicals will not migrate which is equivalent to the case when all $^\bullet$OH radicals are scavenged. In the experiments [LM00a] of 41-mer synthetic oligoDNA irradiated by $^{125}$I in BP plus DMSO solution, DNA strand breaks were contributed only from physical tracks and from the neutralization effect. For the case of BP solution, breaks occur from chemical attacks in addition.

Fifty percent of the DNA strand breaks result from neutralization effect in DNA incorporated $^{125}$I decays [LM00b], although this is not so clear understood but many experimental attempts as well as theoretical. In the next section, an endeavor is made to evaluate the component of neutralization from combination of experiments and simulation and a theoretical calculation is performed. We also try to elucidate the mechanisms of charge transfer in DNA chain induced by decays of this special radioisotope $^{125}$I.

## 2.4    Modeling of Neutralization Effect on DNA

### 2.4.1    Process Description

The $^{125}$I atom is assumed in the following to be incorporated into a cytosine in a synthetic oligodeoxynucleotide in solution.

### I-125 Decay

$^{125}$I decay has been already discussed in detail in Section 2.1. Here, only a short summary is given and the description is focused on points relevant to the neutralization effect. $^{125}$I decays via electron capture. It decays in two steps: first, the nucleus $^{125}$I captures an electron from inner shells and decays to $^{125m}$Te (excited). This hole will be filled up by electron from an outer shells, mostly by kicking out another electron (Auger process). Until $^{125m}$Te is relaxed at time scales $10^{-16} \sim 10^{-15}$ s, about 10 electrons will be emitted into the environment (DNA + water). This is called the first Auger cascade. After $10^{-9}$ s, $^{125m}$Te will release its excited energy by $\gamma$-ray emission (7%) or internal conversion (93%) which again creates the second Auger cascade and decays to $^{125}$Te (stable). In the two Auger cascades, about 21 electrons will be emitted, and $^{125m}$Te will be highly positive charged. It is possible that the *charge transfer* is fast enough to neutralize the $^{125m}$Te during its Auger relaxation, and that the charge will not be accumulated on $^{125m}$Te as high as 10 if it is assumed that each cascade will emit about 10 electrons [Sas92], [Pom02].

Due to the short time of transmutation in the first Auger electron cascade, compared to the vibration time of a molecule, i.e. $10^{-14} \sim 10^{-13}$ s, the atoms in the molecule remain in their relative equilibrium positions. The atom $^{125m}$Te remains in a multiply ionized state, the ionization energy on the atom is equal to the total ionization potential $\eta_n$:

$$\eta_n = \sum_{i=1}^{n} P_i. \tag{2.1}$$

The positive charges, $n$, on the atom will be neutralized by electrons from intramolecular and intermolecular charge transfer, and the decreased potential energy of ionization is used for the emission of further electrons [PBC87], [BPPO87].

### Distance between Te-125m and C$_5$ Atom in Cytosine

The distance between $^{125m}$Te and C$_5$ atom in thymine is the key to understand the consequence of the charge increase for the bond. By performing *Gaussian98* calculations [FTS$^+$98] on $^{125}$I-incorporated cytosine in the present study, the distance increases from 2.056 Å (zero charge) to 1.979 Å (+1 charges) resp. 2.014 Å (+2 charges). For +3 charges, the program cannot find a stable geometry. Pomplun

[Pom00] calculated the distances as 2.07 Å (zero charge) resp. 4.68 Å (+6 charges) by the program `HyperChem`. From this *ab initio* calculations, it implies that during the first cascade, the bond between $^{125m}$Te and $C_5$ will already be broken, $^{125m}$Te perhaps can move away from the original located position. It was also found in experiments [RHS88], [Hal90] that the $^{125m}$Te bond does not survive at ordinary temperature (77K or 295 K) and time scale ($10^{-9}$ s), however, the $^{125m}$Te$^{n+}$ ion probably remains in the close neighborhood of the original $^{125}$I decay site.

**The Fate of the $^{125}$I-incorporated Molecule**

The charge developed in the first Auger cascade redistributes fast ($10^{-15}$ s) over the whole molecule. The cytosine ring is initially positively charged. During the subsequent neutralization, by catching electrons from the solvent molecules, one would expect up to 100 eV of *electronic excitation energy* [Pla54] being deposited on this moiety. This energy leads to a *superexcited state* [Pla62]. A *superexcited state* is a neutral electronic state of a molecule lying at higher energies than the first ionization potential. A number of competing processes such as direct dissociation, autoionization, pre-dissociation, or other processes driven by excited-state interactions can follow this excitation to superexcitated states.

In conjugated molecules, $\pi$-electrons can undergo collective excitation and then the molecule loses its excess energy presumably through emission of a single electron, i.e. intramolecular energy transfer from a superexcited state to the surrounding $\pi$-electron molecules.

Deutzmann and Stöcklin [DS81] suggested a mechanism for the decay-induced fragmentation of uracil according to which the pyrimidine ring should be destroyed during charge neutralization following the first Auger cascade. Linz and Stöcklin [LS85] extended this mechanisms to cytosine (Figure 2.8).

Reiche et al. [RHS88] proposed another scheme:

$$\text{cytosine}^{125}\text{I} \longrightarrow \text{cytosine} \cdots ^{125}\text{Te}^{n+} \longrightarrow \begin{array}{l} \nearrow \text{fragmentation} \\ \searrow \text{cytosine}^{m+} + ^{125m}\text{Te}^{(n-m)+}, \end{array}$$
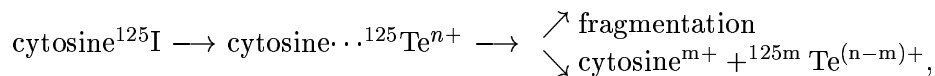
in $10^{-15}$ s, a redistribution of charges occurs which are dispersed to the extremities of the molecule: [cytosine$^{m+}$ + $^{125m}$Te$^{(n-m)+}$]. During the subsequent neutralization of cytosine$^{m+}$, several tens eV ($\sim$ 100 eV) of excitation energy is gained (in $10^{-15}$ up to $10^{-13}$ s) by this moiety which becomes superexcited. In condensed phase, the superexcited state releases energy by several competing pathways: to vibrationally or electronically excited cations or to neutral radicals. Multiply charged cations rapidly become singly charged in the condensed phase by charge transfer with neutral molecules because the second ionization potential is much higher than the first. For cytosine$^{m+}$, the aromatic moiety can escape fragmentation to a great

R = DNA strand
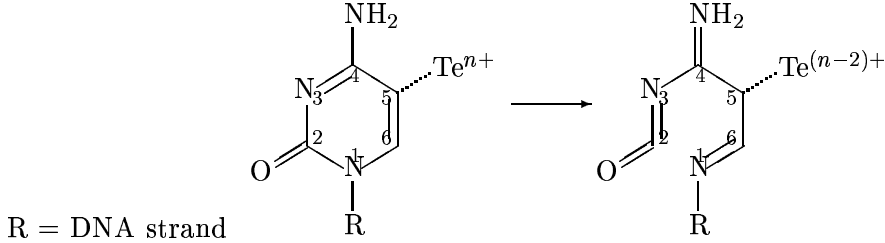
Figure 2.8: Charge transfer mechanism proposed by Deutzmann and Stöcklin: Due to better electron donor properties of the basic amino group at $C_4$, the charge transfer to Te ion should even be easier. $N_3$ may also accept a proton from the positively charged imino group. The Te ion will draw an electron from the neighboring cytosine ring rather than from the sugar via $\sigma$ bonding between $N_1$(base)–$C'_1$(sugar). Because of the overlapping of $\pi$-electrons of DNA bases, resulting positive charges could be distributed to several bases. Finally, the spatial distance between I atom to adjacent base (3.5 Å) is smaller than that between I atom to sugar ($> 5$ Å)

extent. The only explanation is the ability of cytosine$^{m+}$ molecule and adjacent bases surrounding the superexcited $^{125m}$Te$^{(n-m)+}$ atom serves as a energy acceptor, i.e. it takes away excess energy and channels it into collective excitation of their own $\pi$-electrons.

**Charge and Energy Transfer from Base to Base in DNA Chain**

The number of electrons released per $^{125}$I decay can be calculated [PBC87]. The average charge potential, $\eta_n$ is also available [BPPO87]. In addition we need the charge transfer rate within the molecule, i.e. from $^{125m}$Te$^{n+}$ to base cytosine ring, and also between molecules, i.e. from one base $\pi$-stack to the other base $\pi$-stacks. Due to the unpredictable position of $^{125m}$Te$^{n+}$ atom, it is assumed that the charge accumulated on this atom is equivalent to the case that the charge is located on aromatic ring of the cytosine base in which also the $^{125}$I is located. Charge transfer theory has been long introduced in one photon-induced reaction in chemistry and biology [Mar56], [MS85], [BJ99] and in the DNA chain [DB74]. Whether and/or which of these theories could be used for the ca. 10 charges neutralization process of $^{125m}$Te$^{n+}$ atom will be discussed below in Section 2.4.3.

**Energy Deposited in Base Leads to Sugar-phosphate Backbone Breaks – DNA Strand Breaks**

After having obtained the transfer rates from base to base (e.g. charge transfer rates calculated by Dee and Baur [DB74]) the energy transferred to the neighboring and distant bases in the strand can be evaluated. This can be done, e.g. using the program *Master Equation* [MK00] or the technique of "birth and death" process [DB74]. Then assumptions have to be made on the mechanism of how the energy deposited in a base leads to DNA breakage. It should be possible that the ionization potential energy deposited inside aromatic ring can ionize the water molecule and sugar moiety of the DNA molecules nearby. Symons et al. [Sym95] and Box et al. [BBD$^+$01] gave indications to this mechanism from the point of view of experiments how a base radical and an $^\bullet$OH radical lead to a strand break by $\beta$-elimination and electron transfer.

## 2.4.2 Evaluation from Experiment and Simulation

Before one can start to model the strand breaks induced by neutralization effect using charge transfer theory, it would be better to evaluate this component by combining simulated radiation component with experimental data available which include the neutralization component. Here the experiment of Lobachevsky and Martin [LM00a], [LM00b], and simulation data from the PARTRAC code can be used.

Some notations used in the following should be explained first: DNA strand break probability on the $i$th nucleotide site, $p_i$, is also expressed in literature as total DNA breaks frequency on the $i$th nucleotide site; DNA fragment size distribution from $^{32}$P-labeled end to the $i$th nucleotide site, $f_i$, i.e. first DNA breaks frequency for the $i$th nucleotide site. $f_i$ and $p_i$ denote the breaks on the $i$th nucleotide site contributed from radiation and nonradiaition components. *exp* or *sim* on the superscript of the $f_i$ and $p_i$ denote experimental and simulation data, respectively; *nr* or *r* on the subscript mean contribution from non-radiation and radiation components, respectively.

It is assumed that three components, i.e. radiation scavengeable, radiation non-scavengeable and non-radiation are independently contributed to the DNA strand breakage. In experiments, only the number of $^{32}$P dpm in fragments with the length of $i$ nucleotides, i.e. $N_i$ were measured using a Packard counter model 1900CA. The $f_i^{exp}$ can be calculated by $f_i^{exp} = N_i / \sum N_i$ with assumption that $\sum f_i^{exp} = 1$. This means that in the "top" strand after an $^{125}$I decay event there is at least one breakage somewhere between the $^{32}$P and $^{125}$I. In other words, the $^{125}$I-labeled site is always broken, i.e. $p_{125_I} = 1$. This assumption does not mean that there is no possibility that the $^{125}$I-labeled site is not broken. A lower limit for $p_{125_I}$ can be

calculated. It was found that the general conclusions are relatively insensitive to the value of $p_{125I}$ in the range from 0.85 to 1. From Section 2.2.2, it is known that there are 8 data sets for $N_i$, and 8 data sets for $f_i^{exp}$ will be obtained: 4 sets for the DNA strand in which the $^{125}$I is bound (called "top" strand), among them 2 sets for 5′-ends in PB+DMSO solution, 2 sets for 3′-ends in PB solution; 4 sets for the opposite strand (called "bottom" strand). The $p_i^{exp}$ can be calculated by Equation 2.2:

$$p_i^{exp} = \frac{f_i^{exp}}{1 - \sum_{j=1}^{i-1} f_j^{exp}}, \qquad i > 1, \tag{2.2}$$

with assumption $p_1^{exp} \approx f_1^{exp}$ due to $p_1^{exp} = f_1^{exp}/(1 - p_0^{exp})$ with $p_0^{exp} \ll 1$ ($\sim 10^{-2}$–$10^{-3}$ in experiment). There are 4 data sets for $p_i^{exp}$, 2 for the "top" strand in PB+DMSO solution and 2 for the "bottom" strand in PB solution. Data of $p_i^{exp}$ in PB+DMSO solution show the component (only physical tracks contribution without radicals attack) plus non-radiation component; data in PB solution show the contribution from direct physical interactions, from radicals attack as well as from non-radiation component. For evaluating the neutralization component, only data sets in PB+DMSO solution were used.

In the simulation calculation, the total breaks frequency without the non-radiation component, $p_{i,r}^{sim}$, i.e. the DNA strand breaks probability, was first obtained. The first break frequency, $f_{i,r}^{sim}$, i.e. fragment size distribution, can be calculated by using Equation 2.3:

$$f_{i,r}^{sim} = p_{i,r}^{sim}(1 - p_{i-1,r}^{sim})(1 - p_{i-2,r}^{sim}) \cdots (1 - p_{1,r}^{sim})(1 - p_{0,r}^{sim}). \tag{2.3}$$

This means that a fragment with a length of $i$ nucleotides is observed only, if there is a single strand break at site $i+1$ without a break at any of other sites between site $i$ and the $^{32}$P-labeled end.

Eight data sets on fragment size distribution, $f_i^{exp}$, $f_{i,r}^{sim}$ and 4 data sets on strand breaks probability, $p_i^{exp}$, $p_{i,r}^{sim}$ can be compared between this simulation and the experiments mentioned (cf. Sections 3.1.3 and 3.2.1).

In the experiments, $p_i^{exp}$ refers to the experimentally found probability of elimination of the $(i+1)$th nucleotide. In the simulation, $p_{i,r}^{sim}$ refers to the calculated probability of elimination of the $i$th nucleotide. The component contributed from the neutralization effect $p_{i,nr}$ can be obtained by Equation 2.4 subtracting the calculated direct and indirect radiation action component, $p_{i+1,r}^{sim}$, from the $p_i^{exp}$

$$p_{i,nr} = p_i^{exp} - p_{i+1,r}^{sim}. \tag{2.4}$$

These DNA strand breaks contributed only from the neutralization component, $p_{i,nr}$, can be applied to the analysis of the CAP-DNA and free B-DNA data.

Following Equations 2.4, the total strand breaks including the non-radiation component, $p_i$ can be calculated for CAP-DNA and free B-DNA, and, further, the first strand breaks taking into account also the neutralization effect, $f_i$, can also be obtained. It should be pointed out that in the "top" strand for the $^{125}$I-labeled site, $p_{125_I}$ was assumed to be 1 when using Equation 2.3 to calculate the first breaks frequency, $f_i$, for CAP-DNA and free B-DNA. Only the $f_i$ values of those nucleotides, which are inside the range from the $^{32}$P-labeled end to the $^{125}$I-labeled site, can be calculated. For the nucleotides beyond the $^{125}$I-located site, $f_i$ will always be equal to 0.

### 2.4.3  Charge Transfer in DNA

A theoretical introduction on charge and energy transfer dynamics in molecular system was recently given by May and Kühn [MK00]. The electron transfer theory in protein developed by Marcus [MS85] was extended by Jortner [JBLMB98] to the DNA chain. Recently, experiments [MMBG98] and theoretical calculations [GBS00] confirmed that the nucleotide base guanine (G) is the main target for oxidative damage in DNA. Radiation-induced electron migration in nucleic acids was reviewed, e.g. by Fuciarelli et al. [FSMZ94].

Modeling of DNA strand breaks due to the neutralization effect of the positive charged daughter ion $^{125m}$Te$^{n+}$ needs the time dependent hole occupation probability $P_m(t)$ to the neighboring and distant bases $m$. This quantity can be calculated by the *Master Equation* derived by Pauli [MK00]:

$$\frac{\partial}{\partial t}P_m = -\sum_n (k_{mn}P_m - k_{nm}P_n), \qquad (2.5)$$

where $k_{mn}$ is the transition rate from base $m$ to base $n$. The decrease of $P_m$ with time $t$ is the probability of transfer from all other bases $n$ into the base $m$ minus the probability of transfer from base $m$ to all other bases $n$.

In the decay studies with $^{125}$I, $^{125m}$Te$^{n+}$ is assumed to be located at the cytosine base, and the multiply charged ion $^{125m}$Te will first extract electrons from this base. In the following calculation, this cytosine base with the ion $^{125m}$Te will be assumed to be at location $m$. The charge will be transferred to other bases, i.e. $n$, and causes those bases again to become ionize. The charge from those bases can also be transfered to other bases and induces further ionized states, etc. To solve the *Master Equation* mathematically, it can be rewritten to a family of equations of "birth and death" processes [DB74], one special form of Markov processes [Fel65].

$$P'_m(t) = \lambda_{m-1}P_{m-1}(t) - (\lambda_m + \mu_m)P_m(t) + \mu_{m+1}P_{m+1}(t). \qquad (2.6)$$
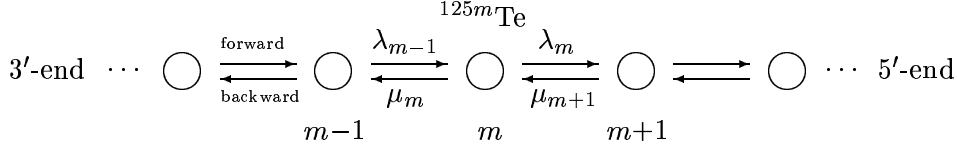
Figure 2.9: Charge transfer procedure in a DNA chain

where $\lambda_m$ is the "forward" transfer probability for an excitation or charge to move from base $m$ to the neighboring base $m+1$, i.e. $k_{m,m+1}$, and $\mu_m$ is the "backward" transfer probability, for reverse movement from base $m$ to base $m$-1, i.e. $k_{m,m-1}$. Here the direction $3'$–$5'$ is defined as the "forward" direction, and $5'$–$3'$ as the "backward" direction. This charge transfer nomenclature is graphically represented in Figure 2.9

According to the work of Dee and Baur [DB74], applying the perturbation approach, the solution of the Equation 2.6 reads

$$
\begin{aligned}
P_m(t) &= P_m^0(t) + P_m'(t) \\
&= e^{-(\lambda+\mu)t}(\mu/\lambda)^{-m/2} \\
&\quad \times \bigg\{ I_m(\alpha t) + \sum_k \Delta_{k,k+1}[(\lambda/\mu)^{1/2}G(k+1,m;t) - G(k,m;t)] \\
&\quad + \Delta_{k,k-1}[(\lambda/\mu)^{-1/2}G(k-1,m;t) - G(k,m;t)] \bigg\},
\end{aligned} \tag{2.7}
$$

where $P_m^0(t)$ is the solution for a uniform DNA chain and $P_m'(t)$ is the first-order correction term for a nonuniform chain, $\alpha = 2\sqrt{\lambda\mu}$ with $\lambda$ and $\mu$ being the transfer rates for "forward" and "backward" transfer, $I_\nu(z)$ is the modified Bessel function [AS68], $\Delta$ is the perturbation matrix incorporating the "deviations" from uniformity due to the specific base sequence of the DNA chain, and

$$
G(k,m;t) = (2/\alpha) \sum_{n=0}^{\infty} I_{|k|+|k-m|+2n+1}(\alpha t), \tag{2.8}
$$

$$
G(k \pm 1,m;t) = (2/\alpha) \sum_{n=0}^{\infty} I_{|k|+|k\pm 1-m|+2n+1}(\alpha t). \tag{2.9}
$$

The solution of the Equation 2.7 for $P_m(t)$ needs the knowledge of the hole transfer rates $k_{\alpha\beta}$ ($\alpha,\beta$ = T, C, A, G) which were calculated by Dee and Baur [DB74] based on the "strong scattering" approximation developed by Glaeser and

Berry [GB66]. These transfer rates were in the order of several $10^{14}$ s$^{-1}$ which implied that the lifetime of the hole staying in one base is about $10^{-15}$ s.

Another way to calculate the transfer rates follows the classical electron transfer theory originally derived by Marcus for protein [Mar56] using the *Golden Rule* which was first discussed by Dirac and Fermi [MK00]. Later this theory is extended by Jortner and Bixon [BJ99] and the rate expression [MS85] reads

$$k = \frac{2\pi}{\hbar} V^2 F, \qquad (2.10)$$

where $V = \langle D|\hat{H}|A \rangle$ is the electronic coupling between a charge donor $D$ and an acceptor $A$, where $\hat{H}$ is the Hamiltonian, $F$ is the thermally averaged Franck-Condon density, incorporating both medium and intramolecular vibrational modes [BJ99]

$$F = \sqrt{\frac{1}{4\pi E_\lambda k_B T}} \exp(-S) \sum_{n=0}^{\infty} \frac{S^n}{n!} \exp\left[ -\frac{(E_\lambda + n\hbar\omega + \Delta G^0)^2}{4\pi E_\lambda k_B T} \right], \qquad (2.11)$$

where $\hbar = h/2\pi$, $h$ is the Max-Planck constant, $k_B$ is the Boltzmann constant, $T$ is the temperature, $S = E_\lambda/\hbar\omega_M$ is the electron vibration coupling constant or the Huang-Phys factor, with medium frequency, $\omega_M$, $E_\lambda$ is the reorganization energy, $\Delta G^0$ is the driving force, the free energy gap, $\omega \cong 1500$ $cm^{-1}$, is the mean intramolecular vibrational frequency.

The base pair electronic coupling matrix element $V$ for electron and hole interaction were calculated by Dee and Baur [DB74]. Extended Hückel calculations were introduced by Beratan's group [PRB96]. Recently, Voityuk et al. [VRBJ00] [VBJR01] reported $V$ for hole transfer for all pairs of nucleotide bases using a two-state model. With these newly evaluated electronic coupling for hole transition (Table 2.2), transfer rate can be calculated using the reorganization energy calculated by the computer program *Gaussian98* [FTS$^+$98] with the Hartree-Fock and Density Functional Method (B3LYP) using the 6-31G* basis set (Table 2.2). The driving force between the bases (Table 2.2) is obtained from the difference between the oxidation potential energy of each base measured by Seidel et al. [SSS96]: $E_{Ox}(T) = 2.11$, $E_{Ox}(C) = 2.14$, $E_{Ox}(A) = 1.96$, $E_{Ox}(G) = 1.49$ eV (V vs NHE).

Experimental results obtained recently are usually interpreted in terms of extended charge transfer theories: superexchange process [MMBG98], [WFS$^+$99], hole hopping model [MKS$^+$98], [GWS$^+$99], [LLL$^+$00], [Gie00], [GAK$^+$01] and phonon assisted polaron hopping [CR00], [HJH$^+$99], [LSS99]. Experiments [WFS$^+$99], [KB99], [MCO$^+$98] focused on the "hole" or electron transfer or transport by either measuring the quenching of the fluorescence of the donor or by analysis of the relative yields of strand breaks at different positions along the DNA strands.

| Base pair | $E_\lambda$ (eV) | $V$ (eV) | $\Delta G^0$ | Base pair | $E_\lambda$ (eV) | $V$ (eV) | $\Delta G^0$ |
|:---:|:---:|:---:|:---:|:---:|:---:|:---:|:---:|
| TT | 0.486 | 0.158 | 0. | AT | 0.436 | 0.105 | 0.15 |
| TC | 0.423 | 0.076 | 0.03 | AC | 0.373 | 0.061 | 0.18 |
| TA | 0.476 | 0.086 | $-0.15$ | AA | 0.452 | 0.030 | 0. |
| TG | 0.621 | 0.085 | $-0.62$ | AG | 0.571 | 0.049 | $-0.47$ |
| | | | | | | | |
| CT | 0.367 | 0.100 | $-0.03$ | GT | 0.509 | 0.137 | 0.62 |
| CC | 0.304 | 0.041 | 0. | GC | 0.446 | 0.110 | 0.65 |
| CA | 0.383 | 0.029 | $-0.18$ | GA | 0.499 | 0.089 | 0.47 |
| CG | 0.502 | 0.042 | $-0.65$ | GG | 0.644 | 0.084 | 0. |

Table 2.2: Reorganization energy, $E_\lambda$, electronic coupling, $V$ and driving force, $\Delta G^0$ between bases

In order to determine the transfer rate experimentally, the rate expression 2.10 can be rewritten for superexchange processes as:

$$k_{CT}(R) = k_0 \exp(-\beta R), \qquad (2.12)$$

where $k_0$ is a preexponential factor, $\beta$ is the so-called falloff parameter and is often used to distinguish between the different charge migration mechanisms, $R$ is the distance from donor to acceptor. For multistep hopping mechanism the transfer rate can be calculated by

$$\ln k_{CT} \propto -\eta \ln N, \qquad (2.13)$$

where the power parameter $\eta$ is here equal to 2, $N$ is the number of hopping steps. Experiments are often performed by measuring steady-state quantum yields and quenching efficiencies [KB99], or excitation spectra [XN00] from fluorescent analogs of adenine (1,$N^6$-ethenoadenine ($A_\varepsilon$), 2-aminopurine ($A_2$) to other bases. Other groups measured strand breaks [MKS$^+$98] by analyzing the hole transfer from the $G^{+\bullet}$ to a GGG unit through one, two, three and four AT base pairs. These experiments were designed to examine the parameters $\beta$ and $\eta$.

Regarding the $^{125}$I decay, the charge transfer problem becomes even more complicated because the $^{125m}$Te is heavily charged. As a first try the transfer rates calculated by Dee and Baur [DB74] for one hole charge were used to calculate the distribution of the multiple charges. The ionization energy transferred to the bases exceeds much the chemical bond energy or even the dissociation energy of most radicals. Hence, it is assumed in the present study that the nucleobase is expected to collapse which will be recorded as a strand break as is pointed out in the experiment [LM00b]: "the experimental end point that is the basis of the data is the

nucleoside gap rather than a DNA strand break. In other words, any one (or more) of a number of chemically different DNA cleavage events, occurring within the one nucleoside unit are scored in the experiment as the same strand 'break'."

# Chapter 3

# Results and Discussions

## 3.1  Calculated Results

### 3.1.1  Track Structures of I-125 Decay

Figure 3.1 presents the track structures of 100 $^{125}$I decays in different scales with the CAP-DNA structure. In the scale of 20×20 cm, only the interactions of photons in the energy range of 27 $\sim$ 35 keV can be resolved as "black dots". In the smaller scale of 40×40 $\mu$m, the tracks of electrons with energies of about 35 keV and a range of 20 $\mu$m are spatially resolved. When zooming in to the $^{125}$I atom, tracks of electrons with energies about 3 $\sim$ 4 keV range of about 300 $\sim$ 500 nm can be seen (1000×1000 nm resolution). In the frame with a size comparable to the CAP-DNA (10×10 nm), events from electrons with energy lower than, say 500 eV (corresponding to about 10 $\sim$ 20 nm range in water [Par87]), deposit most of their energy near this bent DNA and interact with its atoms frequently.

### 3.1.2  Frequency of DNA Hits

The frequency of DNA hits will be presented in terms of direct hits, i.e. contributed from physical track interactions and indirect hits, i.e. from chemical radical attacks. The former part is distance-dependent; the distribution of the nucleotide base distances to the $^{125}$I decay site is shown first. With the distinction between the direct and indirect hits, the portion to DNA damage from primary physical and chemical processes can be estimated and understood.

In the present study the "direct" and "quasi-direct" hits (cf. Appendix A.2) are pooled together and called "direct" hits. They correspond to the radiation nonscavengeable part of experimental results. All other electronic excitations and ionizations are assumed to occur in the bulk water and to undergo radiation chemistry as processed in the chemistry module. After interaction of these chemical species among
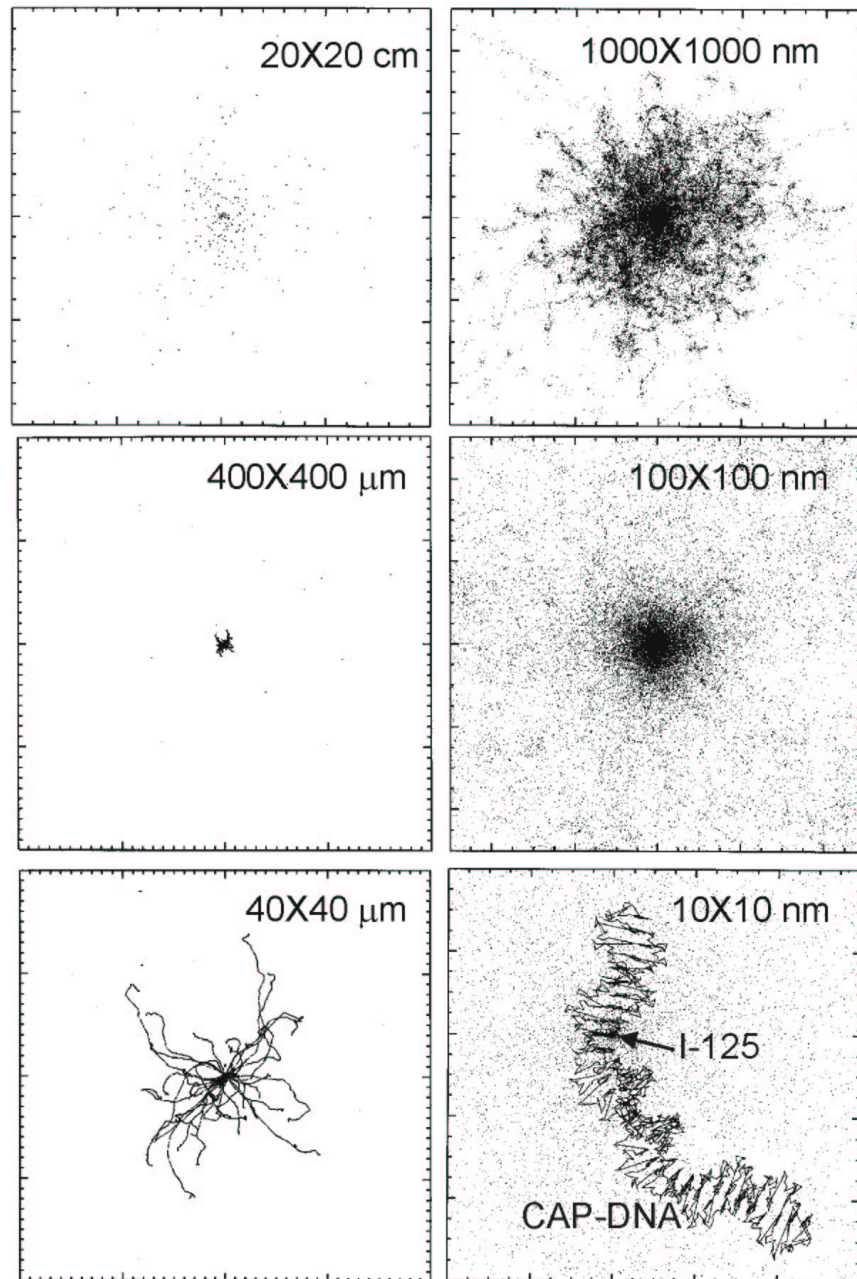
Figure 3.1: Track structures of 100 ^{125}I decays in different scales with CAP-DNA structure. The black dots denote locations of excitations and ionizations

themselves and with DNA molecule, the $^\bullet$OH events which occurred inside the re-action radii of the DNA constituents are scored as "indirect" hits (cf. Appendix A.3). PARTRAC code was first applied to CAP-DNA and free B-DNA without changing the $^\bullet$OH scavengeable condition, i.e. the physiological scavengeable capac-ity in cellular environment [WMF97]. Having reviewed the experiment which was performed in $-70°$ for CAP-DNA and free B-DNA [KZG$^+$99], we assumed in the present study that chemical radicals will not move and interact with DNA, and the simulations for CAP-DNA and free B-DNA should be performed under the full scav-engeable condition. For the 41-mer synthetic oligoDNA, full and none scavengeable conditions were simulated according to the experiment [LM00a]. The scavengeable parameter for plasmid DNA was adopted from ref. [KBR74]. For cellular DNA the physiological scavengeable condition [WMF97] was unchanged. For reference the indirect hit frequency for CAP-DNA and Free B-DNA in physiological scavenging capacity ($\sigma = 4 \times 10^8$ s$^{-1}$) are plotted in Section 3.1.2.

**Nucleotide distances to the I-125 decay site**

As has been pointed out in experiments [LM00b], DNA strand breaks contributed from the radiation component depend on the geometric distance of the nucleotide to the $^{125}$I decay site rather than the genomic distance. The nucleotide distance to the $^{125}$I decay site is defined conventionally as the average distance of the five atoms (four C atoms and one O atom) in the sugar ring to the $^{125}$I decay site.

*CAP-DNA and Free B-DNA*
The geometric distance distributions of the CAP-DNA and B-DNA models are plot-ted in Figure 3.2. In the "top" strand, distance distributions of these two forms of DNA are very similar in the direct environment of the $^{125}$I atom. In the "bottom" strand, sugar molecules of the CAP-DNA in the 3$'$-end direction tend to be farther from the $^{125}$I atom than in the free B-DNA molecules. It should be pointed out that in the "top" strand, the nearest nucleotide sugar molecule to the $^{125}$I atom, is the next one in the 5$'$-end direction other than the one in which the $^{125}$I atom is incorporated. In the "bottom" strand, in the CAP-DNA model, the distances of the nucleotide sugar molecules in the 5$'$-end direction are less than those in the 3$'$-end direction, for free B-DNA, and it is difficult to predict the trend due to its short length of base pair.

*41-mer Synthetic OligoDNA*
It is assumed that the deoxyribosyl moieties are the crucial radiation-sensitive target for DNA strand breakage and that bases are potential radiation targets, as discussed in Section 2.3. The calculated $^{125}$I-deoxyribosyl distances for the 41-mer synthetic

oligoDNA are plotted in Figure 3.3, the "top" strand is numbered with positive integers from number 1 to 41 in the direction from $5'$ to $3'$-end and the "bottom" strand with negative integers from $-1$ to $-41$ in the direction from $5'$ to $3'$-end.

Notice that the $^{125}$I atom is located at the nucleotide number 21 cytosine. In general, the $^{125}$I-deoxyribosyl distances for the nucleotide bases in the "top" strand are less than that in the "bottom" strand especially within 4 bases, say about 6 Å less in both directions. In the "top" strand the nearest base is the base number 20 thymine instead of the base number 21 cytosine and the distribution represents an asymmetrical pattern like that in the "top" strand of bent CAP-DNA model. It may imply that the distortion in CAP-DNA model affects not so much in the "top" strand than in the "bottom" strand. In the "bottom" strand the bases within 5 bases in the $3'$-end direction are less than those in the $5'$-end and they are stacked from 1.1 to 1.3 Å around the decay site, and the nearest base to $^{125}$I atom is the base number $-23$ cytosine in the $3'$-end direction.

### Direct Hits

The direct hit frequency from the physical tracks per decay is plotted in Figure 3.4 for the CAP-DNA and free B-DNA models. All the distributions are plotted for both DNA strands: the "top" strand (Figure 3.4a) with the $^{125}$I source in the attached base and the opposite "bottom" strand (Figure 3.4b).

The maximal direct hit frequency close to the $^{125}$I atom is in the "top" strand, it is about 10 times greater than that in the "bottom" strand. In the "top" strand for these two DNA models, the hit frequency has a peak value about 5 hits per decay at the nucleotide in which $^{125}$I atom is located, it decreases quickly to $1 \sim 1.5$ in the neighboring nucleotides and tends to be smaller than 0.1 hits per decay beyond $7 \sim 8$ nucleotides from the decay site. The prominent peak is due to a large number of hits in the base to which the $^{125}$I atom is attached. Even the $C_5$ atom in the cytosine has on average more than 3 hits per decay. In the model calculations, these hits in the base do not contribute to the strand breakage. In the "bottom" strand, the peak shifts by one nucleotide from the decay site in the $5'$-end direction, as expected from the distance distribution (Figures 3.2 and 3.3), and at this nucleotide the CAP-DNA obtains more hits than the other DNA models. The hit frequency in the "bottom" strand distributes more smoothly than in the "top" strand along the strand. Again, this is in accordance with the distance distribution.

In the "top" strands of these two DNA models, the most frequently hit nucleotides are those in which the $^{125}$I atom is located; however, in the "bottom" strands the peaks of the frequency distribution occurs in the neighboring nucleotides.

The direct hit frequency per decay for 41-mer synthetic oligoDNA is plotted in Figure 3.5. In the "top" strand, there is no difference in the hit frequency between
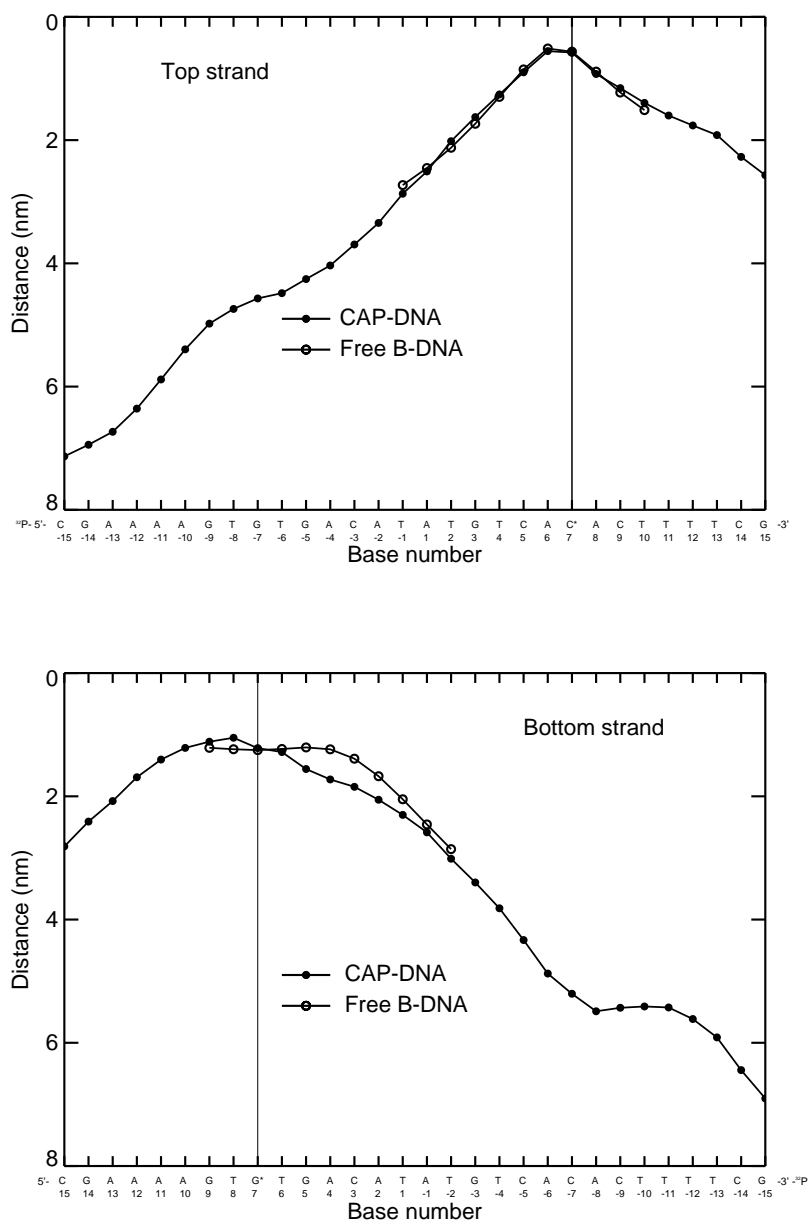
Figure 3.2: Distribution of the nucleotide distance to $^{125}$I atom for CAP-DNA and free B-DNA
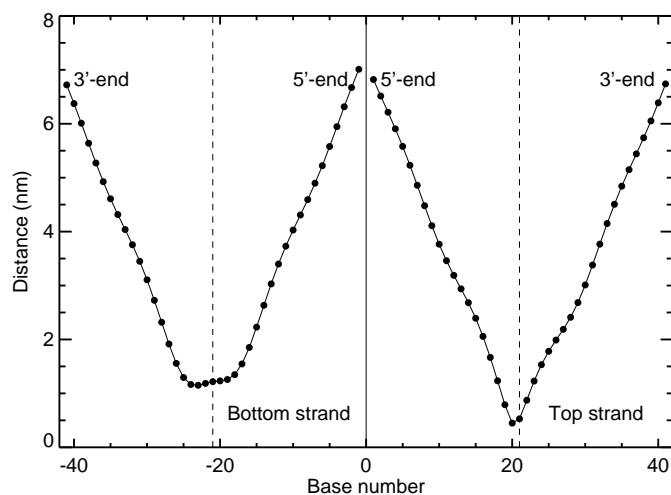
Figure 3.3: Distribution of the nucleotide distance to $^{125}$I atom for 41-mer synthetic oligoDNA. Note the numbering of the bases in both strands (cf. text)

this molecular software generated DNA and the CAP-DNA and free B-DNA. In the "bottom" strand, the peak of hit frequency happened on the base which is the complementary pair to that one $^{125}$I located in the "top" strand. This difference from the free B-DNA (cf. Figure 3.4b) implied that the location of the $^{125}$I atom inside or outside the groove (cf. Figure 2.4 for free B-DNA and 41-mer synthetic oligoDNA) of these double helix models is the key for the direct hit frequency; also the definition of the sugar distance as the index for distance of the nucleobase to the $^{125}$I atom is an influence factor on the direct hit frequency because in the simulation the physical tracks interactions scored the hits on base and phosphate moieties as well (cf. Appendix A.2), and the hits on base moiety have not been taken into account to contribute to the DNA strand breaks yet. The sugar distance as an distance index from each nucleobase to the $^{125}$I atom is just a reference for the direct hit frequency and the strand breaks probability and cannot be regarded as an absolute parameter.

**Indirect Hits**

The indirect hit frequencies contributed from the chemical radical species per decay for the CAP-DNA and free B-DNA models in the physiological scavengeable con-
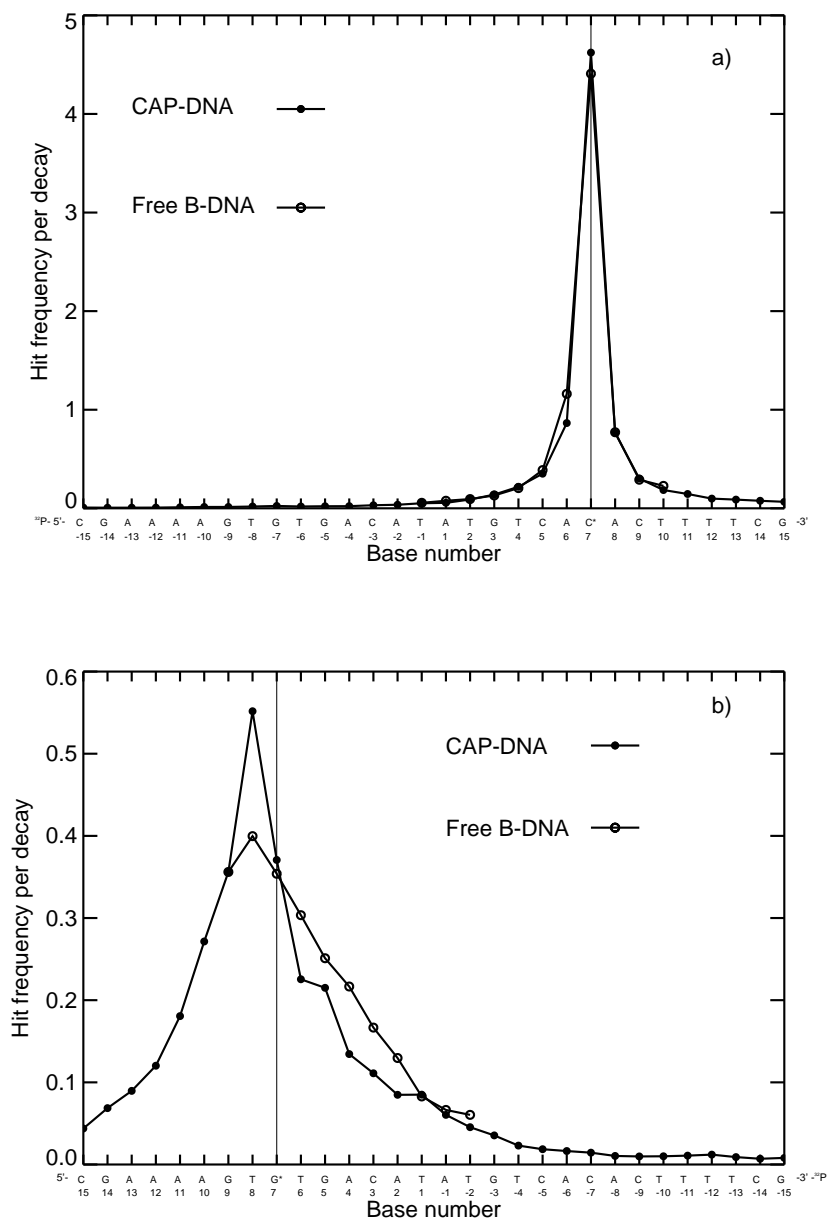
Figure 3.4: Average number of direct hits per $^{125}$I decay in the "top" (a) and in the "bottom" (b) strands for CAP-DNA and free B-DNA

Figure 3.5: Average number of direct hits per $^{125}$I decay in the "top" and in the "bottom" strands for 41-mer synthetic oligoDNA

dition are presented in Figure 3.6a for the "top" strand and in Figure 3.6b for the "bottom" strand. Indirect hits do not show one sharp peak as the direct hits and are more distributed over the strand. This is to be expected because of the diffusion of the radicals. In the "top" strand, the number "3" nucleotide G in the $5'$-end direction from the decay site receives most hits (Figure 3.6a), and in the "bottom" strand the neighboring nucleotides G ("5" and "9") receive more hits than the decay site nucleotide (Figure 3.6b). The structures in the curves are due to the differences in the base sequence. (Guanine receive more radical hits whereas for naked free B-DNA there are no structures since the bases are only A and T.) The peak at the end nucleotide of the "top" strand reflects the higher accessibility to chemical radicals of this nucleotide than of the other inner nucleotides. The magnitude of the distribution of indirect hit frequencies of both strands is more similar to each other than it is the case for direct hits.

The indirect hit frequencies for CAP-DNA and free B-DNA models in the non-scavengeable condition was not analyzed, in view of no comparable experimental data [KZG$^+$99]. However, this component can be estimated from the 41-mer synthetic oligoDNA in Figure 3.7. The radical hit frequency on DNA chain is dependent on guanine according to the experiment-based assumption in PARTRAC chemistry module (cf. Appendix A.3) that the base G receives radical attacks with more probability. Generally the indirect hit frequency of 41-mer oligoDNA is about 2 times larger than that of CAP-DNA, free B-DNA (cf. Figures 3.6 and 3.7) due to $^\bullet$OH radical scavenging. In other words, under the physiological scavengeable condition, 50% $^\bullet$OH radicals will be scavenged. Again it is shown that the indirect hit frequency is independent of the geometric distance because of radicals diffusions in water solution, as seen in Figure 3.8. The diffusion time is cut off at $10^{-7}$ s.

### 3.1.3   Total DNA Strand Breaks from Radiation Components

In this section, the total DNA strand breaks probability from radiation components for CAP-DNA, free B-DNA, 41-mer synthetic oligoDNA, pUC19 plasmid DNA and cellular DNA will be presented. Here radiation components includes physical tracks and chemical radicals attacks contributions excluding neutralization effect, which will be shown in Section 3.1.4.

**CAP-DNA and Free B-DNA**

The total strand breakage under the physiological scavengeable condition is again plotted for CAP-DNA and free B-DNA models in the "top" (cf. Figure 3.9) and in the "bottom" (cf. Figure 3.10) strands to give an idea of how many fractions contributed from physical tracks and chemical radicals in the simulation. In this
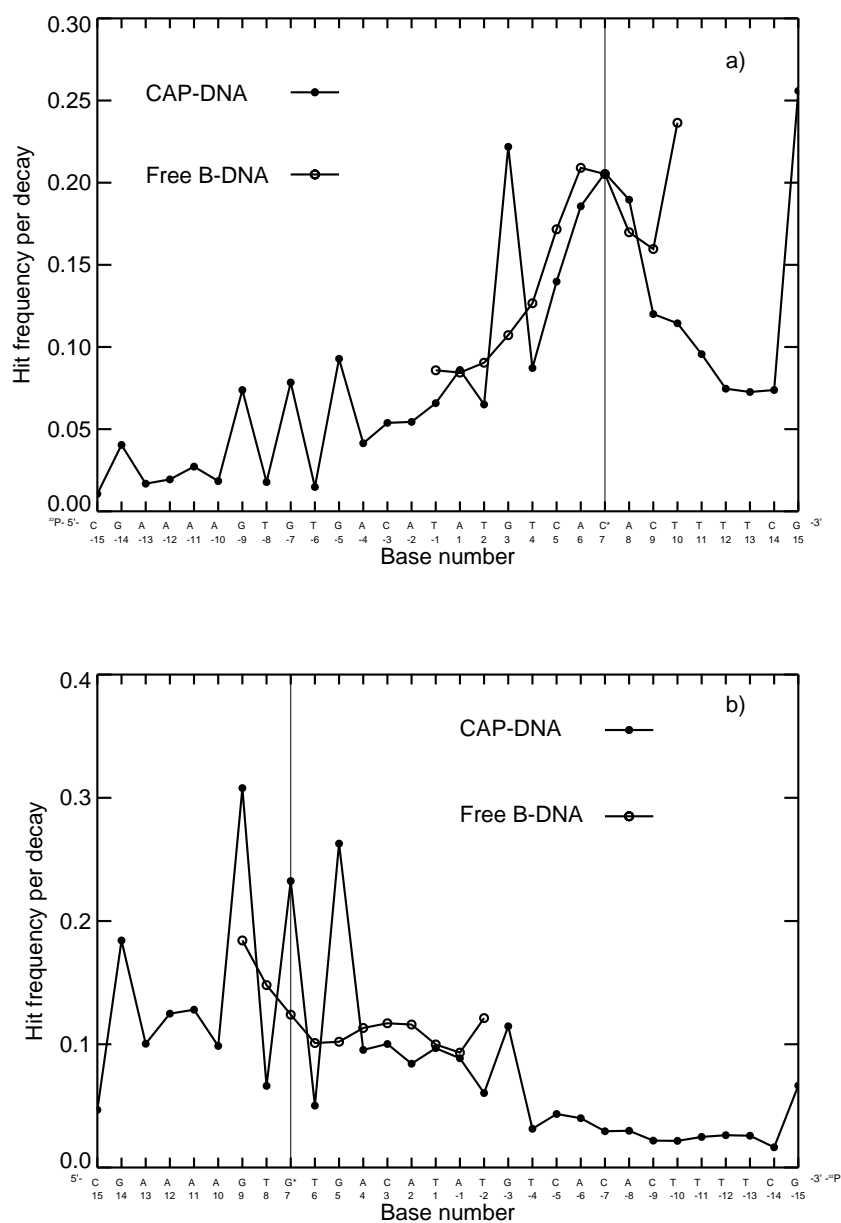
Figure 3.6: Average number of indirect hits per ^{125}I decay in the "top" (a) and in the "bottom" (b) strands for CAP-DNA and free B-DNA
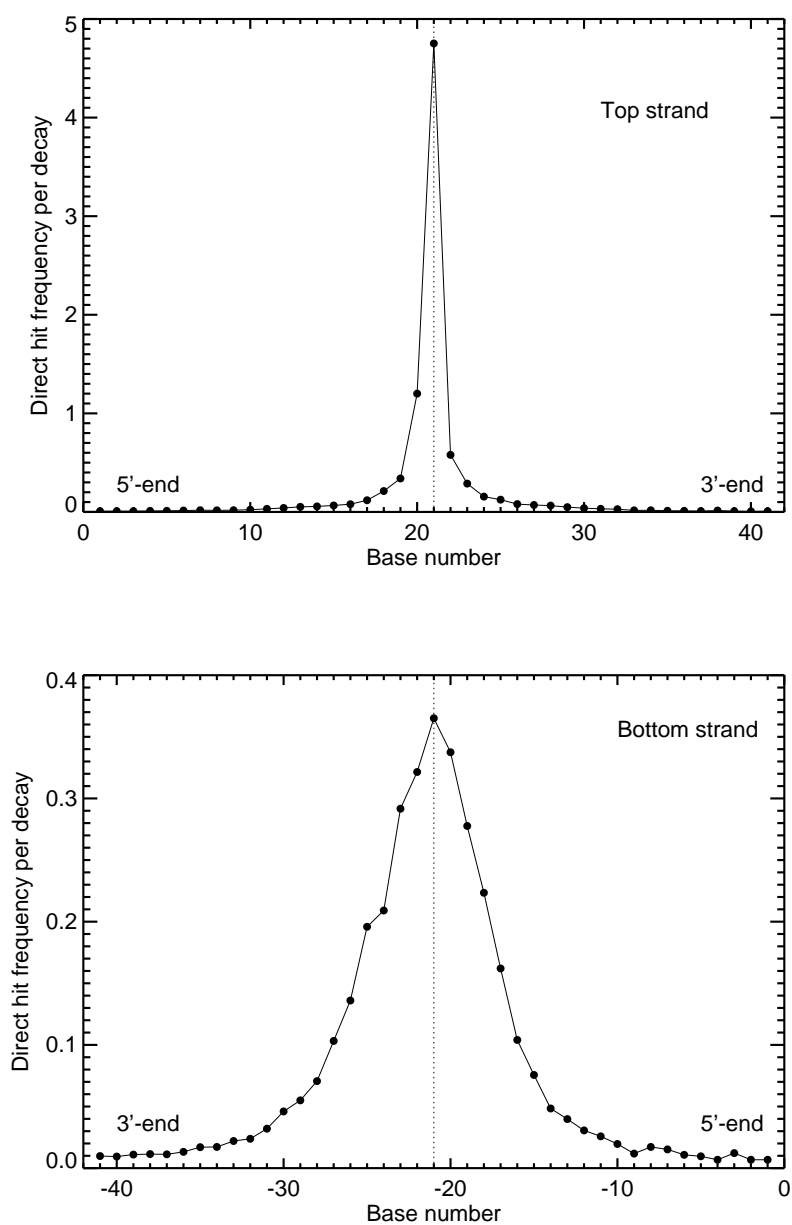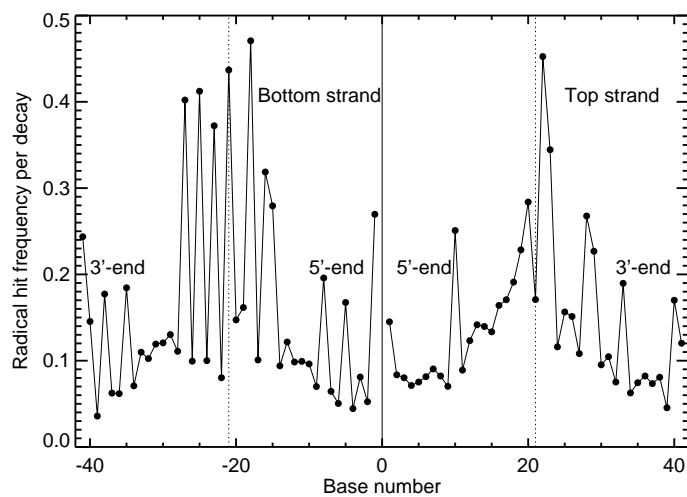
Figure 3.7: Average number of indirect hits per $^{125}$I decay in the "top" and in the "bottom" strands for 41-mer synthetic oligoDNA
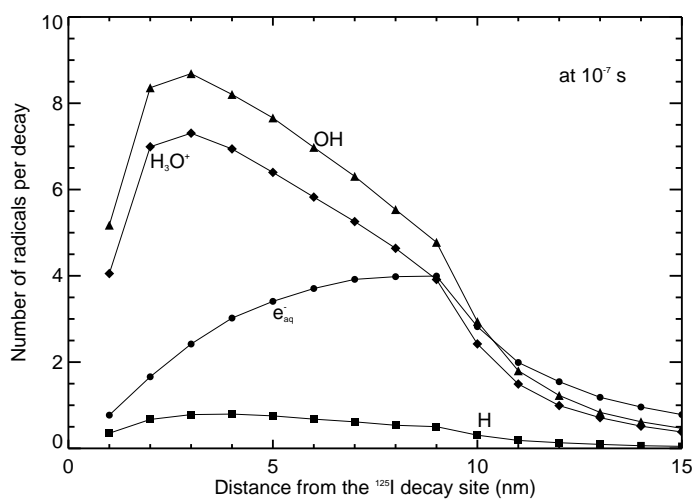


Figure 3.8: Distribution of the diffusion distance of the chemical radicals induced by $^{125}$I decay in water solution at $10^{-7}$ s with the physiological scavengeable condition

context, the total DNA break distribution records all the breakages per decay produced by radioiodine in each strand, whereas the first break distribution includes only the breakage nearest to the $^{32}$P-labeled end. From Figure 3.9, the free B-DNA model shows a larger probability on the total and first breakage in the "top" strand than the CAP-DNA model. The CAP-DNA gives a lower probability at the decay site nucleotide and also at the neighboring nucleotide in the 5′-end direction; this lower probability on CAP-DNA model is perhaps due to reduction of the DNA model volume when CAP-DNA is bent in simulation. Figure 3.10 presents the total and first breakage of simulation results for the "bottom" strand. For the two DNA models in the nucleotides in the 5′-end direction from the decay site, the frequencies are similar, but in the other direction, i.e. 3′-end direction, some difference can be seen due to the larger geometric distance to the decay site of the CAP-DNA than that of the free B-DNA model.

For the two DNA models in the "top" strands, indirect hits do not contribute much to the breakage. There is no appreciable difference between total and first breakage resulting from indirect hits (Figure 3.9). In the "bottom" strand, the frequency of direct hits is smaller and the higher resolution of Figure 3.10 exhibits the small difference between first and total breakages. Indirect hits have a relatively more effect in the "bottom" strand. One should bear in mind that till now the discussion on strand breakage is limited to the physiological scavengeable condition. For the nonscavengeable condition, one can refer to that of 41-mer synthetic oligoDNA in the subsection entitled "**41-mer Synthetic OligoDNA**". Actually only for the fragment size distribution, i.e. first breakage was measured in experiment [KZG$^+$99], the comparison between the simulation and the experimental data will be discussed in Section 3.2.1.

**41-mer Synthetic OligoDNA**

For 41-mer synthetic oligoDNA, DNA total strand breaks in PB solution with full DMSO are plotted in Figure 3.11. Because only the fragment size distribution from the labeled $^{32}$P can be measured, the experimental data of total strand breaks are derived under the assumption that the amount of damage from radiation component declines as an inverse square of distance from a decay point to a sensitive target [LM00b].

In view of the purpose of the present study, i.e. the evaluation of neutralization effect, the total strand break distribution without DMSO will not be discussed here. Results will be not much different from the data with DMSO only, except for the bases which are $5 \sim 6$ bases away from the decay site, and it is clear from experiment that 90% of breakage occur within $5 \sim 6$ nucleotides of the $^{125}$I-dC [LM00a].

|            |                          | DSBs | SSBs | SSBs:DSBs |
|------------|--------------------------|------|------|-----------|
| Simulation | full scavengeable        | 0.3  | 0.8  | 2.7       |
|            | nonscavengeable          | 0.5  | 2.32 | 4.67      |
|            | sodium polyphosphate     | 0.49 | 2.29 | 4.5       |
| Kassis et al. | +DMSO                 | 0.9  | 0.42 | 0.5       |
|            | –DMSO                    | 0.9  | 3.11 | 3.5       |
|            | sodium phosphate buffer  | 1.08 | 3.11 | 2.9       |
| Panyutin et al. | -70°C               | 0.46 | 5.1  | 11        |

Table 3.1: Average number of DSBs and SSBs for pUC19 plasmid DNA per decay of $^{125}$I in experiments and in simulations

**Plasmid DNA**

The distribution of double strand breaks (DSBs) around the $^{125}$I decay site (base number #1339 in reference [YPVM85]) is plotted in Figure 3.12. The number of SSBs and DSBs per $^{125}$I decay in simulation under different scavenging conditions are listed in Table 3.1 for comparison with experimental data available by Kassis et al. [KHA99a], [KHA99b] and by Panyutin et al. [PLPN01]. The simulation data of DSBs $0.3 \sim 0.5$ are reasonable when one bears in mind that neutralization effect must be taken into account (cf. Section 3.2.2). The percentage 26% of DSBs in the plasmid outside the 90-bp fragment containing the $^{125}$I atom agrees with 25% of Panyutin experimentally derived data. However, and the simulation the neutralization is not included, in this point simulation data may appear to be too larger. However, these data and the track structures of $^{125}$I decay (cf. Figure 3.1) brings us to agree with the explanation to the phenomenon that DSBs occurred 100-bp away from the decay site, it is those high-energy electrons and chemical radicals produced by $^{125}$I decay that interact with those DNA molecules and produce DSBs there.

**Cellular DNA**

For cellular DNA under the physiological scavenging condition, cytosine incorporated with $^{125}$I produces about 3.4 SSBs and 0.41 DSBs per cell per decay with the relation SSBs:DSBs = 8.41. Walicka et al. [WAK98b] estimated $1 \sim 2$ DSBs per cell per decay from experimental data. Including the neutralization effect component (cf. Section 3.2.2), the simulation results will be expected to be 1 DSBs per cell per decay.
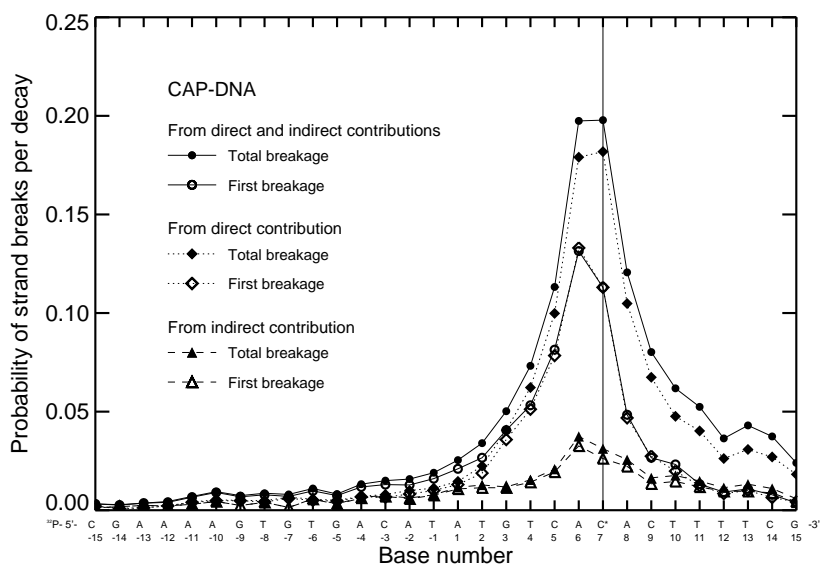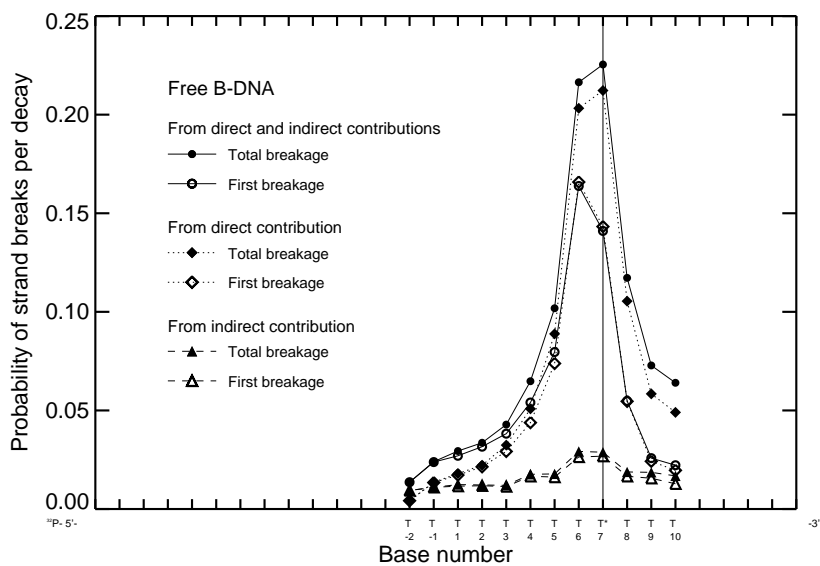
Figure 3.9: Probability of breakage per $^{125}$I decay contributed from direct interaction and from chemical radicals for CAP-DNA and free B-DNA in the "top" strand. First breakage denotes the fragment size distribution from the $^{32}$P-labeled end
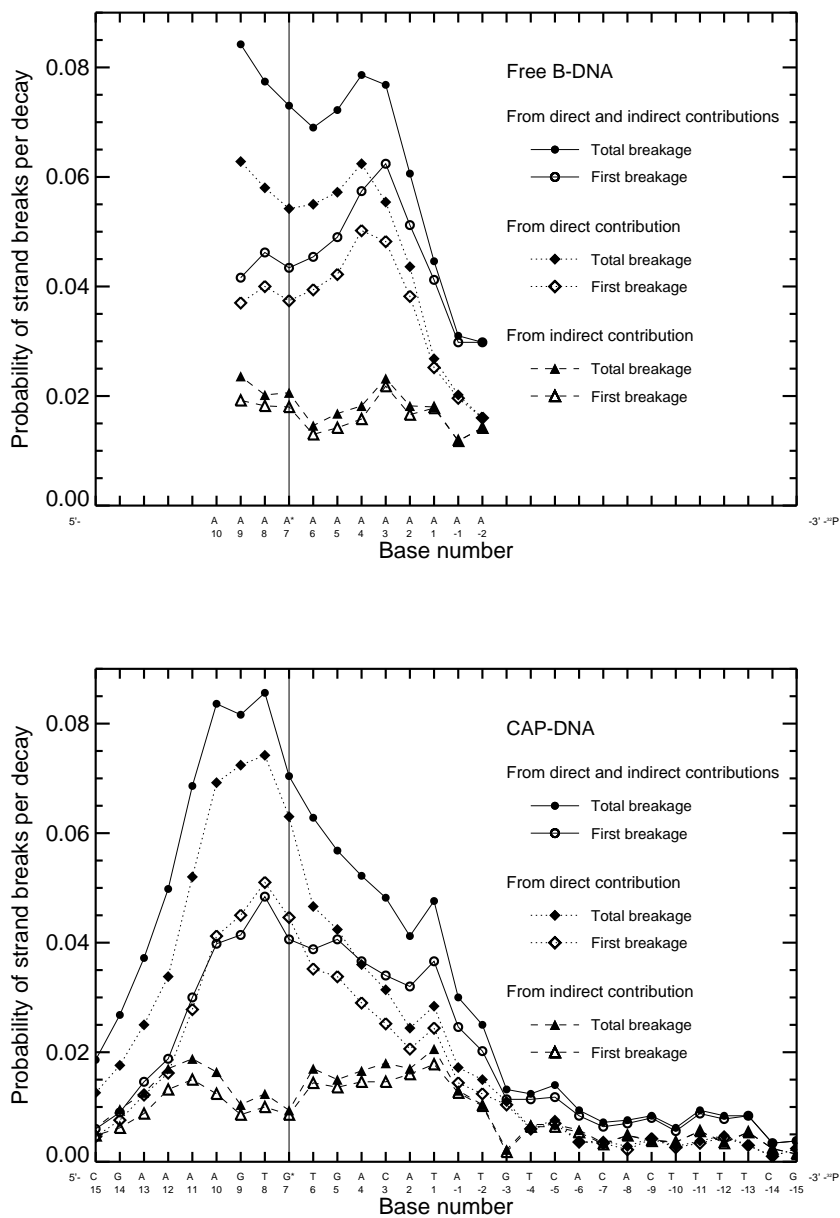
Figure 3.10: Probability of breakage per ^{125}I decay contributed from direct interaction and from chemical radicals for CAP-DNA and free B-DNA in the "bottom" strand
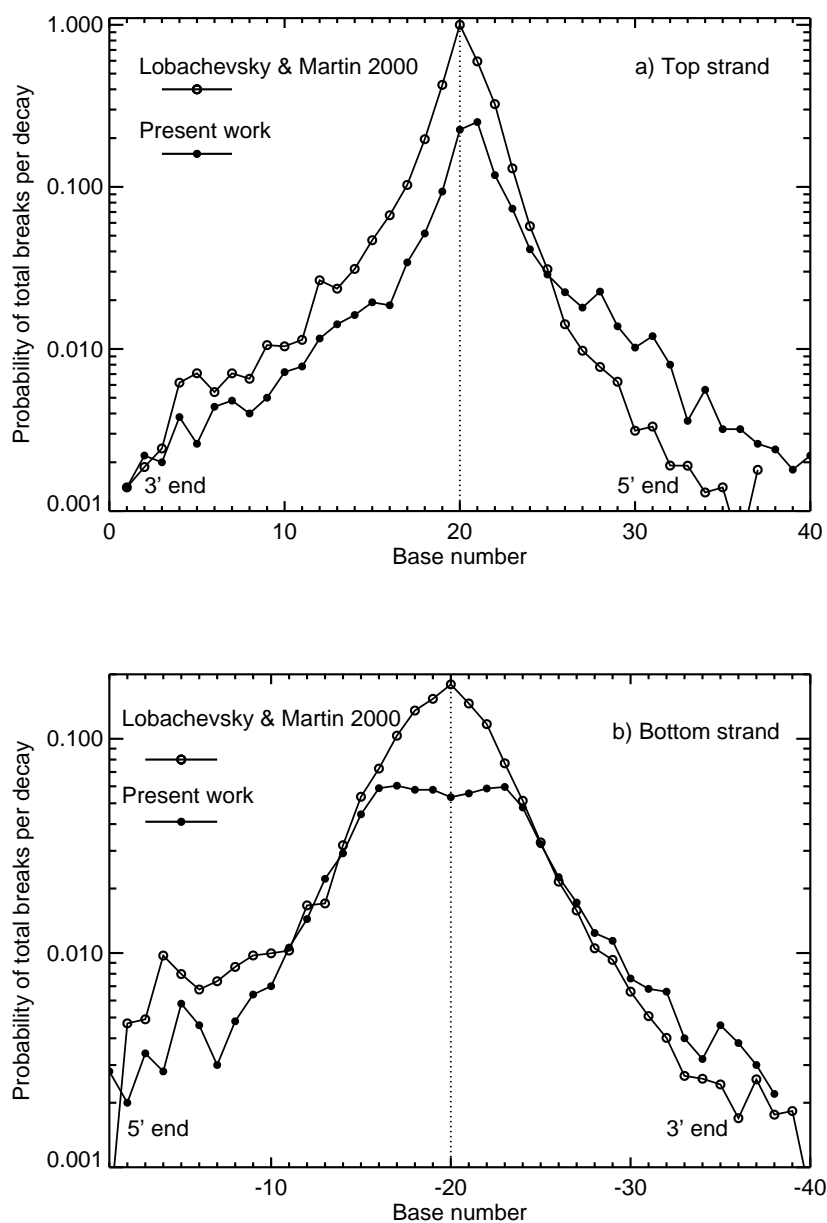
Figure 3.11: Probability of strand breaks per $^{125}$I decay in PB solution with full DMSO in experiment and simulation for 41-mer synthetic oligoDNA in the "top" (a) and in the "bottom" (b) strands
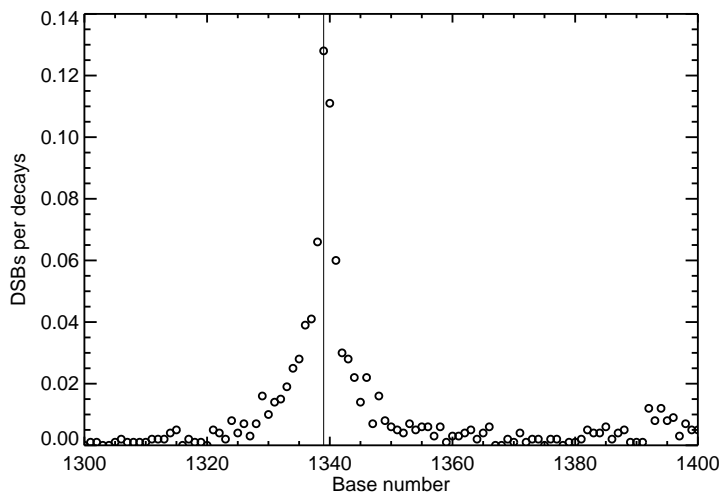
Figure 3.12: DSBs distribution of pUC19 plasmid DNA per $^{125}$I decay in sodium polyphosphate solution (scavenging capacity $\sigma = 5 \times 10^4$ s$^{-1}$)

### 3.1.4  Total DNA Strand Breaks from Neutralization Components

The main intention of the present work is to evaluate the total DNA strand breaks induced by neutralization effect resulting from the multiple charged daughter ion $^{125m}$Te$^{n+}$ when $^{125}$I atom is incorporated into pyrimidine. From the literature it is summarized that the actual mechanism of this toxic isotope to DNA damage is still not fully understood [Hof00] and is in debate [Pom00]. To quantitate the portion of DNA strand breaks contributed from the neutralization effect, Data from simulation and experiment were first combined to give a guide and an attempt was made to calculate this component theoretically.

**Combination with Simulation and Experiment**

The difference of the total strand breaks between the experimentally derived distributions and the simulation with PARTRAC code (Figure 3.11) is regarded as the component from the neutralization effect. The mathematical formulation can be seen in Section 2.4 and reference [LM00b]. The neutralization component thus calculated is plotted in Figure 3.13 together with the experimentally derived component. It should be pointed out that the strand break probability on the decay site in the "top" strand cannot be measured even in the fragment size distribution, this

probability is assumed to be equal to 1 in experiment and this is subtracted from experimental data. The result is less than 1 and around 0.85, and the experimentally derived DNA strand breaks by neutralization are relatively insensitive to this result from 0.85 to 1. In principle, the probability of 1 for this decay site can also be assumed in simulation because in experiment the fragment size distributions in the "top" strand were terminated at bases next to or less than the decay site.

## Theoretical Calculation

With the data combining simulation and experiment in hand, it is possible to test calculation on the neutralization effect based on the charge transfer theory. First the hole transfer rates between bases (Table 3.5) calculated by Dee and Baur [DB74] were used to calculate the distribution along the DNA chain of the multiple charges built up on $^{125m}$Te.

The probability distribution of hole migration in DNA chain was expressed in Equation 2.7 after solving the Equation 2.6 for the "birth and death" process using a perturbation approach. Although it was announced by Dee and Baur [DB74] that their study was for nonuniformly sequenced DNA, the nonuniform chain DNA should be understood as an averaged DNA chain of different types, such as *E. coli* bacterial DNA, DNA for averaged over 10 animal tissues and *Cancer boreali* testis DNA. They used the nearest-neighbor frequencies of bases in different types of DNA with the above transfer rates in a statistic way to obtain an averaged transfer rate along the different DNA chains. From their complicated calculations on different-type DNA chains the assumption that the hole, electron or excitation energy initially located in different bases, after 20 jump times, several $10^{-14}$ s (each "jump time" is equal to $1/\sqrt{\lambda\mu}$ of the oder of $10^{-15}$ s.), the distributions become the same as in uniform DNA chains, especially for the hole transfer (cf. Figures 1 and 5 in reference [DB74]). The first Auger cascade in $^{125}$I decay ends at $10^{-16} \sim 10^{-15}$ s, The holes are transferred from base to base also at several $10^{-15}$ s. It is difficult to distinguish to which molecules the hole will be transferred. The excited ion $^{125m}$Te can extract electrons from its own outer shells and release more Auger electrons or it may capture electrons from the neighboring or water molecules.

The mean pair-occurrence frequencies, $\bar{P}_{\alpha\beta}$, $\alpha$, $\beta$ = T, C, A, G, for the fraction of nearest-neighbor pairs $\alpha\beta$ occurring in the downward direction along the chain, and $_{\beta\alpha}\bar{P} = \bar{P}_{\beta\alpha}$ for $\alpha\beta$ pairs occurring in the upward direction (cf. Section 2.4.3) are used to describe the so-called average uniform DNA chain with parameters,

$$\lambda = \lambda_{\text{Av}}^{3'-5'} = \sum_\alpha \sum_\beta \bar{P}_{\alpha\beta} R_{\alpha\beta},$$

$$\mu = \mu_{\text{Av}}^{5'-3'} = \sum_\beta \sum_\alpha {}_{\beta\alpha}\bar{P} R_{\beta\alpha} = \sum_\beta \sum_\alpha \bar{P}_{\beta\alpha} R_{\beta\alpha}. \tag{3.1}$$
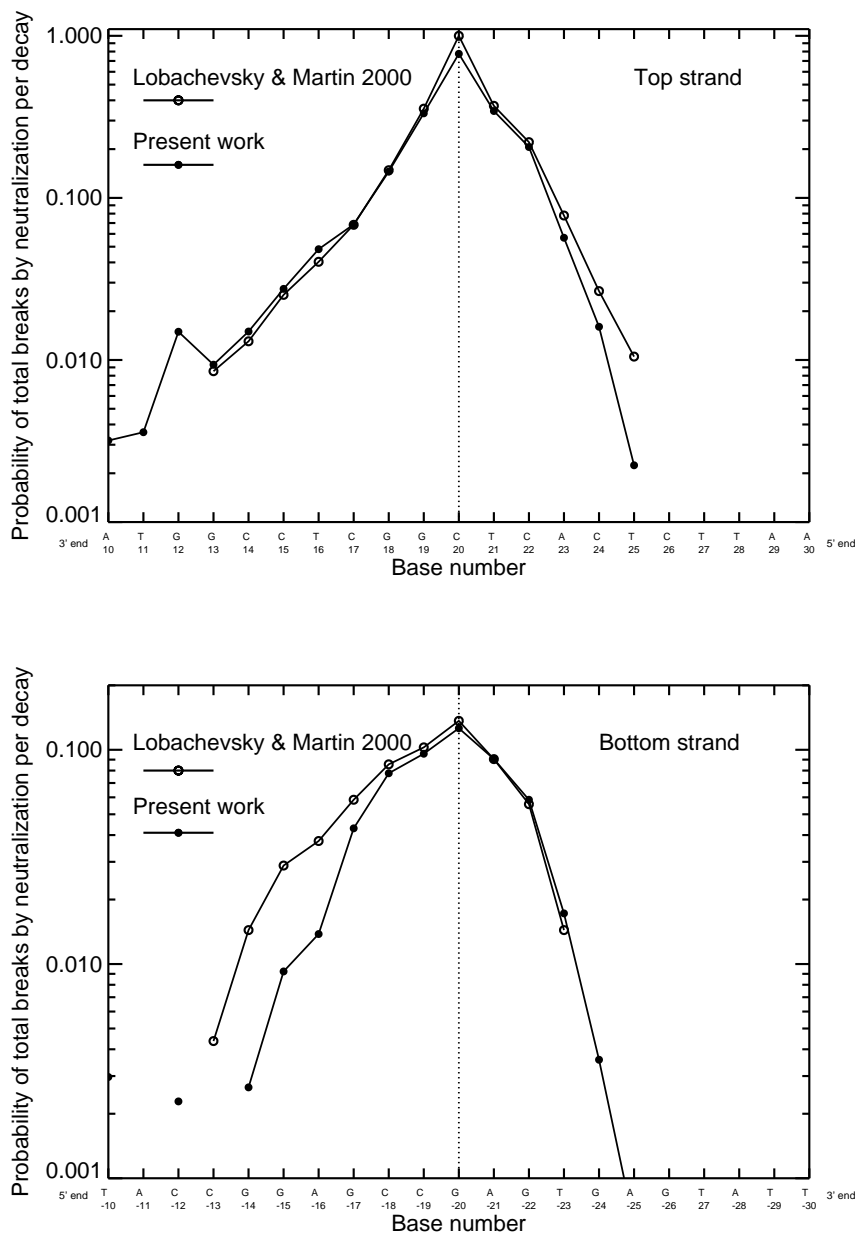
Figure 3.13: Calculated and experimentally derived probabilities of total strand breaks per ^{125}I decay by neutralization effect for 41-mer synthetic oligoDNA in the "top" (a) and in the "bottom" (b) strands

The frequencies $\bar{P}_{\alpha\beta}$ and $\bar{P}_{\beta\alpha}$ for the "top" strand of the 41-mer synthetic oligoDNA used in simulation were calculated and are listed in Table 3.2 and then the average transfer rate, $\lambda_{\mathrm{Av}}^{3'-5'}$ and $\mu_{\mathrm{Av}}^{5'-3'}$ are calculated to be the same $6.0\times10^{14}$ s$^{-1}$.

To calculate the $\Delta_{k,k\pm1}$ matrix the conditional probabilities $Pd_{\alpha\beta}$ and $Pu_{\alpha\beta}$ that a base $\beta$ follow a base $\alpha$ in the forward and backward directions respectively are needed:

$$Pd_{\alpha\beta} = \bar{P}_{\alpha\beta}/P_{\alpha},$$
$$Pu_{\beta\alpha} = \bar{P}_{\beta\alpha}/P_{\beta}, \tag{3.2}$$

where $P_{\alpha}$ and $P_{\beta}$ are the fractions of base of type $\alpha$ or $\beta$. In simulation the base cytosine is located by $^{125}$ atom and is considered as the excitation origin; for convenience of discussion, this cytosine base is set at position zero. the probabilities finding a base $\alpha$ =T, C, A, G at position 1 can be expressed by matrix $Pd_{C\alpha} = (Pd_{CT}\ Pd_{CC}\ Pd_{CA}\ Pd_{CG})$ and a base at position $-1$ by $Pu_{C\alpha} = (Pu_{CT}\ Pu_{CC}\ Pu_{CA}\ Pu_{CG})$. The conditional occurrence probabilities for finding a base $\beta$ at position 2 and $-2$ when base $\alpha$ at zero will be matrix $Pd_{C\alpha\beta}$ and $Pu_{C\alpha\beta}$:

$$Pd_{C\alpha\beta} = (Pd_{CT}\ Pd_{CC}\ Pd_{CA}\ Pd_{CG})\begin{pmatrix} Pd_{TT} & Pd_{TC} & Pd_{TA} & Pd_{TG} \\ Pd_{CT} & Pd_{CC} & Pd_{CA} & Pd_{CG} \\ Pd_{AT} & Pd_{AC} & Pd_{AA} & Pd_{AG} \\ Pd_{GT} & Pd_{GC} & Pd_{GA} & Pd_{GG} \end{pmatrix},$$

$$Pu_{C\alpha\beta} = (Pu_{CT}\ Pu_{CC}\ Pu_{CA}\ Pu_{CG})\begin{pmatrix} Pu_{TT} & Pu_{TC} & Pu_{TA} & Pu_{TG} \\ Pu_{CT} & Pu_{CC} & Pu_{CA} & Pu_{CG} \\ Pu_{AT} & Pu_{AC} & Pu_{AA} & Pu_{AG} \\ Pu_{GT} & Pu_{GC} & Pu_{GA} & Pu_{GG} \end{pmatrix}. \tag{3.3}$$

In the same approach the matrix $Pd_{C\alpha\beta\gamma...}$ and $Pu_{C\alpha\beta\gamma...}$ can be calculated. These DNA statistical parameters for the 41-mer synthetic oligoDNA are listed in Table 3.2.

The transfer rates from position zero to positions $\pm1$ ($\lambda_0$ and $\mu_0$), and from positions $\pm1$ to postions $\pm2$ ($\lambda_1$ and $\mu_1$) $\cdots$ can be calculated as

$$\lambda_0 = Pd_{C\alpha}\overline{k_{\alpha\beta}},$$
$$\mu_0 = Pu_{C\alpha}\overline{k_{\alpha\beta}},$$
$$\lambda_1 = Pd_{C\alpha\beta}\overline{k_{\beta\gamma}},$$
$$\mu_{-1} = Pu_{C\alpha\beta}\overline{k_{\beta\gamma}},$$
$$\vdots \tag{3.4}$$

where the $\overline{k_{\beta\gamma}}$ is the average transfer rate from base $\beta$ to base $\gamma$; it means that the transfer rate at position $n$ is the sum over all base types $\gamma$ of the probability that

| Base pair $(\alpha\beta)$ | $\bar{P}_{\alpha\beta}$ (3′–5′) | $Pd_{\alpha\beta}$ | Base pair $(\alpha\beta)$ | $\bar{P}_{\beta\alpha}$ (5′–3′) | $Pu_{\alpha\beta}$ |
|:---:|:---:|:---:|:---:|:---:|:---:|
| TT | 0.049 | 0.22 | TT | 0.049 | 0.22 |
| TC | 0.098 | 0.45 | TC | 0.146 | 0.67 |
| TA | 0.049 | 0.22 | TA | 0.024 | 0.11 |
| TG | 0.024 | 0.11 | TG | 0.0 | 0.0 |
|    |       |      |    |       |      |
| CT | 0.146 | 0.43 | CT | 0.098 | 0.29 |
| CC | 0.049 | 0.14 | CC | 0.049 | 0.14 |
| CA | 0.049 | 0.14 | CA | 0.122 | 0.36 |
| CG | 0.098 | 0.29 | CG | 0.073 | 0.21 |
|    |       |      |    |       |      |
| AT | 0.024 | 0.09 | AT | 0.049 | 0.18 |
| AC | 0.122 | 0.46 | AC | 0.049 | 0.18 |
| AA | 0.096 | 0.36 | AA | 0.098 | 0.37 |
| AG | 0.024 | 0.09 | AG | 0.073 | 0.27 |
|    |       |      |    |       |      |
| GT | 0.0 | 0.0 | GT | 0.024 | 0.14 |
| GC | 0.049 | 0.29 | GC | 0.073 | 0.43 |
| GA | 0.073 | 0.43 | GA | 0.024 | 0.14 |
| GG | 0.049 | 0.29 | GG | 0.049 | 0.29 |

Table 3.2: Mean base-pair occurrence frequencies $\bar{P}_{\alpha\beta}$ and conditional probabilities $Pd_{\alpha\beta}$ in the "top" strand in forward direction (3′–5′) and $\bar{P}_{\beta\alpha}$, $Pu_{\alpha\beta}$ in backward directions (5′–3′) for 41-mer synthetic oligoDNA

| Site $k$ | $-5$ | $-4$ | $-3$ | $-2$ | $-1$ | $0$ |
|---|---|---|---|---|---|---|
| $\Delta_{k,k+1}$ | 0.0525 | 0.0545 | 0.0452 | 0.08 | -0.341 | -0.207 |
| $\Delta_{k,k-1}$ | -0.023 | -0.023 | -0.023 | -0.023 | -0.026 | -0.123 |
| Site $k$ | 5 | 4 | 3 | 2 | 1 | |
| $\Delta_{k,k+1}$ | -0.0356 | -0.0345 | -0.0360 | -0.0272 | -0.0614 | |
| $\Delta_{k,k-1}$ | 0.0522 | 0.055 | 0.046 | 0.0881 | -0.524 | |

Table 3.3: The matrix $\Delta$ ($\times 10^{14}$) for hole transfer in 41-mer synthetic oligoDNA

a base of type $\gamma$ is at position $n$ mutilply by the average transfer rate from base $\gamma$ to all other four bases. The perturbation matrix $\Delta_{k,k\pm1}$ can be obtained and are shown in Table 3.3.

$$\Delta_{k,k+1} = \lambda_k - \lambda_{AV},$$
$$\Delta_{k,k-1} = \mu_k - \mu_{AV}. \qquad (3.5)$$

The charge transfer probability distribution after the first jump time at $1.7\times10^{-15}$ and $3.4\times10^{-14}$ s with this average transfer rate parameter after taking into account the matrix perturbation in the "top" strand of the 41-mer synthetic oligoDNA is presented in Figure 3.14. It is found that the probability distributions are nearly symmetric with respect to the zero position, since the average forward and backward hole transfer rates for cytosine are similar.

As is pointed out before, the first Auger cascade finishes at time $\sim 10^{-15}$ s, and the second cascade comes at time $1.6\times10^{-9}$ s, if the hole transfer rates above is suitable for the charge transfer phenomenon resulted from $^{125}$I decay, the charge built up on the daughter ion $^{125}$Te will never be beyond 10 [Pom02], the half of the total charges 21, corresponding 21 electrons released in $^{125}$I decay in condensed phase. From Equation 2.1, the ionization potential energy $\eta_n = 820$ eV corresponding to 10 positive charges [BPPO87] was used in the present study.

Kelley and Barton [KB99] reported that H-bond-mediated interstrand connection between $A_2$ and its complementary thymine is an important component in the overall electron transfer pathway for the interstrand reaction. Xu and Nordlund [XN00] calculated from their measured data and found out that a maximum of 7.7% of excitation energy transferred from one base in one strand into the complementary base in the opposite strand. In the present study, 7.7% of ionization potential energy is distributed from the "top" strand into the "bottom" strand. With more than 100 eV potential energy, the base moiety will be collapsed, but this energy will

| Base number | 3'-end      | 15     | 16    | 17    | 18    | 19    | 20   |
|-------------|-------------|--------|-------|-------|-------|-------|------|
| "Top"       | Energy (eV) | 2.0    | 10.4  | 43.6  | 141.1 | 325.9 | 467  |
|             | SSBs        | 0.003  | 0.018 | 0.07  | 0.2   | 0.5   | 0.8  |
| "Bottom"    | Energy (eV) | 0.2    | 0.9   | 3.6   | 11.8  | 27.2  | 39   |
|             | SSB         | <0.001 | 0.003 | 0.012 | 0.04  | 0.09  | 0.15 |

Table 3.4: Ionization potential energy deposited in bases in the "top" and in the "bottom" strands and estimated induced DNA strand breaks in both strand for 41-mer synthetic oligoDNA

also ionize the the sugar and phosphate groups and lead to strand breaks. Scaling the charge distribution at $1.7 \times 10^{-15}$ s to the simulation results in Figure 3.15, one obtains the energy deposited in each base in both strands and the strand break probability listed in Table 3.4. The calculation shows that 1 eV energy deposited inside a nucleotide base will make strand breaks with a probability of 0.2%.

Following the charge transfer theory of Marcus and Jortner (cf. Section 2.4.3), the hole transfer rates can be calculated using Equations 2.11 and 2.10, and results are listed together with that calculated by Dee and Baur in Table 3.5. Generally the newly calculated hole transfer rates are 100-fold less than those of Dee and Baur [DB74]. According to the Marcus and Jortner theory those rates from base G to other bases are almost negligible. From the experimentally measured data (cf. Figure 3.13), one sees no trapping in the G bases (number "18" and "19" to the 3'-end direction). In the same time one should keep in mind that this theory is derived for one electron or hole transfer in the DNA chain; whether it applies to the $^{125m}$Te with 10 charges is still a question. Other methods such as Drift-Diffusion equation in the current transport theory might be a next try, in view of the multiple hole transfer through the DNA chain [Ins96].

## 3.2   Comparison with Experimental Data

Because only the fragment size distribution can be measured in experiments [KZG$^+$99], [LM00a], the simulated data were plotted from different $^{32}$P-labeled ends for CAP-DNA, free B-DNA and 41-mer synthetic oligoDNA and compared with experimentally measured results.

| Base pair | $k_{\alpha\beta}\dagger$ | $k_{\alpha\beta}\ddagger$ | Base pair | $k_{\alpha\beta}\dagger$ | $k_{\alpha\beta}\ddagger$ |
|-----------|------------|------------|-----------|------------|------------|
| TT | $5.5\times10^{14}$ | $3.5\times10^{12}$ | AT | $2.9\times10^{14}$ | $7.9\times10^{10}$ |
| TC | $13.0\times10^{14}$ | $8.5\times10^{11}$ | AC | $6.1\times10^{14}$ | $2.0\times10^{10}$ |
| TA | $9.0\times10^{14}$ | $1.5\times10^{13}$ | AA | $3.0\times10^{14}$ | $1.8\times10^{11}$ |
| TG | $9.8\times10^{14}$ | $1.5\times10^{14}$ | AG | $1.7\times10^{14}$ | $4.0\times10^{13}$ |
| | | | | | |
| CT | $3.2\times10^{14}$ | $9.0\times10^{12}$ | GT | $4.1\times10^{14}$ | $6.5\times10^{3}$ |
| CC | $10.0\times10^{14}$ | $1.7\times10^{12}$ | GC | $6.2\times10^{14}$ | $6.9\times10^{2}$ |
| CA | $5.8\times10^{14}$ | $6.0\times10^{12}$ | GA | $6.3\times10^{14}$ | $1.2\times10^{6}$ |
| CG | $3.9\times10^{14}$ | $3.2\times10^{13}$ | GG | $5.2\times10^{14}$ | $1.9\times10^{11}$ |

Table 3.5: Hole transfer rates, $k_{\alpha\beta}$ (in s$^{-1}$), between bases calculated by Dee and Baur$\dagger$ and in the present work$\ddagger$
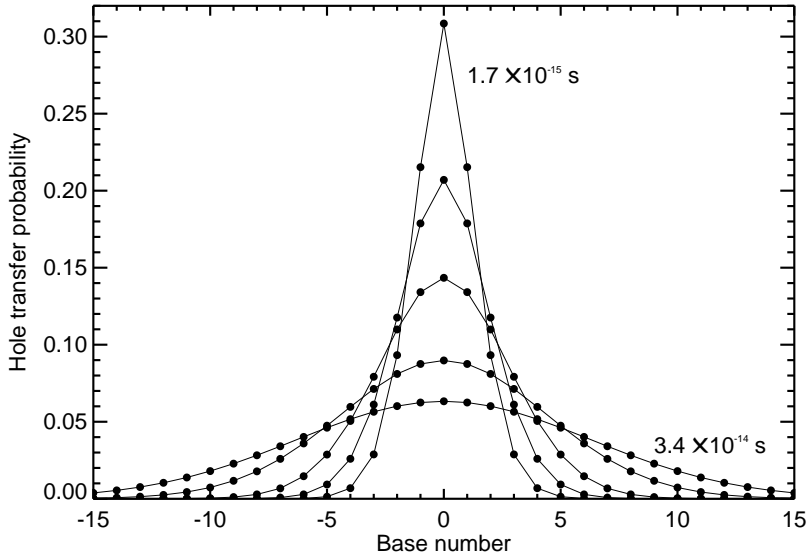


Figure 3.14: Calculated positive charge transfer probability distribution for 41-mer synthetic oligoDNA in the "top" strand from first jump time, $1.7\times10^{-15}$ s over 2, 4 and 10 jumps to 20 jump times at time $3.4\times10^{-14}$ s
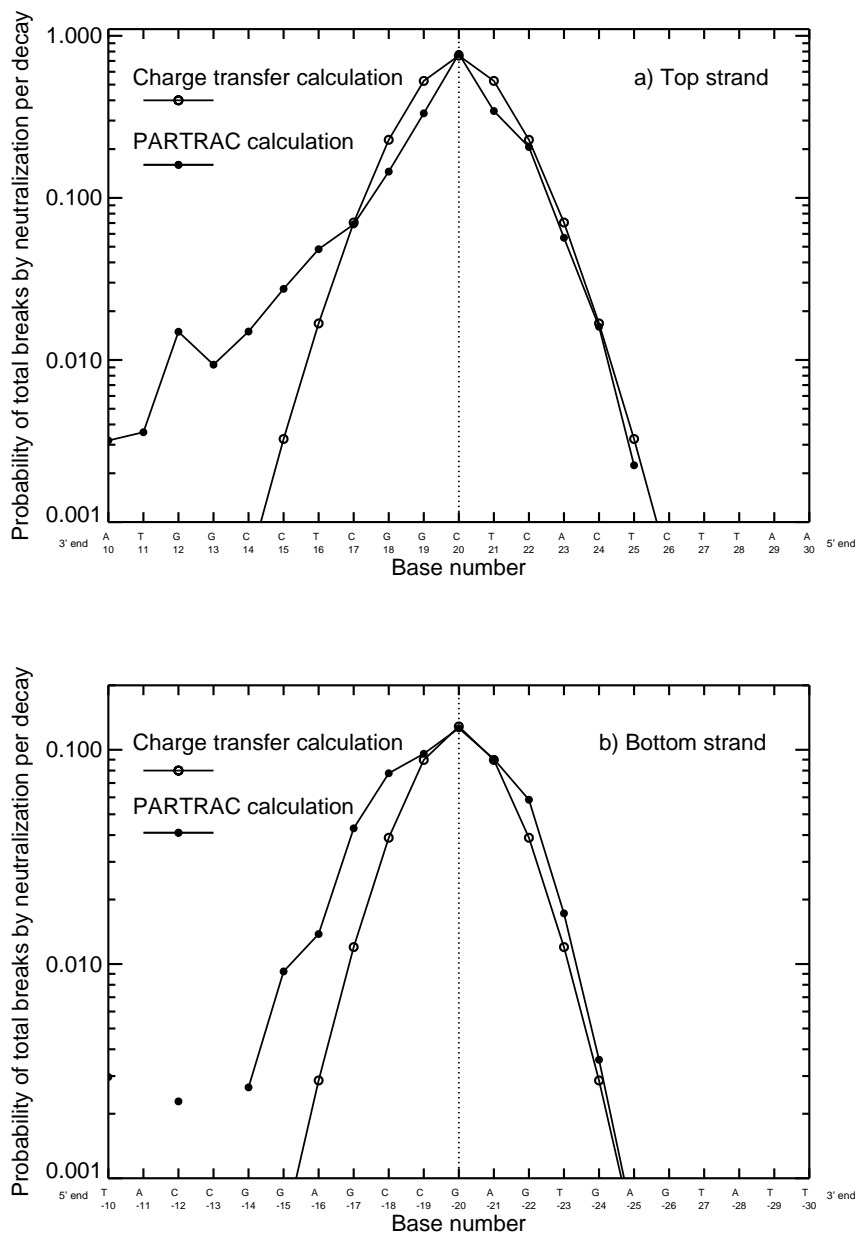
Figure 3.15: Comparison of total DNA strand breaks induced by neutralization per ^{125}I decay between Monte Carlo simulation and charge transfer calculation for 41-mer synthetic oligoDNA in the "top" strand (a) and in the "bottom" strand (b)

### 3.2.1 Fragment Size Distribution

**41-mer Synthetic OligoDNA**

Comparison was made first on the fragment size distribution for 41-mer synthetic oligoDNA in PB solution with full DMSO, which means that only strand breaks contributed from physical tracks and neutralization effect was considered for reducing the uncertainty resulting from chemical radicals attacks. From the data of the "top" strand shown in Figure 3.16, for both $^{32}$P-labeled 5'- and 3'-ends, the simulation results are always less than the experimental data inside $\sim 7$ base nucleotides from the decay site, and in the "bottom" strand (Figure 3.17), only inside $\sim 4$ base nucleotides from the decay site. Beyond 7 bases in the "top" strand and 4 bases in the "bottom" strand, the simulation data agree well with the measured data. This agreement between the simulation and experiment indicates that the physical tracks module of the PARTRAC code is very refined. To test the chemistry module (cf. Appendix A.3) of the PARTRAC code, comparison of results in PB solution without DMSO was plotted in Figure 3.18 for the "top" strand and in Figure 3.19 for the "bottom" strand. The scavenging capacity of $\sigma = 5 \times 10^4$ s$^{-1}$ [KBR74] was used. Except the $6 \sim 7$ bases from the $^{125}$I located site, simulated fragment size distributions from both $^{32}$P-labeled ends agree very well with experimental data in the "top" strand (Figure 3.18); in the "bottom" strand, one sees the agreement between simulation and experiment beyond the $3 \sim 4$ bases from the decay site. Results proved the methods and parameters used in the modeling of radiation chemicals attacks to DNA in the PARTRAC code. It is concluded that the simulated radiation non-scavengeable component results can be used, in combination with the experimental data, to evaluate DNA strand breaks by the neutralization effect more precisely (cf. Section 3.1.4).

**CAP-DNA and Free B-DNA**

The initial concept of the present work is to test and confirm that whether the measured fragment size distribution of CAP-DNA can be used as a radioprobing for the DNA distortion such as DNA kicks like other chemical and biological assays. Thus, the simulation data before and after taking into account the neutralization effect were compared in Figures 3.20 and 3.22.

The simulated data plotted in Figure 3.20 concern radiation-induced strand breaks without neutralization effect. The simulated frequency is $\sim 30\%$ less in the "top" and in the "bottom" strands than the measured data which were plotted after considering 13 days of exposure, a time during which only 14% of the $^{125}$I atom has decayed. In the "top" strand the shape between simulation and experiment is similar, however the shape of the curve in the "bottom" strand is quite different. Figure

| Endpoint | Contribution | Experiment | Simulation |
|----------|--------------|------------|------------|
| SSBs | Neutralization | 3.02 (2.37, 0.65) | - |
|  | Radiation nonscavengeable | 1.99 (1.24, 0.75) | 1.86 (1.08, 0.79) |
|  | Radiation scavengeable | 1.11 (0.68, 0.43) | 0.96 (0.56, 0.40) |
| DSBs | All contributions | 0.8 | - |
|  | Radiation only | - | 0.55 |

Table 3.6: Comparison of average number of DNA strand breaks between experiment and simulation for 41-mer synthetic oligoDNA. The first and second numbers in the parentheses denote the fraction in the "top" and in the "bottom" strands, respectively

3.21 is presented here to give a comprehension picture of total strand breaks from different components: radiation with and without scavenger, radiation scavengeable effect and neutralization effect.

In experiment the fragment size distribution is directly measured and included already the neutralization effect. In simulation the total DNA strand breaks were first obtained directly by performing PARTRAC, which does not include neutralization effect, and by adding the total strand breaks by neutralization component derived in Section 3.1.4. The fragment size distribution with neutralization component is recalculated by Equation 2.3 and is showed in Figure 3.22, in this Figure the experimental data are also scaled according to the measurement efficiency (cf. the cumulative distribution of fragment size distribution per decay in Figure 3.23). After including the neutralization component in simulated data the fragment size distributions agree well with measured data by Karamychev et al. [KZG$^+$99].

### 3.2.2  Yields of Single and Double Strand Breaks

The yields of SSBs and DSBs from different contribution for 41-mer synthetic oligoDNA are listed in Table 3.6. The DSBs contributed from neutralization effect per $^{125}$I decay is estimated to be $0.8 - 0.5 \approx 0.3$. The result is valid also for plasmid and cellular DNA. The values $0.8 \sim 1.0$ for DSBs and 4.2 for SSBs per $^{125}$I decay simulated previously [CH88], [Pom91], [PT94] are a little larger since they do not include the neutralization effect as measured in experiments [MH81], [LL84].

## 3.3  Discussions

In the present study, the $^{125}$I atom is always considered to be incorporated into pyrimidine of DNA molecules, i.e. replacing the H$_5$ atom in cytosine and the methyl
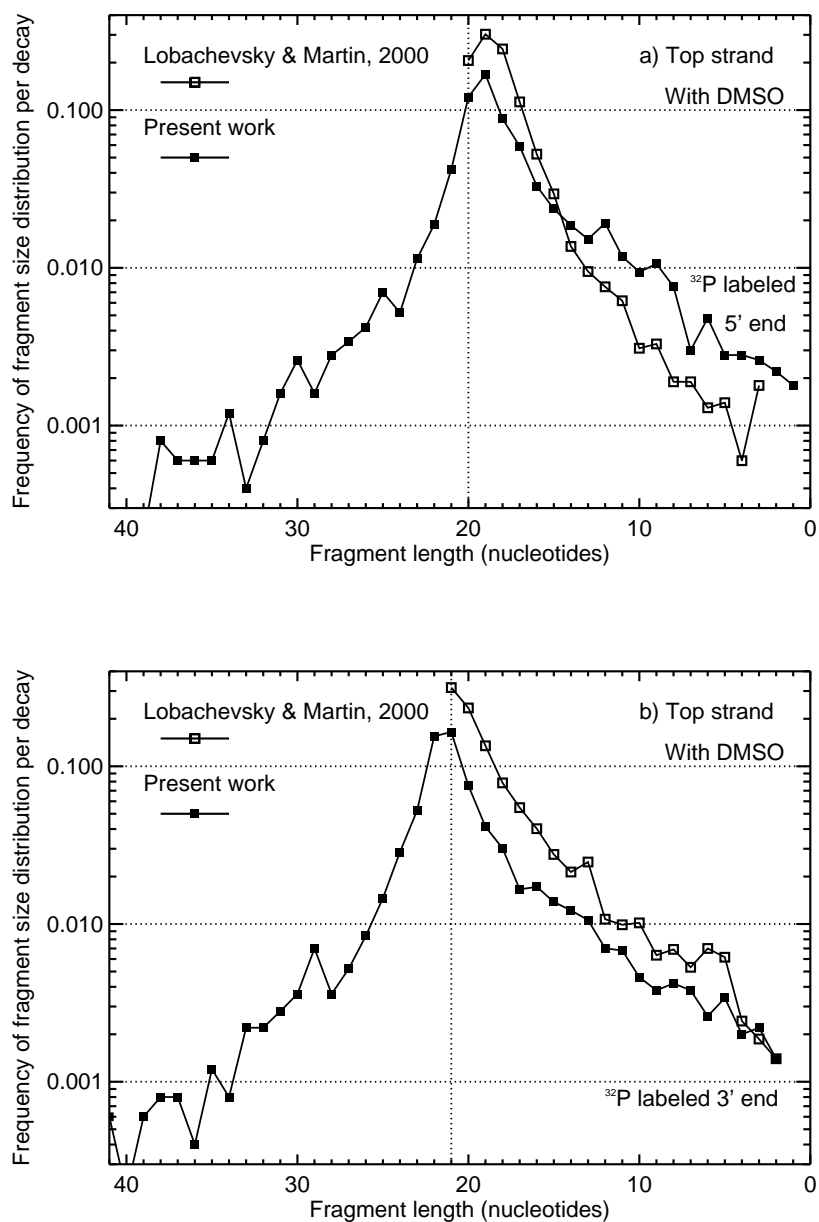
Figure 3.16: Comparison of fragment size distribution from ^{32}P-labeled end per ^{125}I decay between simulation and measurement for 41-mer synthetic oligoDNA in the "top" strand from 5′-end (a) and 3′-end (b) in PB solution with full DMSO
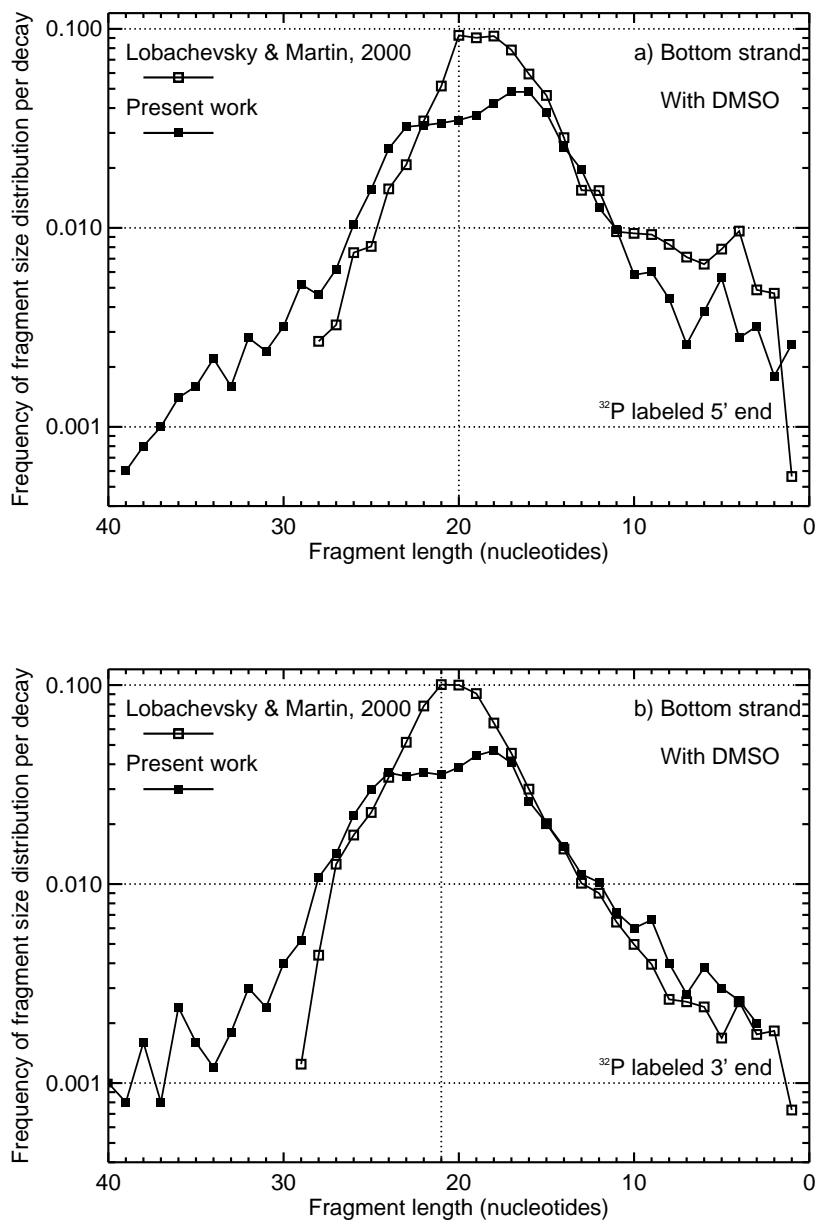
Figure 3.17: Comparison of the fragment size distribution from ^{32}P-labeled end per ^{125}I decay between simulation and measurement for 41-mer synthetic oligoDNA in the "bottom" strand from 5'-end (a) and 3'-end (b) in PB solution with full DMSO
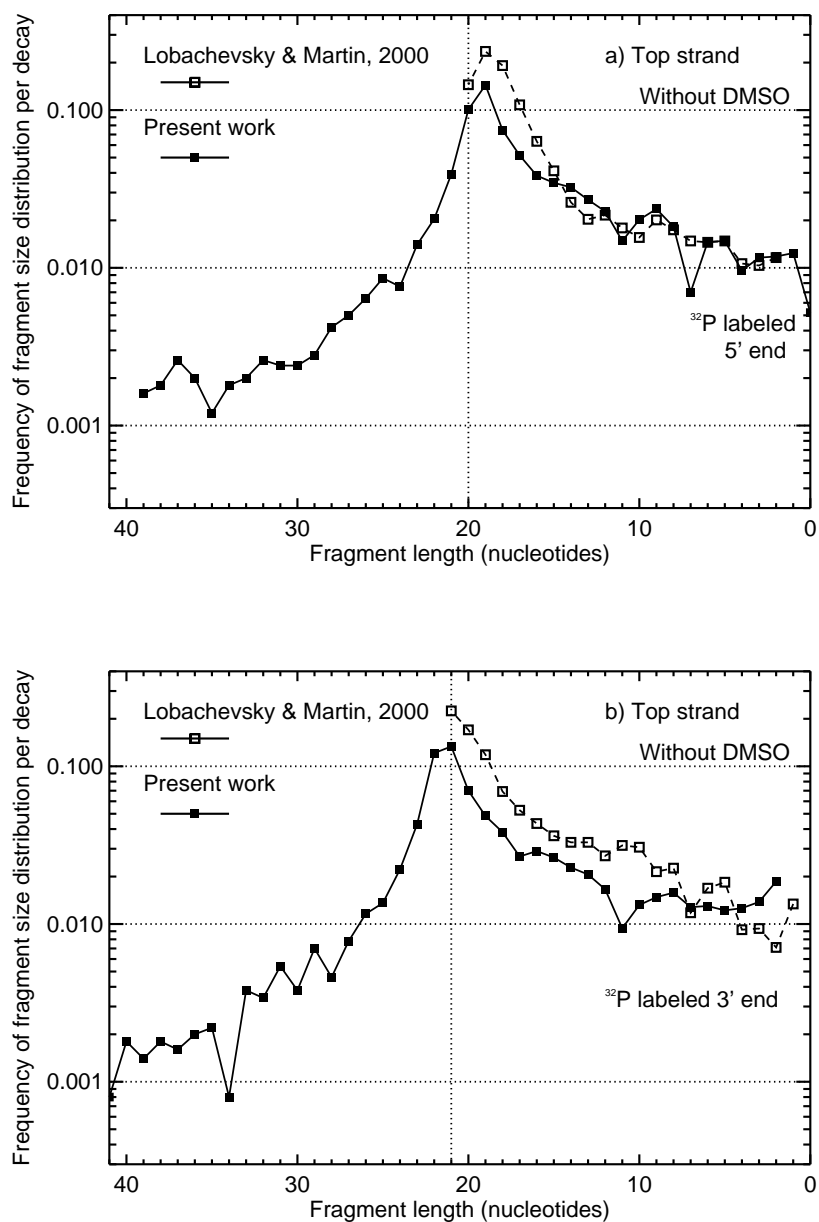
Figure 3.18: Comparison of the fragment size distribution from ^{32}P-labeled end per ^{125}I decay between simulation and measurement for 41-mer synthetic oligoDNA in the "top" strand from 5′-end (a) and 3′-end (b) in PB solution without DMSO
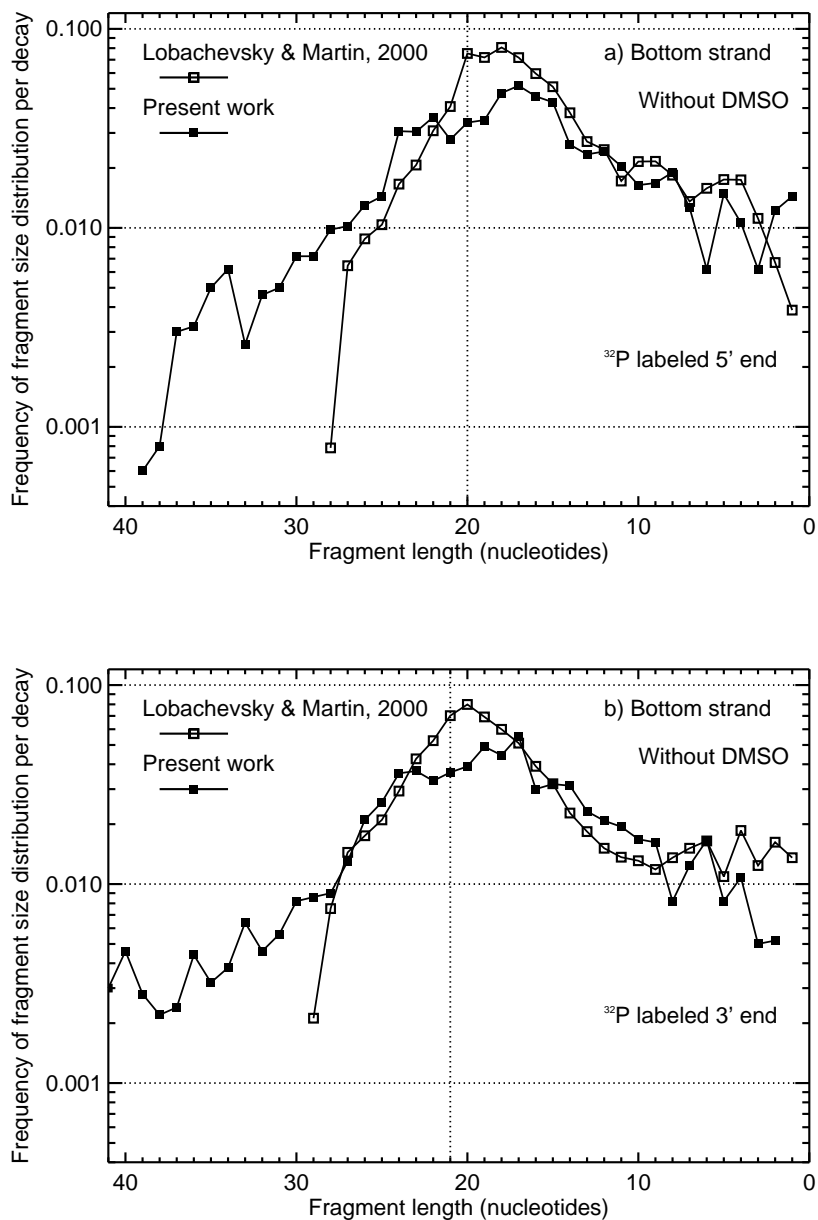
Figure 3.19: Comparison of the fragment size distribution from ^{32}P-labeled end per ^{125}I decay between simulation and measurement for 41-mer synthetic oligoDNA in the "bottom" strand from 5′-end (a) and 3′-end (b) in PB solution without DMSO
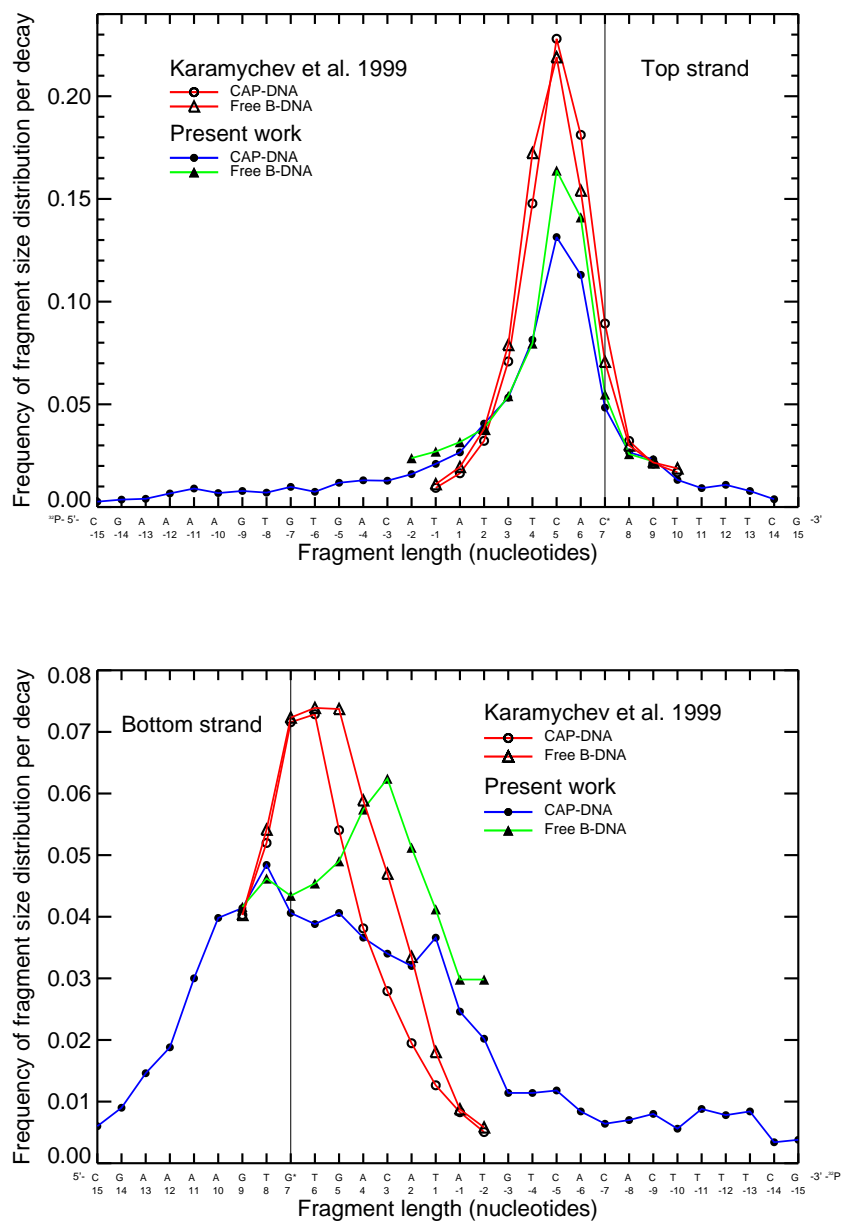
Figure 3.20: Comparison of the fragment size distribution from $^{32}$P-labeled end per $^{125}$I decay between simulation and measurement for CAP-DNA and free B-DNA before taking into account the neutralization effect
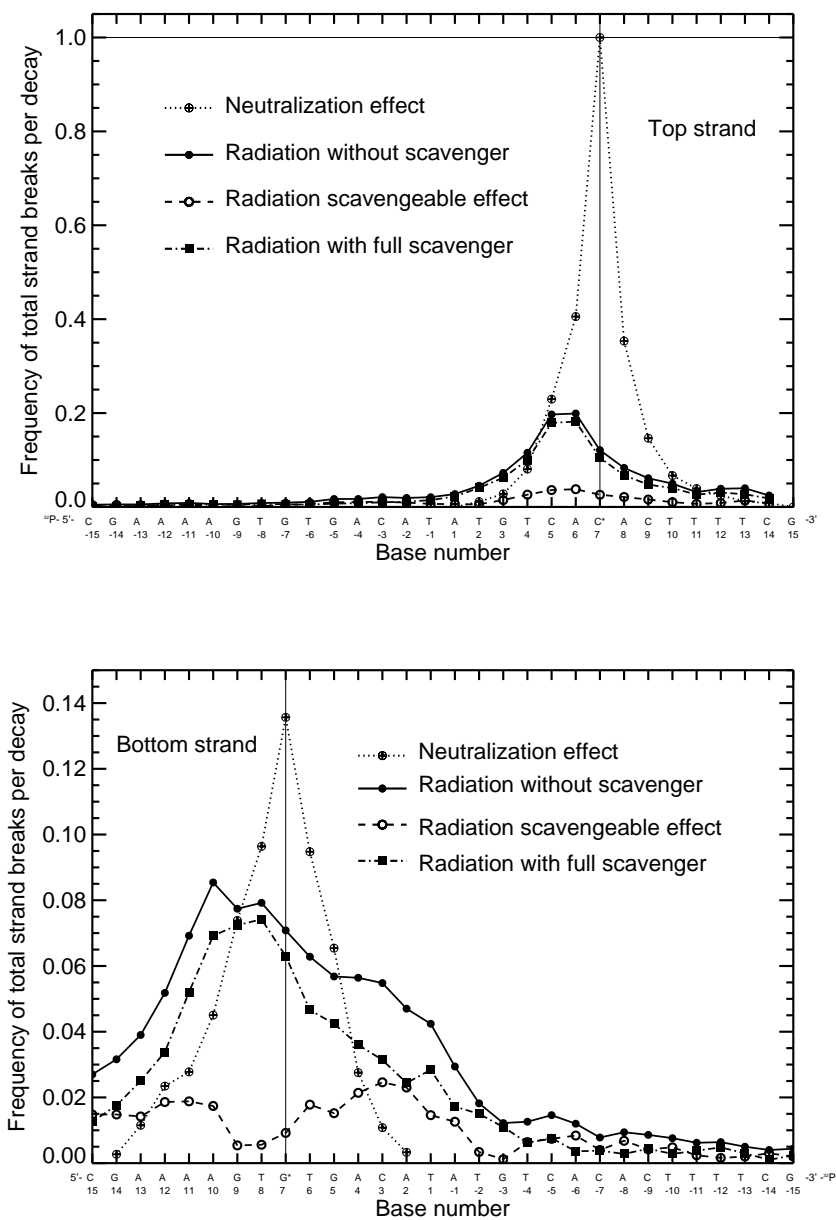
Figure 3.21:  Contribution of different components to the frequency distribution of total strand breaks per ^{125}I decay for CAP-DNA
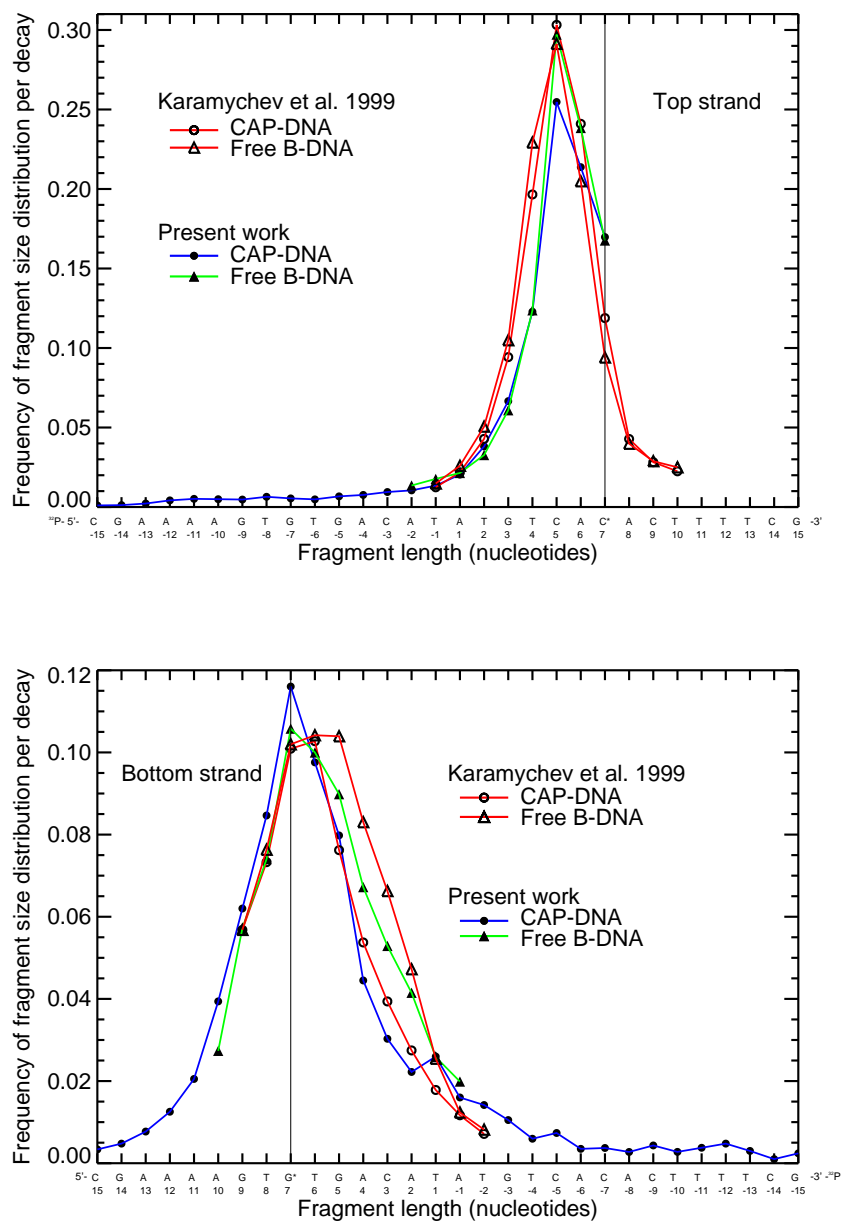
Figure 3.22: Comparison of the fragment size distribution from $^{32}$P-labeled end per $^{125}$I decay between simulation and measurement for CAP-DNA and free B-DNA after taking into account the neutralization effect
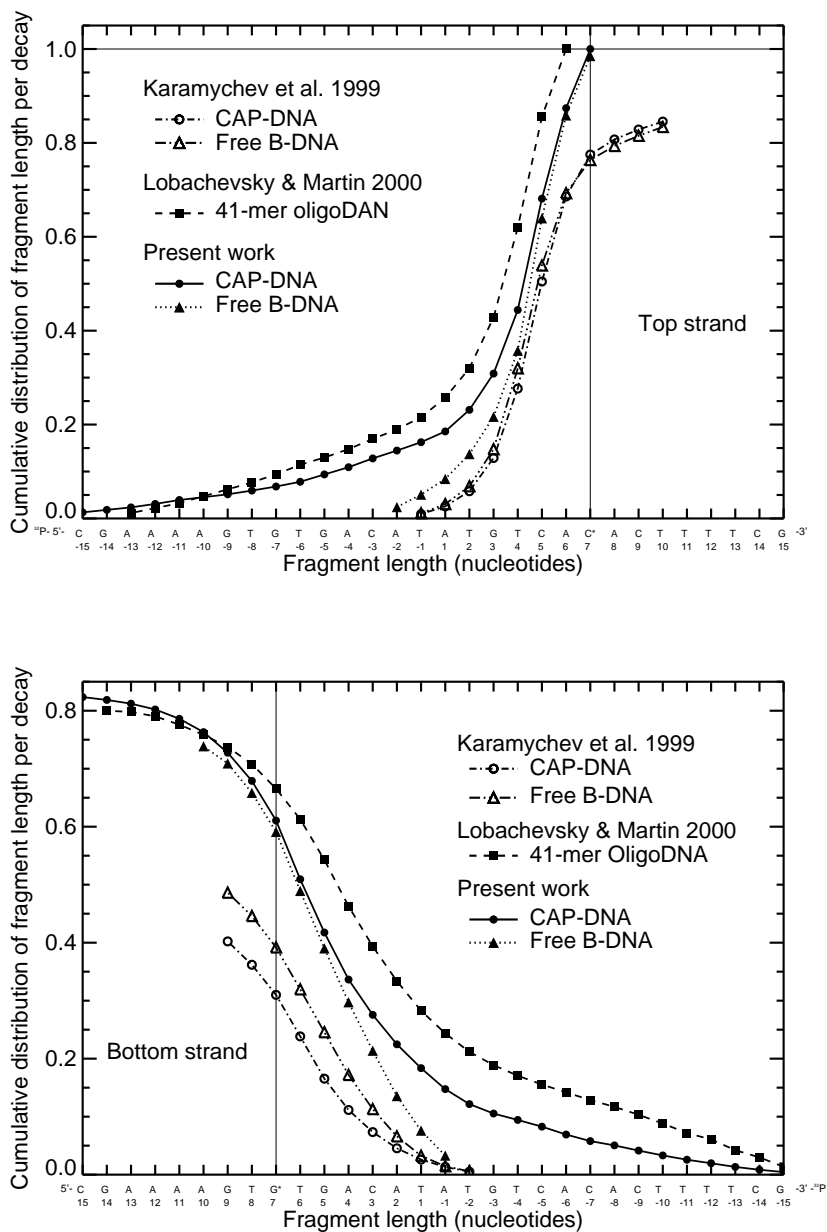
Figure 3.23: Comparison of the cumulative distribution of fragment size from $^{32}$P-labeled end per $^{125}$I decay between simulation and measurement for CAP-DNA, free B-DNA and 41-mer synthetic oligoDNA after taking into account the neutralization effect

group $CH_3$ in thymine and bonding to $C_5$ atom (cf. Figure 2.7), and the environment of DNA molecules is assumed to be surrounded by water molecules. This presupposition is emphasized here just to distinguish the case of $^{125}I$ atom decaying in isolation or in gaseous phase, where the molecules are in collision-free space and the molecule virtually explodes due to highly charged regions repelling one another under the coulombic forces; this phenomenon is known in literature as "Coulomb explosion".

In the present study the disintegration of an $^{125}I$ atom is newly considered according to the timing of decay scheme and the charge transfer rate as follows: The iodine is transmuted first to excited-state tellurium when an $^{125}I$ atom decays, about 10 electrons are released in the first Auger cascade process, the multiple charged $^{125m}Te$ could be neutralized at $10^{-15} \sim 10^{-12}$ s depending on the adoption of transfer rates by extraction of electron from neigboring DNA and/or water molecules before the second Auger cascade begins at $1.6\times10^{-9}$ s; during the latter cascade, another 10 electrons will be emitted and another neutralization procedure will be complete.

The physical mechanisms of the decay are well understood and the transport of Auger electrons in liquid water can be described by Monte Carlo technique. However, the mechanisms of the neutralization procedures in the two Auger cascades are not fully understood. The key question is how fast the holes will move from the $^{125m}Te$ atom to an other molecule. In a short time, i.e. $10^{-15} \sim 10^{-12}$ s, the extraction of 10 electrons from neighboring DNA and water molecules to the $^{125m}Te$ atom ionizes those DNA molecules and may lead to base damage and strand breaks; the ionized or excited water molecules can also interact with DNA molecule and make damage. For a long time, simulation of $^{125}I$-induced DNA strand breaks concentrates on radiation interaction with DNA with some extra ionization potential energy deposits around the decay site to mimic the neutralization effect.

By simulation and comparison of the fragment size distribution of CAP-DNA with experimental data, it is found that the simulated fragment size distributions on both strands are about 30% less than the measured data. At the same time comparison between the simulated fragment size distribution and the total strand breaks probability of the 41-mer synthetic oligoDNA with the experimental data has shown that strand breaks by neutralization effect is of the same oder of magnitude as that induced by radiation only. The fragment size distribution and total strand breaks probability calculated by the available track structure model, PARTRAC code, are smaller than experimental data. From these observations it is substantiated that the biophysical simulation code–PARTRAC is a refined Monte Carlo radiation track structure simulation program for modeling the irradiation transport in liquid water; this code also describes the migration and diffusion of the chemical radicals produced by radiation in liquid water.

The agreement of the fragment size distribution between the simulations and the experiments [CH88], [MH81], [NMC+96], [KLDM96], [NLT+00], [NPT+00] stimulated us for a time to try to find out the reason why our simulated results with PARTRAC code were always less than the experimentally measured data. The series work of the Stöcklin group [DS81], [LS85] and their charge transfer explanation produced by heavily charged daughter ion $^{125m}$Te led our attention to the work of Halpern et al. [RHS88], [Hal90]. Meantime Lobachevsky and Martin reported the fragment size distributions from $^{32}$P-labeled 3'- and 5'-ends on both strands with and without DMSO [LM00a], and derived from a simple model based on their measured data the total strand breaks induced from different components. Thus, they demonstrated that the total strand breaks by neutralization effect constitute about 50% in the whole strand breaks by DNA incorporated-$^{125}$I. The agreement between our simulated physical-tracks-induced fragment size distribution with the measured data with full DMSO allowed us to evaluated the total strand breaks by neutralization effects.

Our evaluation of the DNA total strand breaks including neutralization effect of $^{125m}$Te for short piece of DNA can be used to estimate the portion of DNA strand breakage in plasmid und cellular environment when $^{125}$I incorporated into DNA molecule. However, the underlying mechanism is still not fully understood. The charge transfer calculations give us some hints that the charge cumulative on $^{125m}$Te atom will not exceed 10 because the charge may be redistributed to other bases or water molecules at least $10^{-10}$ s before the second Auger cascade at $1.6 \times 10^{-9}$ s.

If the agreement of the total strand breaks calculated with the hole transfer rates of Dee and Baur [DB74] with the simulation-experiment derived data is reasonable (cf. Figure 3.14), then the charge transfer from $^{125m}$Te to other bases and water molecules are of the oder of $10^{-15}$ s, faster even than the molecular vibration period ($10^{-14} \sim 10^{-13}$ s); such a fast transfer phenomenon is difficult to understand physically.

According the calculated hole transfer rate using the Marcus and Jortner theory, the hole will be transfer in a period of the oder of $10^{-2}$ s. However, according to their theory, it is not allowed for hole from base G to transfer to other bases, in contradiction to the measured data. Bearing in mind that the charge transfer rates of Dee and Baur [DB74], and of Marcus and Jortner are based on one charge calculation, it should be reasonable to modify the charge transfer theory for multiple charge/electrons process from the point of view of quantum chemistry.

# Chapter 4

# Summary

By virtue of low-energy Auger electrons emitted in its decays, radioisotope $^{125}$I has a high potential in applications in nuclear medicine, e.g. diagnostics, therapeutics and radiopharmaceuticals. Experimental studies show that the radionuclide distributions at cellular and subcellular levels within tumors are needed for cancer therapy. Radiation microdosimetry shows that the dose distribution of the low-energy Auger electrons in tumors is highly inhomogeneous. Oligonucleotides targeting agents, e.g. $^{125}$IUdR attack specific nucleotide sequences in the genome of cancer cells. Radiobiological studies found an extremely high radiotoxicity of $^{125}$I when it is incorporated into DNA. The toxic damage to DNA results not only from excitation and ionization by low-energy Auger electrons but also from the neutralization of the highly positive charged daughter ion $^{125m}$Te with thermal electrons.

Recently, an attempt has been made by Karamychev et al. [KZG$^+$99] to analyze the DNA kinks in a protein-DNA complex with $^{125}$I-induced DNA strand breakage. For comparison, a free B-DNA was also studied. Notice that the $^{125}$I can be used for radio-probing and identifying DNA distortions, provided that the idea has been tested and confirmed, e.g. in a corresponding theoretical simulation. The present work contributes to this analysis. The catabolite gene activator protein (CAP) or cAMP receptor protein (CRP) of the CAP-DNA complex is connected with a specific sequence of 30 base pairs in DNA, and the same complex indicates that the DNA is bent by $90°$. The $^{125}$I atom is incorporated into the position of the $H_5$ atom of the cytosine near the center of the DNA. In experiments only the fragment size distribution from the $^{32}$P-labeled end can be measured. Results of the present work for fragment size distribution calculated with the biophysical simulation code, PARTRAC, (i.e. without accounting for neutralization effect) are about 30% less than the experimental data for both CAP-DNA and the free B-DNA.

Lobachevsky and Martin [LM00a], [LM00b] measured the number of strand breaks induced in a 41-mer synthetic oligoDNA by $^{125}$I decay, analyzed their results

using a simple model, and concluded that 50 percent of the DNA strand breaks were attributable to the neutralization of multiply charged daughter ions of $^{125m}$Te. Detailed track structure simulations of the present work led to a yield of strand breaks in the oligoDNA also less than experimental results, especially near the $^{125}$I decay site. The difference between the total number of strand breaks, derived from experiment, and the results of the track structure simulations can be interpreted to represent contributions from the neutralization effect; it amounts to nearly the same fraction as Lobachevsky and Martin [LM00a], [LM00b] stated. Thus, the present work confirms their conclusion on a much firmer basis.

A moral of the present study is that, also concerning the fragment size distribution, mere comparison between track effect simulations and experiments might overlook a non-radiation effect such as the neutralization effect and is in general insufficient for fully establishing a biophysical model for the action of DNA incorporated-$^{125}$I decay [CH88], [MH81], [NMC$^{+}$96], [KLDM96], [NLT$^{+}$00], [NPT$^{+}$00]. The total strand break probability should be the endpoint for comparison. After taking into account the neutralization component for CAP-DNA and B-DNA, the calculated fragment size distribution of the present work agrees well with the measured data [KZG$^{+}$99].

A theoretical calculation, independent of the above analysis, was also attempted to obtain the neutralization contribution using the charge transfer theory. Calculations based on the transfer rates given by Dee and Baur [DB74] show that the energy of 1 eV deposited inside a nucleotide will produce a strand break at the probability of 0.2%. This result gives a basic support to the importance of the neutralization in the interpretation of the total number of strand breaks discussed earlier. As known in the literature, the $^{125}$I nucleus decay occurs in two steps: first, into $^{125m}$Te with electron capture followed by the emission of about 10 Auger electrons in $10^{-15}$ s, and second, into $^{125}$Te in $1.6 \times 10^{-9}$ s followed by the emission of also about 10 electrons. The transfer rates [DB74] are of the order of magnitudes of $10^{15}$ s$^{-1}$, meaning that the atomic charge resulting from the nuclear decay stays for about $10^{-15}$ s, comparable to the first step and much shorter than the second step of the decay process. Thus, the calculations imply that a charge higher than 10 units will not build up on a $^{125m}$Te atom, because the potential energy deposited on the bases near a decay site, amounts to $40 \sim 400$ eV and will destroy those bases completely according to the hole transfer rates given by Dee and Baur [DB74].

Furthermore, a cellular DNA model and a simple pUC19 plasmid DNA model, both based on track structure calculations, were examined to evaluate the single and double strand breaks when $^{125}$I is incorporated into DNA. It is found that the results of previous simulations [CH88], [Pom91], [PT94], i.e. $0.8 \sim 1.0$ for DSBs and 4.2 for SSBs per decay, are too high since they did not include the neutralization

effect. The present study shows that only 0.5 of DSBs and 3 of SSBs per $^{125}$I decay can be obtained by direct and indirect radiation action from the simulation of track structures alone (i.e. without neutralization effect).

In conclusion, the present work has firmly established the crucial importance of the neutralization effect in the understanding of the total number of DNA strand breaks and of the fragment size distribution produced by $^{125}$I decays. However, further work remains to be carried out for clarifying precise chemo-physical mechanisms of the neutralization effect.

# Appendices

# Appendix A

# PARTRAC — The Biophysical Radiation Track Structure Simulation Code

For a review on general radiation track structure theory and details of the calculation, see ref. [Par87]. The PARTRAC code (PARticle TRACks) is based on the MOCA series of Monte Carlo simulation codes which were originally developed by Paretzke [Par74], [Par80] for understanding the radiation transport and energy deposition in matter and its action on radiation detectors and on biological matter. Many theoretical calculations were done on the cross sections of electron [Par88] and photon interaction with gaseous water which are needed for calculating radiation tracks, i.e. the $x$, $y$, $z$-coordinates of activation events at time $t$ in the target materials. After successfully applying the code to radiation induced chromosome aberrations in human cells [HP92], efforts were made to model the chromatin structure of the DNA [FJPS98], [FJP$^+$99] which is considered to be the main target of radiation damage in cells [vS87]. Interaction cross sections for liquid water were recently developed for electrons [DHIP98] and protons [DIP00]; the cross sections for $\alpha$-particles, heavy ions and for interactions with DNA are still under development.

To model radiation induced DNA damage, the mechanisms of DNA damage should be known. Radiation biology and chemistry have accumulated a huge amount of experimental data on DNA damage from which many yields for direct and indirect effects can be derived. The former are caused by the absorption of energy in the DNA molecule itself, the latter by chemical radicals produced by radiation in water which then diffuse to and act on the DNA. The PARTRAC code models the physical and chemical processes and allows to evaluate the yields of DNA strand breaks and fragment size distributions which are normally measured in experiments and indexed as the observed lesions. However, here certain assumptions on the conversion of

absorbed energy into new chemical species have to be made. In addition to modeling radiation damage to DNA in cells, the PARTRAC code has been used for a refined Monte Carlo approach to understand and to evaluate doses in nuclear medicine [LFP+01]. In the following, a short description of important modules in PARTRAC is presented according to the time scale [AJ80] given in Table A.1, To be consistent with the time scale implemented in PARTARC code, the chemistry stage is divided into physicochemical (i.e. pre-chemical) and chemical stages.

## A.1    Track Structure Module

The PARTRAC code can generate tracks of primary photons, electrons [FJP+99] and protons [FBJ+02] in liquid water. Essentially all energy from photons, high-energy electrons, a large fraction of the energy lost by fast ions and by neutrons is transferred to and transported in irradiated matter by secondary and higher generation electrons. Thus, electrons are of utmost importance for the production of track structures. A set of differential electron inelastic scattering cross sections in liquid water has been evaluated within the first Born approximation using five excitation levels (two electronic excitations $\tilde{A}^1B_1$ and $\tilde{B}^1A_1$, two Rydberg series Ryd A+B and Ryd C+D, and diffuse bands) and five ionization shells; electron-exchange effects and semiempirical corrections to account for non-Born effects at low energies have also been incorporated [DHIP98]. With these cross sections for the model substance "liquid water" the electron track structures are calculated also for organic materials like cells and cell nuclei. The electron energy-loss in solid, dry DNA is very similar to that in liquid water [LP95]; thus, the track structure simulation in liquid water is expected to be a reasonable approximation for the energy deposition pattern inside DNA and its environment.

The interaction of photons by photoelectric effect including Auger electrons and fluorescence electron emission, by Compton effect and by coherent scattering is simulated on the basis of a mixture of respective atomic cross sections. Starting points, energies and directions of secondary electrons are input data of the electron module of PARTRAC.

Ionizations and electronic excitations, regarded as "activation events", are further analyzed in the geometry module of PARTRAC.

## A.2    Geometry Module

The geometry module is permit to superpose a simulated physical track with the spatial coordinates of the target material, here the DNA in the cell nucleus. The DNA model describes higher-oder chromatin and chromosome structure [FJPS98]. Ionization and excitation events falling inside one van der Waals radius of the DNA

| Time (s) | Process occurring |
|---|---|
| **Physical stage** | |
| $10^{-18}$ | Fast particle traverses small atom |
| $10^{-16}$ – $10^{-17}$ | Ionization: $H_2O \longrightarrow H_2O^+ + e^-$ |
| | |
| **Physicochemical stage** | |
| $10^{-15}$ | Electronic excitation: $H_2O \longrightarrow H_2O^*$ |
| $10^{-14}$ | Ion-molecule reactions, e.g. $H_2O^+ + H_2O \longrightarrow {}^\bullet OH + H_3O^+$ |
| $10^{-13}$ | Molecular vibration $\to$ dissociation of excited state: $H_2O^* \longrightarrow H^\bullet + {}^\bullet OH$ |
| $10^{-12}$ | Rotation relation, thermalization of hot electrons, hydration of electrons: $e^- \to e^-_{aq}$ |
| | |
| **Chemical stage** | |
| $<10^{-12}$ | Reactions of $e^-$ before hydration with reactive solute at high concentrations |
| $10^{-10}$ | Reactions of $e^-_{aq}$ and other radicals with reactive solute (concentration $\sim 1$ mol·dm$^{-3}$) |
| $<10^{-7}$ | Reactions in spurs |
| $10^{-7}$ | Homogeneous distribution of radicals |
| $10^{-3}$ | Reactions of $e^-_{aq}$ and other radicals with reactive solutes (concentration $\sim 10^{-7}$ mol·dm$^{-3}$, i.e. $\sim 0.01$ ppm) |
| 1 | Free-radical reactions largely completed |
| $10^3$ | Biochemical processes |
| | |
| **Biological stage** | |
| Hours | Cell division affected in prokaryotic and eukaryotic cells |
| Days | Damage to central nervous system and gastrointestinal tract evident |
| Weeks | Haemopoietic effects |
| Several months | Late kidney damage, lung fibrosis |
| Years | Carcinogenesis and genetic effects |

Table A.1: The time scale of physical, chemical and biological stages of radiation action

atoms are scored as "direct" hits and are further analyzed in the effect module of the PARTRAC code. The water shell of the DNA is modeled as a 0.22 nm shell around the van der Waals radii of the DNA atoms [MB94]. Events occurring inside this shell are classified into three categories: (1) for the volume attached to phosphate group atoms, 60% of the events are taken as "quasi-direct" hits and further processed as "direct" hits, and 40% are further processed in the chemistry module, (2) for the volume attached to sugar group atoms, all events are transferred to the chemistry module and (3) for the volume attached to bases, the events are supposed to result in base damage. All other electronic excitations and ionizations are assumed to occur in the bulk water and to lead to radiation chemistry as is then processed in the chemistry module.

## A.3   Chemistry Module

The indirect radiation effect caused by chemical radicals produced by radiation in water is considered to be of the same or of even higher importance in radiation damage to DNA. After completion of the physical stage, different new chemical species are obtained, e.g. the sub-excitation electrons, $e_{\mathrm{sub}}$; ionized water molecules, $H_2O^+$; excitations: $\tilde{A}^1B_1$ and $\tilde{B}^1A_1$; Rydberg states; diffuse bands and dissociative excitations are obtained [BBM$^+$00]. Ionized water molecules are assumed to react immediately following the scheme: $H_2O^+ + H_2O \rightarrow H_3O^+ + {}^\bullet OH$. Excited water molecules are assumed either to relax, autoionize or to dissociate in many possible ways following the schemes listed in Table A.2. This scheme proposed by Cubut et al. [CFP$^+$98] was adapted in order to obtain – starting from the output of the physical tracks of the PARTRAC code – the reported initial yields of water radiolysis products [LP91] at $10^{-12}$ s.

The PARTRAC models the production, diffusion and interaction of reactive species during the physicochemical and chemical stages. The physicochemical from $10^{-15}$ to $10^{-12}$ s after irradiation considers the production of chemical species ($e_{\mathrm{aq}}^-$, $H_3O^+$, ${}^\bullet OH$, $H^\bullet$, $H_2$), starting from ionized and excited water molecules. For the initial positioning of the chemical species produced, the scheme proposed by Turner [THW$^+$88] was adopted. A randomly selected positioning according to a theoretical frequency distribution for the potential positions of the chemical species at $10^{-12}$ s after the interaction event is used. During the physicochemical stage, electrons with energies too low to excite electronic states of a water molecule are assumed to thermalize further and to become solvated. The thermalization distances of these subexcitation electrons have been investigated using theoretical stochastic and experimental approaches [MS87], [KRT88], [RHTB94], [GPJG88], [GJGF$^+$96]. Since the calculated time dependent yields do not depend much on the "actual" initial distribution, the PARTRAC code simplified the mean thermalization distance, $\langle r_{\mathrm{therm}} \rangle$, as on a function of subexcitation electron energy $E$ by a straight line, i.e.

$\langle r_{therm} \rangle = c_{therm} E$ for all cases, where the value of $c_{therm}$ was adopted from Ritchie et al. [RHTB94].

Concerning the chemical stage, i.e. the diffusion and reaction of chemical species from $10^{-12}$ to $10^{-6}$ s after irradiation, a step-by-step approach [TMW$^+$83] is adopted following the general scheme proposed by Stabin et al. [SHTB94]. A series of time steps was simulated, during each time step of length $\tau$, which varies from 0.1 ps at short times up to 30 ps at longer times, each species was allowed to randomly diffuse with a diffusion coefficient $D$, assuming pure diffusion within the time step itself. The square root mean distance traveled, $\lambda$, was calculated according to $\lambda = \sqrt{6D\tau}$. The actual distance was extracted from a gaussian distribution. After each diffusion step, distances between each pair of radicals are checked: if radicals are closer than their reaction radius they are considered to react and are replaced by appropriate products. The reactions included, reaction rate constants $k$ for the principal reactions considered and diffusion coefficient $D$ adopted are listed in Table A.2. Reaction radii $\alpha$ for each pair of interacting species are derived from the relation $k = 4\pi D\alpha$, where $k$ and $D$ were derived from experimental data. In the PARTRAC code, the effective reaction radius $R$ is modified, assuming the more accurate Noyes boundary conditions for all reactions, i.e. partially diffusion-controlled reactions [Noy63]:

$$k_{obs} = 4\pi D' R \frac{R}{R + \sqrt{\pi D' \tau}} \tag{A.1}$$

where $k_{obs}$ is the experimentally observed reaction rate constant, $D' = D_A + D_B$ is the relative diffusion coefficient for reactions between species A and B, and $\tau$ is the length of the time step. "Jump-through" are considered corrections according to Hamm et al. [HTS98] in order to avoid underestimation of the yield of reactions when time steps are larger. This allows one to adopt longer time steps without losing a significant number of reactions due to the possibilities of unrecognized crossing of the reaction spheres of the species during a time step.

It is assumed that $^\bullet$OH radicals contribute mainly damage to DNA interacting with nucleotides and sugar-phosphate moieties, but they can also be scavenged in the cytoplasm. The probability for an $^\bullet$OH radical to be scavenged within a time step $\tau$ is given by $P = 1 - e^{-\sigma\tau}$, where the scavenging capacity $\sigma$ is assumed to be equal to $4 \times 10^8$ s$^{-1}$ [WMF97] in a cell nucleus. For the interaction of $^\bullet$OH radicals with constituents of the DNA, reaction radii derived from Buxton et al. [BGHR88] (i.e. 0.085, 0.29, 0.29, 0.43 and 0.30 nm for reactions with deoxyribose, adenine, cytosine, guanine and thymine, respectively) are used. These events are called the "indirect" hits and are scored for further analysis in the effect module of the PARTRAC code.

The parameters included in PARTRAC were chosen after an extensive evaluation of the influence of each parameter on the time dependent yields of water radiolysis products [BBM$^+$00]. Good agreement was obtained between calculated time dependent radical yields in pure water and experimental data or values obtained by

| Dissociation schemes | | |
|---|---|---|
| Excitation | Decay channel | Probability |
| $\tilde{A}^1B_1$ | $H_2O+\Delta E$ | 35% |
| | $H^\bullet+{}^\bullet OH$ | 65% |
| | $H_2+O$ | - |
| $\tilde{B}^1A_1$ | $H_2O+\Delta E$ | 23% |
| | $H_3O^++{}^\bullet OH+ e_{aq}^-$ | 50% |
| | $H^\bullet+{}^\bullet OH$ | 20% |
| | $2H^\bullet+O$ | 3.9% |
| | $H_2+O$ | |
| | $H_2+H_2O_2$ | 3.2% |
| Ryd, dB, dE | $H_2O+\Delta E$ | 50% |
| | $H^\bullet+{}^\bullet OH$ | - |
| | $H_3O^++{}^\bullet OH+ e_{aq}^-$ | 50% |

| Reaction rate constant $k$ ($10^{10}$ M$^{-1}$ s$^{-1}$) | |
|---|---|
| Reaction type | $k$ |
| 1. $e_{aq}^-+e_{aq}^-+2H_2O \rightarrow H_2+2OH^-$ | 0.5 |
| 2. $e_{aq}^-+{}^\bullet OH \rightarrow OH^-$ | 3.0 |
| 3. $e_{aq}^-+H^\bullet+H_2O \rightarrow H_2+OH^-$ | 2.5 |
| 4. $e_{aq}^-+H_3O^+ \rightarrow H^\bullet+H_2O$ | 2.3 |
| 5. $e_{aq}^-+H_2O_2 \rightarrow OH^-+{}^\bullet OH$ | 1.1 |
| 6. ${}^\bullet OH+{}^\bullet OH \rightarrow H_2O_2$ | 0.44 |
| 7. ${}^\bullet OH+H^\bullet \rightarrow H_2O$ | 1.44 |
| 8. $H^\bullet+H^\bullet \rightarrow H_2$ | 1.0 |
| 9. $H_3O^++OH^- \rightarrow 2H_2O$ | 14.3 |

| Diffusion coefficient $D$ ($10^{-9}$ m$^2$ s$^{-1}$) | |
|---|---|
| Chemical species | $D$ |
| 1. $e_{aq}^-$ | 4.5 |
| 2. ${}^\bullet OH$ | 2.8 |
| 3. $H^\bullet$ | 7.0 |
| 4. $H_3O^+$ | 9.0 |
| 5. $H_2$ | 4.8 |
| 6. $OH^-$ | 5.0 |
| 7. $H_2O_2$ | 2.3 |

Table A.2: Chemistry parameters used in the PARTRAC code

Pimblott and LaVerne [PL92], [LP91] through the inverse Laplace transform technique, which provides a reliable estimate for most of the species involved.

## A.4 Effect Module

In the effect module of PARTRAC, the direct hits (including the quasi-direct hits occurring at atoms in the DNA) as well as interactions of $^\bullet$OH radicals with sugar atoms are processed to calculate DNA strand breaks and fragments. A single strand break (SSB) is assumed to occur in the DNA if (1) an ionization or an excitation involving a local energy deposition greater than the ionization threshold of liquid water, i.e. 10.79 eV [DHIP98], has been found inside an atom, i.e. within one van der Waals radius of the sugar-phosphate backbone, or (2) if an ionization/excitation event has been scored as a quasi-direct hit in the water shell attached to phosphate, or (3) if an $^\bullet$OH radical has interacted with the sugar moiety. This "threshold energy" was chosen since the deposition events are quantified according to the shells of liquid water. Strand breaks at adjacent nucleotides on the same strand are scored as one SSB. Two SSBs on opposite strands within a genomic distance of no more than 10 bp are scored as one double strand breaks (DSBs).

# Appendix B

# The Geometric Algorithm to Calculate the "Missing DNA Atoms" in a CAP-DNA Complex

## B.1 Introduction

This section describes a geometric algorithm used in our simulation to calculate the missing DNA atoms in the CAP-DNA complex. In the CAP-DNA data set of the Protein Data Bank [BWF$^+$00] (PDB ID entry number 1CGP on the web site http://www.rcsb.org/pdb) the following atoms are missing: (1) All the H-atoms in the sugar group, i.e. $H_1$, $H_{21}$, $H_{22}$, $H_3$, $H_4$, $H_{51}$ and $H_{52}$. (2) Some H-atoms in bases, $H_2$ and $H_8$ in base A, $H_8$ in base G, $H_5$ and $H_6$ in base C, $H_6$, $H_{91}$, $H_{92}$ and $H_{93}$ in base T. (3) Two single phosphate groups (one phosphorus and two oxygen atoms) in the nucleotide number 33 (base T) of chain C and in the nucleotide number 33 (base T) of chain D. According to the numbering used in the present work (cf. Figure 2.3) these nucleotides have the numbers 2 in the "top" strand and -2 in the "bottom" strand.

## B.2 Method

### B.2.1 Two DNA Data Sets

To reconstruct the positions of the missing atoms, two data sets were used, one is the B-DNA coordinates [CA89], denoted as set 1 and the other one is the PDB CAP-DNA coordinates [SSS91], denoted as set 2 (Figure B.1).
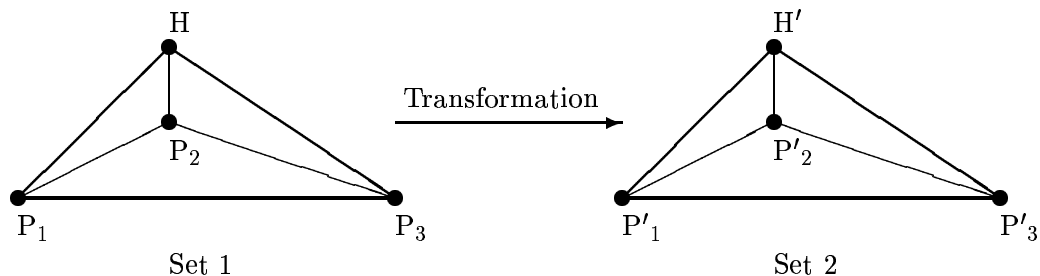
Figure B.1: Two data sets of DNA coordinates. H′ in set 2 is missing

## B.2.2  The Principle of the Algorithm

The basic idea of this calculation is based on the assumption that when the B-DNA duplex is bent, the relative position of the atoms inside the basic constituent units sugar, base and phosphate groups are not distorted. To calculate the position of each missing atom, the positions of three neighboring atoms were used. In set 1 no atom is missing, the relative position of these four atoms are known. The relative position of these four atoms is assumed to be unchanged in the bent DNA in set 2 (Figure B.1). From the solid geometry and vector calculations, the position of H′ corresponding to the missing atom in set 2 was evaluated. Table B.1 lists the atoms which were used to reconstruct the positions of the missing atoms.

## B.3  Results

Figure B.2 shows the PDB CAP-DNA, all missing DNA atoms and the CAP-DNA with the reconstructed atoms. The colors of the atoms are the same as in Figure 2.3.

|  | Missing atom | Neighboring atom 1 | Neighboring atom 2 | Neighboring atom 3 |
|---|---|---|---|---|
| Sugar | $H_1$ | $C_1$ | $C_2$ | $O_4$ |
|  | $H_{21}$ | $C_1$ | $C_2$ | $C_3$ |
|  | $H_{22}$ | $C_1$ | $C_2$ | $C_3$ |
|  | $H_3$ | $C_2$ | $C_3$ | $C_4$ |
|  | $H_4$ | $C_3$ | $C_4$ | $C_5$ |
|  | $H_{51}$ | $C_4$ | $C_5$ | $O_4$ |
|  | $H_{52}$ | $C_4$ | $C_5$ | $O_4$ |
| Base A | $H_2$ | $N_1$ | $C_2$ | $N_3$ |
|  | $H_8$ | $N_7$ | $C_8$ | $N_9$ |
| Base G | $H_8$ | $N_7$ | $C_8$ | $N_9$ |
| Base C | $H_5$ | $C_4$ | $C_5$ | $C_6$ |
|  | $H_6$ | $N_1$ | $C_6$ | $C_5$ |
| Base T | $H_6$ | $N_1$ | $C_6$ | $C_5$ |
|  | $H_{91}$ | $C_9$ | $C_5$ | $C_6$ |
|  | $H_{92}$ | $C_9$ | $C_5$ | $C_6$ |
|  | $H_{93}$ | $C_9$ | $C_5$ | $C_6$ |
| Phosphate | P | $O_3$ | $O_4$ | $C_5$ |
|  | $O_1$ | $O_3$ | $O_4$ | $C_5$ |
|  | $O_2$ | $O_3$ | $O_4$ | $C_5$ |

Table B.1: List of the atoms which were used to reconstruct the missing atoms in CAP-DNA
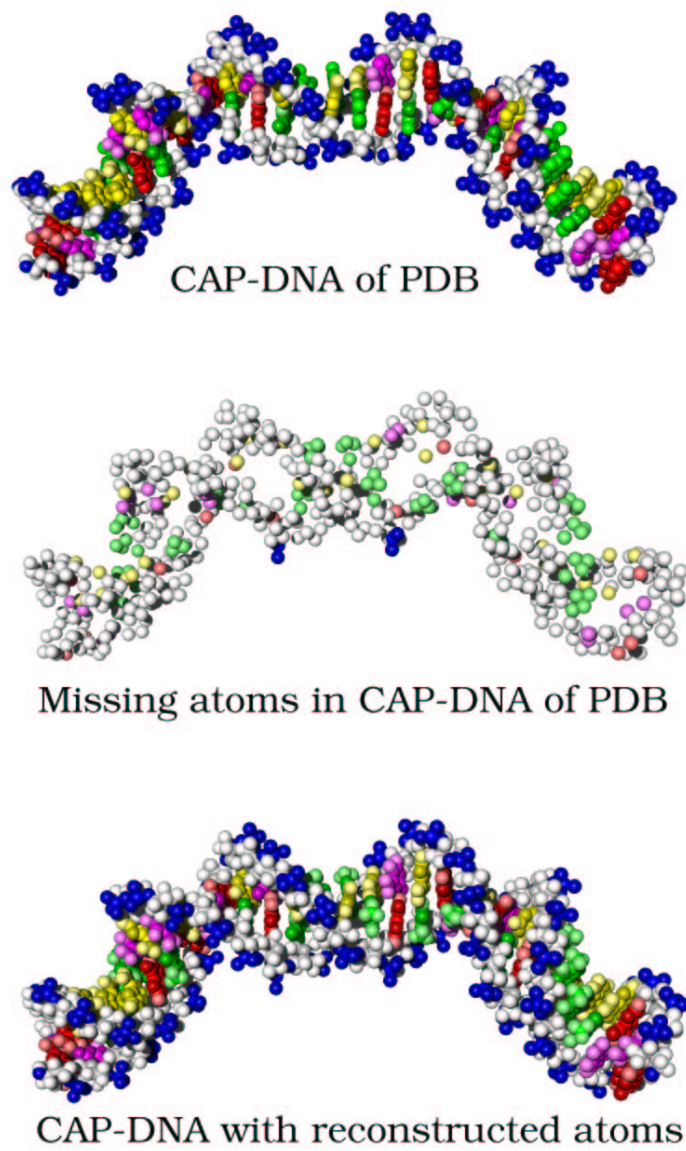
Figure B.2: CAP-DNA of PDB, missing atoms and completed CAP-DNA

# Appendix C

# Abbreviations

| | |
|---|---|
| $^{125}$IAP | $^{125}$I-Iodoantipyrine |
| $^{125}$IdCTP | 5-[$^{125}$I]iodine-2'-deoxycytidine 5'-triphosphate |
| $^{125}$IdU | 5-[$^{125}$I]iodine-2'-deoxyuridine |
| $^{125}$IH | [$^{125}$I]iodoHoechst 33342 |
| $^{125}$IVME2 | E-17$\alpha$[$^{125}$I]iodovinyl-11$\beta$methoxyestradiol |
| $^{125}$I-TFO | $^{125}$I-triplex forming oligonucleotide |
| CAP-DNA complex | Catabolite gene activator protein DNA complex |
| CHOER | ER-expressing Chinese hamster ovary |
| CRP-DNA complex | cAMP receptor protein DNA complex |
| DMSO | Dimethyl sulphoxide |
| DNA | Deoxyribonucleic acid |
| DSBs | Double strand breaks |
| IRT | Independent reaction time |
| PB | Sodium phosphate buffer |
| SSBs | Single strand breaks |

# Bibliography

[Ade92]      S. J. Adelstein. Biophysical aspects of auger processes: A review of the literature 1987–1991. In R. W. Howell, V. R. Narra, K. S. R. Sastry, and D. V. Rao, editors, *Biophysical Aspects of Auger Processes*, pages 1–13. American Institute of Physics, Inc., Woodbury, New York, 1992.

[AJ80]       G. E. Adams and D. G. Jameson. Time effects in molecular radiation biology. *Radiat. Environ. Biophys.*, 17:95–113, 1980.

[AK96]       S. J. Adelstein and A. Kassis. Strand breaks in plasmid DNA following positional changes of Auger-electron-emitting radionuclides. *Acta Oncol.*, 35(7):791–801, 1996.

[AS68]       M. Abramowitz and I. A. Stegun. *Handbook of Mathematical Functions, Applied Mathematics Series*, volume 55. Dover Publications, New York, 1968.

[AW00]       P. Auffinger and E. Westhof. Water and ion binding around RNA and DNA (C,G) oligomers. *J. Mol. Biol.*, 300:1113–1131, 2000.

[BBD+01]     H. C. Box, E. E. Budzinski, J. Dawidzik, H. B. Patrzyc, and H. G. Freund. A novel double lesion in X-irradiated DNA consists of a strand break and a base modification. *Radiat. Res.*, 156:215–219, 2001.

[BBM+00]     F. Ballarini, M. Biaggi, M. Merzagora, A. Ottolenghi, M. Dingfelder, W. Friedland, P. Jacob, and H. G. Paretzke. Stochastic aspects and uncertainties in the prechemical and chemical stages of electron tracks in liquid water: a quantitative analysis based on Monte Carlo simulations. *Radiat. Environ. Biophys.*, 39(3):179–188, 2000.

[BCA75]      E. W. Bradely, P. C. Chan, and S. J. Adelstein. The radiotoxicity of mammalian cells. I. Effects on the survival curve of radioiodine incorporated into DNA. *Radiat. Res.*, 64:555–563, 1975.

[BGHR88]     G. V. Buxton, C. L. Greenstock, W. P. Helman, and A. B. Ross. Critical review of rate constants for reactions of hydrated electrons, hydrogen atoms and hydroxyl radicals in aqueous solutions. *J. Phys. Chem. Ref. Data*, 17:513–886, 1988.

[BJ99]       M. Bixon and J. Jortner. Electron transfer — from isolated molecules to biomolecules. *Adv. Chem. Phys.*, 106:35–202, 1999.

[BPPO87]   J. Booz, H. G. Paretzke, E. Pomplun, and P. Olko. Auger-electron cascades, charge potential and microdosimetry of iodine-125. *Radiat. Environ. Biophys.*, 26:151–162, 1987.

[BRB+94]   A. Bishayee, D. V. Rao, L. G. Bouchet, W. E. Bolch, and R. W. Howell. Protection by DMSO against cell death caused by intracellularly localized iodine-125, iodine-131 and polonium-210. *Radiat. Res.*, 137:385–393, 1994.

[BRFB73]   H. J. Burki, R. Roots, L. E. Feinendegen, and V. P. Bond. Inactivation of mammalian cells after disintegration of $^3$H or $^{125}$I in cell DNA at -196 degrees C. *Int. J. Radiat. Biol.*, 4:363–375, 1973.

[BWF+00]   H. M. Berman, J. Westbrook, Z. Feng, G. Gilliland, T. N. Bhat, H. Weissig, I. N. Shindyalov, and P. E. Bourne. The protein data bank. *Nucleic Acids Res.*, 28:235–242, 2000.

[CA89]   R. Chandrasekaran and S. Arnotte. The structures of DNA and RNA helices in oriented fibers. In W. Saenger, editor, *Landdolt-Börnstein, Numerical Data and Functional Relationship in Science and Technology*, New Series VII, 1b, pages 31–170. Springer, Berlin, 1989.

[CFP+98]   V. Cobut, Y. Frongillo, J.P. Patau, T. Goulet, M.-J. Fraser, and J.-P. Jay-Gerin. Monte Carlo simulation of fast electron and proton tracks in liquid water. I. Physical and physicochemical aspects. *Radiat. Chem. Phys.*, 51:229–243, 1998.

[CH88]   D. E. Charlton and J. L. Humm. A method of calculating initial DNA strand breakage following the decay of incorporated $^{125}$I. *Int. J. Radiat. Biol.*, 53(3):353–365, 1988.

[Cha86]   D. E. Charlton. The range of high LET effects from $^{125}$I decays. *Radiat. Res.*, 107(2):163–171, 1986.

[CHvLS94]   D. E. Charlton, K. G. Hofer, N. van Loon, and M. N. Schneiderman. Double-strand breaks from $^{125}$I incorporated in the DNA and cell death. *Int. J. Radiat. Biol.*, 66(5):437–447–440, 1994.

[CJ81]   D. E. Charlton and Booz J. A Monte Carlo treatment of the decay of $^{125}$I. *Radiat. Res.*, 87(1):10–23, 1981.

[CLLA76]   P. C. Chan, E. Lisco, H. Lisco, and S. J. Adelstein. The radiotoxicity of iodine-125 in mammalian cells II. A comparative study on cell survival and cytogenetic responses to $^{125}$IUdR, $^{131}$TUdR, and $^3$HTdR. *Radiat. Res.*, 67(2):332–343, 1976.

[CLLA78]   P. C. Chan, E. Lisco, H. Lisco, and S. J. Adelstein. Cell survival and cytogenetic responses to $^{125}$I-UdR in cultured mammalian cells. *Curr. Top Radiat Res Q.*, 12(1–4):426–435, 1978.

[CMS90]     P. M. Cullis, J. D. Mcclymont, and M. C.R. Symons. Electron conduction and trapping in DNA. An electron spin resonances study. *J. Chem. Soc. Faraday Trans. I*, 86:591–592, 1990.

[CPB87]     D. E. Charlton, E. Pomplun, and J. Booz. Some consequences of the auger effect: fluorescence yield, charge potential, and energy imparted. *Radiat. Res.*, 111(3):553–564, 1987.

[CR00]      E. M. Conwell and S. V. Rakhmanova. Polarons in DNA. *Proc. Natl. Acad. Sci. USA*, 97:4556–4560, 2000.

[CW64]      T. A. Carlson and R. M. White. Formation of fragment ions from $HC_3{}^{125}Te$ and $C_3H_5{}^{125}Te$ following the nuclear decays of $HC_3{}^{125}I$ and $C_3H_5{}^{125}I$. *J. Chem. Phys.*, 38:2930–2934, 1964.

[DB74]      D. Dee and E. Baur. Charge and excitation migration in DNA chains. *J. Chem. Phys.*, 60(2):542–560, 1974.

[Des75]     J. P. Desclaux. A multiconfiguration relativistic Dirac-Fock program. *Comput. Phys. Commun.*, 9:31–45, 1975.

[DHIP98]    M. Dingfelder, D. Hantke, M. Inokuti, and H. G. Paretzke. Electron inelastic-scattering cross sections in liquid water. *Radiat. Phys. Chem.*, 53:1–18, 1998.

[DIP00]     M. Dingfelder, M. Inokuti, and H. G. Paretzke. Inelastic-collision cross sections of liquid water for interactions of energetic protons. *Radiat. Phys. Chem.*, 59:255–275, 2000.

[DS81]      R. Deutzmann and G. Stöcklin. Chemical effects of iodine-125 decay in aqueous solution of 5-Iodouricil. Ring fragmentation as a consequence of the Auger effect. *Radit. Res.*, 87:24–36, 1981.

[EFH70]     H. H. Ertl, L. E. Feinendegen, and H. J. Heiniger. Iodine-125, a tracer in a cell biology: Physical properties and biological aspects. *Phys. Med. Biol.*, 15:447–456, 1970.

[FBJ$^+$02]  W. Friedland, P. Bernhardt, P. Jacob, H. G. Paretzke, and M. Dingfelder. Simulation of DNA damage after proton and low LET irradiation. *Radiat. Prot. Dosim.*, 99(1–4):99–102, 2002.

[FEB71]     L. E. Feinendegen, H. H. Ertl, and V. P. Bond. Biological toxicity associated with the Auger effect. In H. Ebert, editor, *Proceedings of the Symposium on Biological Aspects of Radiation Quality*, pages 419–430, Vienna, 1971. IAEA.

[Fel65]     W. Feller. *An Introduction to Probability Theory and its Applications*, volume I. Wiley Inc., New York, 3rd edition, 1965.

[FGF$^+$98]  Y. Frongillo, T. Goulet, M.-J. Fraser, V. Cobut, J. P. Patau, and J.-P. Jay-Gerin. Monte Carlo simulation of fast electron and proton tracks in liquid water — II. Nonhomogenous chemistry. *Radiat. Phys. Chem.*, 51(3):245–254, 1998.

[FJP+99]    W. Friedland, P. Jacob, H. G. Paretzke, M. Merzagora, and A. Ot-
            tolenghi. Simulation of DNA fragment distribution after irradiation
            with photons. *Radiat. Environ. Biophys.*, 38(1):39–47, 1999.

[FJPS98]    W. Friedland, P. Jacob, H. G. Paretzke, and T. Stork. Monte Carlo
            simulation of the production of short fragments by low-linear en-
            ergy transfer radiation using higher-order DNA models. *Radiat. Res.*,
            152(2):170–182, 1998.

[FSMZ94]    A. F. Fuciarelli, E. C. Sisk, J. H. Miller, and J. D. Zimbrick. Radiation-
            induced electron migration in nucleic acids. *Int. J. Radiat. Biol.*,
            66(5):505–509, 1994.

[FTS+98]    M. J. Frisch, G. W. Trucks, H. B. Schlegel, G. E. Scuseria, M. A.
            Robb, J. R. Cheeseman, V. G. Zakrzewski, Jr. J. A. Montgomery,
            R. E. Stratmann, J. C. Burant, S. Dapprich, J. M. Millam, A. D.
            Daniels, K. N. Kudin, M. C. Strain, O. Farkas, J. Tomasi, V. Barone,
            M. Cossi, R. Cammi, B. Mennucci, C. Pomelli, C. Adamo, S. Clif-
            ford, J. Ochterski, G. A. Petersson, P. Y. Ayala, Q. Cui, K. Mo-
            rokuma, D. K. Malick, A. D. Rabuck, K. Raghavachari, J. B. Fores-
            man, J. Cioslowski, J. V. Ortiz, A. G. Baboul, B. B. Stefanov, G. Liu,
            A. Liashenko, P. Piskorz, I. Komaromi, R. Gomperts, R. L. Martin,
            D. J. Fox, T. Keith, M. A. Al-Laham, C. Y. Peng, A. Nanayakkara,
            C. Gonzalez, M. Challacombe, P. M. W. Gill, B. Johnson, W. Chen,
            M. W. Wong, J. L. Andres, C. Gonzalez, M. Head-Gordon, E. S. Re-
            plogle, , and J. A. Pople. *Gaussian98, Revision A.7*. Gaussian, Inc.,
            Pittsburgh, PA, 1998.

[GAK+01]    B. Giese, J. Amaudrut, A.-K. Köhler, M. Spormann, and S. Wessely.
            Direct observation of hole transfer through DNA by hopping between
            adenine bases and by tunnelling. *Nature*, 412:318–320, 2001.

[GB66]      R. M. Glaeser and R. S. Berry. Mobilities of electrons and holes in
            organic molecular solids. Comparison of bond and hopping models. *J.
            Chem. Phys.*, 44:3797–3810, 1966.

[GBS00]     F. C. Grozema, Y. A. Berlin, and L. D. A. Siebbeles. Mechnism of
            charge migration through DNA: Molecular wire behavior, single-step
            tunneling or hopping. *J. Am. Chem. Soc.*, 122:10903–10909, 2000.

[Gie00]     B. Giese. Long-distance charge transport in DNA: the hopping mech-
            anism. *Acc. Chem. Res.*, 33:631–636, 2000.

[GJGF+96]   T. Goulet, J. P. Jay-Gerin, Y. Frongillo, V. Cobut, and M. J. Fraser.
            Rôle des distances de thermalisation des électrons dans la radiolyse
            de l'eau liquide. *J. Chim. Phys.*, 93:111–116, 1996.

[GPJG88]    T. Goulet, J. P. Patau, and J. P. Jay-Gerin. Thermalization distances
            and times for subexcitation electrons in solid water. *Radiat. Prot.
            Dosim.*, 31:33–36, 1988.

[GV91]      W. Glass and N. Varma, editors. *Physical and Chemical Mechanisms in Molecular Radiation Biology.* Plenum Press, New York, 1991.

[GWS+99]    B. Giese, S. Wessely, M. Spormann, U. Lindemann, E. Meggers, and M. E. Michel-Beyerle. On the mechanism of long-range electron transfer through DNA. *Angew. Chem. Int. Ed.*, 38:996–998, 1999.

[GZO95]     A. A. Gorin, V.B. Zhurkin, and W. K. Olson. B-DNA twisting correlates with base-pair morphology. *J. Mol. Biol.*, 247:34–48, 1995.

[Hal90]     A. Halpern. Intra- and intermolecular energy transfer and superexcition in post-auger processes. *Radiochimica Acta*, 50:129–134, 1990.

[HH71]      K. G. Hofer and W. L. Hughes. Radiotoxicity of intranuclear tritium, iodine-125 and iodine-131. *Radiat. Res.*, 47:94–109, 1971.

[HJH+99]    P. T. Henderson, D. Jones, G. Hampikian, Y. Kan, and G. B. Schuster. Long-distance charge transport in duplex DNA: The phonon-assisted polaron-like hopping mechanism. *Proc. Natl. Acad. Sci. USA*, 96:8353–8358, 1999.

[HLS00]     K. G. Hofer, X. Lin, and M. H. Schneiderman. Paradoxical effects of iodine-125 decays in parent and daughter DNA: A new target model for radiation damage. *Radiat. Res.*, 153:428–435, 2000.

[Hof96]     K. G. Hofer. Biophysical aspects of Auger processes: A review. *Acta Oncol.*, 35:789–796, 1996.

[Hof00]     K. G. Hofer. Biophysical aspects of Auger processes. *Acta Oncol.*, 39(6):651–657, 2000.

[HP92]      S. Henß and H. G. Paretzke. Biophysical modeling of radiation induced damages in chromosomes. In K. H. Chadwick, G. Moschini, and N. W. Varma, editors, *Biophysical Modeling of Radiation Effects*, pages 67–76. Adam Hilger, Bristol, 1992.

[HPH69]     K. G. Hofer, W. Prensky, and W. L. Hughes. Death and metastatic distribution of tumor cells in mice monitored with[125]I-iododeoxyuridine. *J. Nat. Cancer Inst.*, 43:763–773, 1969.

[HRS89]     R. W. Howell, D. V. Rao, and K. S. R. Sastry. Macroscopic dosimetry for radioimmunotherapy: Nonuniform activity distributions in solid tumors. *Med. Phys.*, 16:66–74, 1989.

[HTS98]     R. N. Hamm, J. E. Turner, and M. G. Stabin. Monte Carlo simulations of diffusion and reactions in water radiolysis: A study of reactant "jump through" and jump distances. *Radiat. Environ. Biophys.*, 36:229–234, 1998.

[HvLSC92]   K. G. Hofer, N. van Loon, M. H. Schneiderman, and D. E. Charlton. The paradoxical nature of DNA damage and cell death induced by ^{125}I decay. *Radiat. Res.*, 130(1):121–124, 1992.

[ICR83]     ICRP. *Radionuclide transformations: Energy and intensity of emissions.* Annals of the ICRP, ICRP Publication 38. Pergamon Press, Oxford – New York – Frankfurt, 1983.

[Ins96]     Institut für Hochfrequenztechnik, TU Braunschweig. *Organische Leuchtdioden*, 1996.

[JBLMB98]  J. Jortner, M. Bixon, T. Langenbacher, and M. E. Michel-Beyerle. Charger transfer and transport in DNA. *Proc. Natl. Acad. Sci. USA*, 95:12759–12765, 1998.

[KB99]      S. O. Kelley and J. K. Barton. Electron transfer between bases in double helical DNA. *Science*, 283:375–381, 1999.

[KBR74]     Y. Kobayashi, A. Barkatt, and J. Rabani. Yields of radiation products in sodium metaphosphate glasses. *J. Phys. Chem.*, 78(7):752–756, 1974.

[KFK$^+$89]  A. I. Kassis, F. Fayad, B. M. Kinsey, K. S. R. Sastry, and S. J. Adelstein. Radiotoxicity of an $^{125}$I labeled DNA intercalator in mammalian cells. *Radiat. Res.*, 118(2):283–294, 1989.

[KHA99a]    A. I. Kassis, R. S. Harapanhalli, and S. J. Adelstein. Comparison of strand breaks in plasmid DNA after positional changes of Auger electron-emitting iodine-125. *Radiat. Res.*, 151:167–176, 1999.

[KHA99b]    A. I. Kassis, R. S. Harapanhalli, and S. J. Adelstein. Strand breaks in plasmid DNA after positional changes of Auger electron-emitting iodine-125: Direct compared to indirect effects. *Radiat. Res.*, 152:530–538, 1999.

[KKS76]     R. E. Krisch, F. Krasin, and C. J. Sauri. DNA breakage, repair, and lethality of $^{125}$I decay in rec$^+$ and recA strains of Escherichia coli. *Int. J. Radiat. Biol.*, 25:37–50, 1976.

[KL74]      R. E. Krisch and R. D. Ley. Induction of lethality and DNA breakage by the decay of iodine-125 in bacteriophage T$_4$. *Int. J. Radiat. Biol.*, 25:21–30, 1974.

[KLDM96]    S. Kandaiya, P. N. Lobachevsky, G. D'Cunha, and R. F. Martin. DNA strand breakage by $^{125}$I-decay in synthetic oligodeoxynucleotide: Fragment distribution and evaluation of DMSO protection effect. *Acta Oncol.*, 35(7):803–808, 1996.

[KRT88]     V. V. Konovalov, A. M. Raitsimring, and Y. D. Tsvetkov. Thermalization lengths of subexcitation electrons in water determined by photoinjection from metals into electrolyte solutions. *Radiat. Phys. Chem.*, 32(4):623–632, 1988.

[KSA87]     A. I. Kassis, K. S. R. Sastry, and S. J. Adelstein. Kinetics of uptake, retention and radiotoxicity of $^{125}$IdUdR in mammalian cell: Implications of localized energy deposition by Auger processes. *Radiat. Res.*, 109:78–89, 1987.

[KWA00]     A. I. Kassis, M. A. Walicka, and S. J. Adelstein. Double-strand breaks yield following $^{125}$I decay. Effects of DNA conformation. *Acta Oncologica*, 39(6):721–726, 2000.

[KZG$^+$99]   V. N. Karamychev, V. B. Zhurkin, S. Garges, R. D. Neumann, and I. G. Panyutin. Detecting the DNA kinks in a DNA-CRP complex in solution with iodine-125 radioprobing. *Nat. Strut. Biol.*, 6(8):747–750, 1999.

[LFJ00]      W. Li, W. Friedland, and P. Jacob. Simulation of $^{125}$I induced DNA strand breaks in a CAP-DNA complex. GSF-Bericht 11/00, GSF-Forchungszentrum, Neuherberg, Germany, 2000.

[LFP$^+$01]   W. B. Li, W. Friedland, E. Pomplun, P. Jacob, H. G. Paretzke, M. Lassmann, and C. Reiners. Track structures and dose distributions from decays of $^{131}$I and $^{125}$I in and around water spheres simulating micrometastases of differentiated thyroid cancer. *Radiat. Res.*, 156:419–429, 2001.

[LHBL96]     G. Ludwików, K. G. Hofer, S.-P. Bao, and F. Ludwików. The effect of $^{125}$I decay at different stages of S-phase on survival, expression of micronuclei and chromosome aberrations in CHO cells. *Int. J. Radiat. Biol.*, 70:177–187, 1996.

[LL84]       P. K. LeMotte and J. B. Little. DNA damage induced in human diploid cells by decay of incorporated radionuclides. *Cancer Res.*, 44:1337–1342, 1984.

[LLL$^+$00]   F. D. Lewis, X. Liu, J. Liu, S. E. Miller, R. T. Hayes, and M. R. Wasielewski. Direct measurement of hole transport dynamics in DNA. *Nature*, 406:51–53, 2000.

[LM96]       P. N. Lobachevsky and R. F. Martin. DNA strand breakage by $^{125}$I-decay in a synthetic oligodeoxynucleotide: Quantitive analysis of fragment distribution. *Acta Oncol.*, 35(7):809–815, 1996.

[LM00a]      P. N. Lobachevsky and R. F. Martin. Iodine-125 decay in a synthetic oligodeoxynucleotide. I. Fragment size distribution and evaluation of breakage probability. *Radiat. Res.*, 153:263–270, 2000.

[LM00b]      P. N. Lobachevsky and R. F. Martin. Iodine-125 decay in a synthetic oligodeoxynucleotide. II. The role of auger electron irradiation compared to charge neutralization in DNA breakage. *Radiat. Res.*, 153:271–278, 2000.

[LP91]       J. A. LaVerne and S. M. Pimblott. Scavenger and time dependences of radicals and molecular products in the electron radiolysis of water: Examination of experiments and models. *J. Phys. Chem.*, 95:3196–3206, 1991.

[LP95]       J. A. LaVerne and S. M. Pimblott. Electron energy-loss distribution in solid, dry DNA. *Radiat. Res.*, 141:208–215, 1995.

[LS85]      U. Linz and G. Stöcklin. Chemical and biological consequences of the radiative decay of iodine-125 in plasmid DNA. *Radiat. Res.*, 101:262–278, 1985.

[LSS99]     D. Ly, L. Sanii, and G. B. Schuster. Mechanism of charge transport in DNA: Internally-linked anthraquinone conjugates support phonon-assisted polaron hopping. *J. Am. Chem. Soc.*, 121:9400–9410, 1999.

[LZ64]      H. Leutz and K. Ziegler. The electron capture ratio in the decay of $^{125}$I. *Nucl. Phys.*, 50:648–656, 1964.

[Mar56]     R. A. Marcus. On the theory of oxidation-reduction reactions involving electron transfers. I. *J. Chem. Phys.*, 24(5):966–978, 1956.

[MB94]      V. Michalik and M. Begusova. Target model of nucleosome particles for track structure calculations and DNA damage modelling. *Int. J. Radiat. Biol.*, 66(3):267–277, 1994.

[MCO$^+$98] M. T. Melvin, S. M. Cunniffe, P. O'Neill, A. W. Parker, and T. Roldan-Arjona. Guanine is the target for direct ionisation damage in DNA, as detected using excision enzymes. *Nucleic Acids Res.*, 26:4935–4942, 1998.

[MF81]      N. Miyazaki and Y. Fujiwara. Mutagenic and lethal effects of [5-$^{125}$I]iodo-2′-deoxyuridine incorporated into DNA of mammalian cells, and their RBEs. *Radiat. Res.*, 88(3):456–465, 1981.

[MH81]      R. F. Martin and W. A. Haseltine. Range of radiochemical damage to DNA with decay of iodine-125. *Science*, 213:896–898, 1981.

[MK00]      V. May and O. Kühn. *Charge and Energy Transfer Dynamics in Molecular System*. Wiley–VCH Verlag Berlin GmbH, Berlin, first edition, 2000.

[MKS$^+$98] E. Meggers, D. Kusch, M. Spichty, U. Wille, and B. Giese. Electron transfer through DNA in the course of radical-induced strand cleavage. *Angew. Chem., Int. Ed.*, 37:460–462, 1998.

[MMBG98]    E. Meggers, M. Michel-Beyerl, and B. Giese. Sequence dependent long range hole transport in DNA. *J. Am. Chem. Soc.*, 120:12950–12955, 1998.

[MS85]      R. A. Marcus and N. Sutin. Electron transfers in chemistry and biology. *Biochimca et Biohpysica Acta*, 811:265–322, 1985.

[MS87]      M. Michaud and L. Sanche. Absolute vibrational excitation cross sections for slow electrons (1–18 eV) scattering in solid $H_2O$. *Phys. Rev. A*, 36:4684–4699, 1987.

[NLT$^+$00] H. Nikjoo, C. A. Laughton, M. Terrissol, I. G. Panyutin, and D. T. Goodhead. A method for radioprobing DNA structures using Auger electrons. *Int. J. Radiat. Biol.*, 76(12):1607–1615, 2000.

[NMC+96]   H. Nikjoo, R. F. Martin, D. E. Charlton, M. Terrissol, S. Kandaiya, and P. Lobachevsky. Modelling of Auger-induced DNA damage by incorporated $^{125}$I. *Acta Oncol.*, 35:7, 1996.

[Noy63]    R. M. Noyes. Effects of diffusion rates on chemical kinetics. In G. Porter and B. Stevens, editors, *Progress in Reaction Kinetics*, volume 1, pages 129–160. Pergamon, Oxford, 1963.

[NPT+00]   H. Nikjoo, I. G. Panyutin, M. Terrissol, J. M. Vridneaud, and C. A. Laughton. Distribution of strand breaks produced by Auger electrons in decay of $^{125}$I in triplex DNA. *Acta Oncol.*, 39(6):707–712, 2000.

[Par74]    H. G. Paretzke. Comparison of track structure calculations with experimental results. In J. Booz and H. G. Ebert, editors, *Proceed. 4th Int. Symp. on Microdosimetry*, pages 141–165, Brussels, 1974. Comm. Europ. Communities.

[Par80]    H. G. Paretzke. Advances in energy deposition theory. In R. H. Thomas and V. Perez-Mendez, editors, *Advances in Radiation Protection and Dosimetry in Medicine*, pages 51–73. Plenum, New York, 1980.

[Par87]    H. G. Paretzke. Radiation track structure theory. In G. R. Freeman, editor, *Kinetic of Nonhomogeneous Processes*, pages 89–170. Wiley, New York, 1987.

[Par88]    H. G. Paretzke. Simulation von Elektronenspuren im Energiebereich 0,01-10 keV in Wasserdampf. GSF-Bericht 24/88, GSF-Forchungszentrum, Neuherberg, Germany, 1988.

[PBC87]    E. Pomplun, J. Booz, and D. E. Charlton. A Monte Carlo simulation of auger cascades. *Radiat. Res.*, 111(3):533–552, 1987.

[PL92]     S. M. Pimblott and J. A. LaVerne. Molecular product formation in the electron radiolysis of water. *Radiat. Res.*, 129:265–271, 1992.

[Pla54]    R. L. Platzman. Subexcitation electrons. *Radiat. Res.*, 2:1–7, 1954.

[Pla62]    R. L. Platzman. Superexcited states of molecules. *Radiat. Res.*, 17:419–425, 1962.

[PLPN01]   I. V. Panyutin, A. N. Luu, I. G. Panyutin, and R. D. Neumann. Strand breaks in whole plasmid DNA produced by the decay of $^{125}$I in a triplex-forming oligonucleotide. *Radiat. Res.*, 156:158–166, 2001.

[PN94]     I. G. Panyutin and R. D. Neumann. Sequence-specific DNA double-strand breaks induced by triplex forming $^{125}$I labeled oligonucleotides. *Nucl. Acid Rec.*, 22(23):4979–4982, 1994.

[PN96]     I. G. Panyutin and R. D. Neumann. Sequence-specific DNA breaks produced by triplex-directed decay of iodine-125. *Acta Oncol.*, 35(7):817–823, 1996.

[PN97]       I. G. Panyutin and R. D. Neumann. Radioprobing of DNA: distribu-
             tion of a triplex-forming oligonucleotide correlates with geometry of
             the triplex. *Nucl. Acid Rec.*, 25:883–887, 1997.

[Pom91]      E. Pomplun. A new DNA target model for track structure calculations
             and its first application to I-125 Auger electrons. *Int. J. Radiat. Biol.*,
             59:625–642, 1991.

[Pom00]      E. Pomplun. Auger electron spectra. *Acta Oncol.*, 39(6):673–679,
             2000.

[Pom02]      E. Pomplun. Private communication, February 2002. "Unter
             der geschilderten Voraussetzung sollten beide Kaskaden im Mittel
             etwa die gleiche Zahl emittierter Elektronen aufweisen. Die relativen
             Wahrscheinlichkeiten für die einzelnen Elektronenschalen hinsichtlich
             electron capture und internal conversion differieren nur geringfügig.
             Da jede Kaskade aber stochastisch abläuft, können bei individuellen
             Zerfällen natürlich zwei ganz unterschiedliche Kaskaden auftreten".

[PRB96]      S. Priyadarshy, S. M. Risser, and D. N. Beratan. DNA is not a molec-
             ular wire: Protein-like electron-transfer predicted for an extended $\pi$-
             electron system. *J. Phys. Chem.*, 100:17678–17682, 1996.

[PT94]       E. Pomplun and M. Terrissol. Low-energy electrons inside active DNA
             models: a tool to elucidate the radiation action mechanisms. *Radiat.
             Environ. Biophys.*, 33:279–292, 1994.

[PWG+96]     G. Parkinson, C. Wilson, A. Gunasekera, Y. W. Ebright, R. E.
             Ebright, and H. Berman. Structure of the CAP-DNA complex at
             2.5 Å resolution: A complete picture of the protein-DNA interface. *J.
             Mol. Biol*, 260:395–408, 1996.

[PY78]       R. B. Painter and B. R. Young. Anomalous effects of $^{125}$I after its
             incorporation into mammalian cell DNA. *Curr. Top. Radiat. Res. Q.*,
             12(1–4):472–479, 1978.

[PYB74]      R. B. Painter, B. R. Young, and H. J. Burki. Non-repairable strand
             breaks induced by $^{125}$I incorporated into mammalian DNA. *Proc.
             Natl. Acad. Sci. USA*, 71(12):4836–4838, 1974.

[RHS88]      M. Reiche, A. Halpern, and G. Stöcklin. Chemical effects of the decay
             of $^{125}$I in [$^{14}$C, $^{125}$I]Iodobenzene in different solvents. *Radiochimica
             Acta*, 43:191–196, 1988.

[RHTB94]     R. H. Ritchie, R. N. Hamm, J. E. Turner, and W. E. Bolch. Interaction
             of low-energy electrons with condensed matter: relevance for track
             structure. In N. Varma and A. Chatterjee, editors, *Computational
             Approaches in Molecular Radiation Biology*, pages 155–166. Plenum,
             New York, 1994.

[Sae84]      W. Saenger. *Principles of Nucleic Acid Structure*. Springer-Verlag,
             Berlin – New York – Heidelberg, 1984.

[Sas92]      K. S. R. Sastry. Biological effects of the Auger emitter iodine-125: A review. Report No. 1 of AAPM Nuclear Medicine Task Group No.6. *Med. Phys.*, 19(6):1361–1370, 1992.

[SHTB94]     M. G. Stabin, R. N. Hamm, J. E. Turner, and W. E. Bolch. Track structure simulation and determination of product yields in the electron radiolysis of water containing various solutes. *Radiat. Prot. Dosim.*, 52:255–258, 1994.

[SPB98]      B. Schneider, K. Patel, and H. M. Berman. Hydration of the phosphate group in double-helical DNA. *Biophys. J.*, 75:2422–2434, 1998.

[SSS90]      S. C. Schultz, G. C. Shields, and T. A. Steitz. Crystallization of *Escherichia coli* catabolite gene activator protein with its DNA bending site. *J. Mol. Biol.*, 231:159–166, 1990.

[SSS91]      S. C. Schultz, G. C. Shields, and T. A. Steitz. Crystal structure of a CAP-DNA complex: The DNA is bent by 90°. *Science*, 253:1001–1007, 1991.

[SSS96]      C. A. M. Seidel, A. Schulz, and M. H. M. Sauer. Nucleobase-specific quenching of fluorescent dyes. I. Nucleobase one-electron redox potential and their correlation with static and dynamic quenching efficiencies. *J. Phys. Chem.*, 100:5541–5553, 1996.

[Sym95]      M. C. R. Symons. Electron spin resonance studies of radiation damage to DNA and to protein. *Radiat. Phys. Chem.*, 45(6):837–845, 1995.

[Ter94]      M. Terrissol. Modelling of radiation damage by $^{125}$I on a nucleosome. *Int. J. Radiat. Biol.*, 66:447–451, 1994.

[THW$^+$88]  J. E. Turner, R. N. Hamm, H. A. Wright, R. H. Ritchie, J. L. Magee, A. Chatterjee, and W. E. Bolch. Studies to link the basic radiation physics and chemistry of liquid water. *Radiat. Phys. Chem.*, 32:503–510, 1988.

[TMW$^+$83]  J. E. Turner, J. L. Magee, H. A. Wright, A. Chatterjee, R. N. Hamm, and R. H. Ritchie. Physical and chemical development of electron tracks in liquid water. *Radiat Res*, 96:437–449, 1983.

[VBJR01]     A. A. Voityuk, M. Bixon, J. Jortner, and N. Rösch. Electronic coupling between Watson-Crick pairs for hole transfer and transport in deoxyribonucleic acid. *J. Chem. Phys.*, 114(13):5614–5620, 2001.

[VLK$^+$92]  A. V. Vologodskii, S. D. Levene, K. V. Klenin, M. Frank-Kamenetskii, and N. R. Cozzarelli. Conformational and thermodynamics properties of supercoiled DNA. *J. Mol. Biol.*, 227:1224–1243, 1992.

[vLWdHH86]   D. van Lith, J. M. G. Warman, M. P. de Haas, and A. Hummel. Electron migration in hydrated DNA and collagen at low temperature. Part I, Effect of water concentration. *J. Chem. Soc. Farady Trans. I*, 82:2933–2943, 1986.

[VRBJ00]   A. A. Voityuk, N. Rösch, M. Bixon, and J. Jortner. Electronic coupling for charge transfer and transport in DNA. *J. Phys. Chem.*, 104:9740–9745, 2000.

[vS87]     C. von Sonntag. *The Chemical Basis of Radiation Biology*. Taylor & Francis, London – New York – Philadelphia, 1987.

[VV95]     D. Voet and J. G. Voet. *Biochemistry*. Wiley & Sons Inc., New York, 2nd edition, 1995.

[WAK98a]   M. A. Walicka, S. J. Adelstein, and A. I. Kassis. Indirect mechanism contribute to biological effects produced by decay of DNA-incorporated iodine-125 in mammalian cells in vitro: Clonogenic survival. *Radiat. Res.*, 149:142–146, 1998.

[WAK98b]   M. A. Walicka, S. J. Adelstein, and A. I. Kassis. Indirect mechanism contribute to biological effects produced by decay of DNA-incorporated iodine-125 in mammalian cells in vitro: Double-strand breaks. *Radiat. Res.*, 149:134–141, 1998.

[WAK01]    M. A. Walicka, S. J. Adelstein, and A. I. Kassis. Chemical modification of 5-[$^{125}$I]iodo-2'-deoxyuridine toxicity in mammalian cells in vitro. *Int. J. Radiat. Biol.*, 77(5):625–630, 2001.

[WDAK00]   M. A. Walicka, Y. Ding, S. J. Adelstein, and A. I. Kassis. Toxicity of DNA-incorporated iodine-125: Quantifying the direct and indirect effects. *Radiat. Res.*, 2000:326–330, 2000.

[WDR$^+$99]   M. A. Walicka, Y. Ding, M. Roy, R. S. Harapanhalli, S. J. Adelstein, and A. I. Kassis. Cytoxicity of [$^{125}$I]iodoHoechst 33342: contribution of scavengeable effects. *Int. J. Radiat. Biol.*, 75:1579–1587, 1999.

[WFS$^+$99]   C. Wan, T. Fiebig, O. Schiemann, J. K. Barton, and A. H. Zewail. Femtosecond direct observation of charge transfer between bases in DNA. *Proc. Natl. Acac. Sci. USA*, 96:8353–8358, 1999.

[WMF97]    J. F. Ward, J. R. Milligan, and R. C. Fahey. Factors controlling the radiosensitivity of the cellular DNA. In D. T. Goodhead, P. O'Neill, and H. G. Menzel, editors, *Microdosimetry – An Interdisciplinary Approach*, pages 57–64, UK, 1997. The Royal Society of Chemistry.

[XN00]     D.-G. Xu and T. M. Nordlund. Sequence dependence of energy transfer in DNA oligonucleotides. *Biophys. J.*, 78:1042–1058, 2000.

[YHD96]    L. S. Yasui, A. Hughes, and E. R. DeSombre. DNA damage induction by $^{125}$I-estrogen. *Acta Oncol.*, 35:841–847, 1996.

[YHD01]    L. S. Yasui, A. Hughes, and E. R. DeSombre. Relative biological effectiveness of accumulated $^{125}$IdU and $^{125}$I-estrogen decays in estrogen receptor-expressing MCF-7 human breast cancer cells. *Radiat. Res.*, 155:328–3354, 2001.

[YPVM85]   C. Yanisch-Perron, J. Vieira, and J. Messing.   Improved M13 phage cloning vectors and host strains: Nucleotide sequences of the M13mp18 and pUC19 vectors. *Gene*, 33(1):103–119, 1985.

# Danksagung

Ich danke Herrn Prof. Dr. Herwig G. Paretzke ganz herzlich, dass er mich nach München eingeladen und betreut hat. Seine Ermutigung, auch den Ladungstransfer in DNS Ketten zu modellieren, hat mich in diese Theorie gebracht.

Herrn Prof. Dr. Erich Sackmann danke ich gleichfalls herzlich für die Vertretung meiner Arbeit an der Fakultät für Physik der Technischen Universität München.

Ich bedanke mich bei Herrn Dr. Peter Jacob für Annahme in seiner Arbeitsgruppe und für seine wertvollen Diskussionsbeiträge über die Kombination von Ergebnissen der Simulation mit den experimentellen Daten.

Herrn Dr. Werner Friedland danke ich besonders für die Einführung in die Welt des PARTRAC Codes bzw. Unix, IDL und POV-Ray.

Ich danke Herrn Dr. Michael Dingfelder für seine vielfache Hilfe nicht nur in wissenschaftlichen Bereichen, sondern auch im privaten Leben. Bedanken möchte ich mich auch für die Zeit, die ich und meine Frau Ying mit ihm in Barcelona verbracht haben. Er hat meine Dissertation ausführlich durchgelesen und hat viele positive Vorschläge vorgebracht.

Herr Philipp Bernhardt hat mir viel geholfen beim Verständnis der „charge transfer theory" und hat mir auch die Parameter, die ich für die Ladungstransferraten brauche, mit *Gaussian98* ausgerechnet. Ich danke ihm herzlich.

Herr Dr. Mitio Inokuti hat die Kapitel 1 und 4 und den Abschnitt 2.1 aufmerksam und ausführlich durchgelesen. Er hat nicht nur Form sondern auch Inhalt meiner Dissertation korrigiert und verbessert. Ich danke ihm.

Ich danke Herrn Dr. Ekkehard Pomplun für die Genehmigung der Verwendung seiner ausgerechneten Zerfallsdaten von I-125.

Herr Prof. Dr. James E. Turner hat die Dissertation durchgelesen. Ich danke Ihm herzlich.

Auch den anderen Mitgliedern der ISAR Gruppe danke ich persönlich.

Ich danke Christoph Utz von Weiden für seine Freundschaft genauso wie Florian Gering, Yeter Göksu, Stephan Hübner, Matthias Niedermayer und Tobias Sahr für die schöne Zeit in München und in der GSF Neuherberg.

Zum Schluss danke ich meinen Eltern, die in Luoyang leben, und meiner geliebten Frau Ying, Beijing, für ihr Verständnis und ihre Unterstützung von ganzem Herzen.

Wei Bo Li, 19.06.2002, München

# Lebenslauf

**Persönliche Daten**

| | |
|---|---|
| Name: | Li |
| Vorname: | Weibo |
| Geburtstag: | 17. May 1966 |
| Geburtsort: | Luoyang, P. R. China |
| Staatsangehörigkeit: | chinesisch |
| Familienstand: | verheiratet |

**Schulbildung**

1982.09 — 1985.07     Das erste Gymnasium (Internat), Luoyang, VR China
                      Abitur

**Hochschulausbildung**

1985.09 — 1989.01     Studium der Physik an der Nanhua Universität,
                      Hunan, VR China. Abschlussnote: gut

1989.02 — 1989.07     Bachelorarbeit in nuklearer Instrumentierung
                      Note: gut. Titel: Bachelor in Science (B. S.)

**Masterstudium**

1991.09 — 1992.07     Masterstudium der Biophysik
                      an der Academy of Military Medicine Sciences,
                      Beijing, VR China
                      Note: gut

1992.08 — 1994.07     Masterarbeit an der Academy of Military
                      Medicine Sciences, Beijing, VR China
                      Note: sehr gut. Titel: Master in Science (M. S.)
                      Mit einem umgerechneten Notenmittel von 1,9 von
                      der Technischen Universität München

**Berufstätigkeit**

1989.07 — 1991.08     Tätigkeit als Ingenieur an der Henan
                      Academy of Sciences, Zhengzhou, VR China

1994.08 — 1997.10     Tätigkeit als Wissenschaftlicher Mitarbeiter
                      am Institute of Radiation Medicine,
                      Beijing, VR China

1997.11 — 1999.06     Tätigkeit als Gastwissenschaftler
                      am GSF-Forschungszentrum für Umwelt und
                      Gesundheit, Institut für Strahlenschutz, Neuherberg

1999.07 — 2002.07     Immatrikuliert an der Technischen Universität München.
                      Promotion am GSF-Forschungszentrum für
                      Umwelt und Gesundheit, Neuherberg